BERICHTE

aus dem

INSTITUT FÜR MEERESKUNDE

an der

CHRISTIAN–ALBRECHTS–UNIVERSITÄT KIEL

Nr. 250

1994

Modelling water and salt

exchange through the Belt and

Sound

von

Erdem Sayın

Diese Arbeit wurde von der Mathematisch–

Naturwissenschaftlichen Fakultät der

Universität Kiel als Dissertation angenommmen.

Abstract

The time dependent 3-dimensional stratified Princeton Model was used, to analyse the dynamics in Belt and Sound. The Belt and Sound are narrow passages between the North Sea and the Baltic two regimes that have different density stratifications and sea level elevations due to different, natural processes in each basin. Three basic experiments were done. The first one of these is a two-basin experiment. Effects of rotation, topography, friction, different stratification and barotropic forcing were studied in these experiments, to analyse the water exchange and the control between the two basins. The flow has two distinct phases, one of them being linear adjustment in which Kelvin and Poincaré dynamics set up the boundary and interior circulations, and the second being the nonlinear phase in which topographic effects and stratification play an important role and instabilities can occur.

The heigh resolution in time and space of the model used here facilitates work on strait problems and the presentation of results. Several possible mechanisms of channel dynamics are presently under discussion. Some questions are, for example, which type of control determines the dynamics in straits and gives the best prediction of the transport through a channel? Is the Rossby deformation radius important? Do barotropic or baroclinic processes play an important role? If both of them, how and when? Why is the time dependent motion important? What are the effects of instabilities and turbulence from the point of view of energy propagation? Is it possible to see solitary waves, bore formations and also time dependent cylinders of rotating fluid in the system? Some of these questions are clear, but some need some clarifications and further research.

The second experiment is performed to determine the effects of barotropic forcing on the stratified Baltic. The resulting circulations with and without barotropic forcing both show expected, realistic patterns. The thermohaline circulation loses its two-layer character with barotropic forcing which is in these experiments given as a prescribed surface elevation at the boundaries of the model region. Unidirectional flow permits larger transport of volume and salt than bidirectional flow in a channel.

Chapter 1

Introduction

The Danish Straits are narrow and shallow channels which connect the Baltic Sea
and the North Sea. They are of fundamental importance for the water exchange
between both areas. The flow in the straits can be considered as a two–layer flow
over a sill which separates two basins of different stratification.

Sea level differences between North Sea and Baltic play an important role in the
water exchange. Due to variable meteorological conditions the system has to adjust
to varying conditions.

Adjustment problems have generally three distinct phases. Two of them are related
to the channel itself and the third to the connected basins. The final quasi-steady
state – if it exists – has less energy than the initial one.

The first phase is characterized by rapid modifications on the inertial time scale. This
is the so-called geostrophic adjustment process, which involves Kelvin and Poincaré
waves. The latter waves can remove some energy from the system. However, there
are cases in which, for some reason, Poincaré or other waves cannot remove energy
from the system (KILLWORTH, 1992a). Additional processes must then occur. One
of the candidates is the tilting of the isopycnals due to strong velocities, such, that
heavy fluid can overlay light fluid (LILLY and KLEM, 1979). This causes static
instabilities and rapid mixing. The dissipative and friction terms start to dominate
over the nonlinear terms in the change of kinetic energy.

In a channel only odd internal Poincaré waves occur (KRAUSS, 1979b; FENNEL
and LASS, 1989). These waves have zero group velocity. Poincaré waves cannot

propagate in the along direction (because of the walls of the finite basin, where they are reflected), they are responsible for the crossoscillations.

Superinertial ($\omega \geq f$) oscillations are important for the vertical energy propagation. Only waves with frequencies exceeding the inertial frequency can carry information downward. In this phase entrainment and detrainment cause bottom intensified or surface intensified flow (or both) in the channel. That means that one of the layers will be more active or the two layers flow opposite to each other. By this a vertical shear is developed and Kelvin–Helmholtz instabilities can occur. At the end of the first stage subinertial oscillations ($\omega \leq f$) exist locally (in the connected basins). Due to eddy viscosity the superinertial oscillations are damped. In the low frequency limit ($\omega \sim 0$), the well known coastal jet follows (Coastal trapped waves, CSANADY, 1977).

The second adjustment is a nonlinear one over topography (McDONALD, 1993). It determines the time scale of the geostrophic flow in the channel. Topography is an obstacle for the fluid, at the same time regulates it and prepares the physical conditions for the next basin. The length scale of motion will change while the water flows into the connected basin. Increase in a length scale causes a decreasing of the Rossby number. This means that the rotational effect will be stronger in a subbasin than in a channel.

The third phase depends on the initial energy of the system; the system has a comparatively large amount of energy in the forced case, but relatively less energy in the density driven case. Water which is flowing over topography, accumulates behind the sill (dome–shape) in the density driven case. GILL (1977) meant that friction is important for this dome–shape in the basin and emphasized the occurence of hydraulic control in the immediate neighbourhood of the topography. The advection of the accumulated water away from the topography is more obvious in the forced case. Cyclonic eddy formation can be seen at the lee of the sill. The development after the accumulation of water is beyond the scope of this study.

The complex geometry can lead to enhanced sea surface amplitude modulation and increased velocities, giving rise to local instabilities, mixing, internal bores, jumps,

and other striking phenomena at small scale. Numerical general circulation models handle topography rather crudely. Topography and associated form drag can effect the current. The problem involving rotating, stratified flow and topographic interactions is too complicated for analytical methods. Some studies which show the importance of topography, are PRATT (1983, 1984, 1986), BAINES (1984), GILL et al. (1986), KILLWORTH (1989a, 1989b), JOHNSON (1990), JOHNSON and DAVEY (1990) and McDONALD (1993).

The Baltic Sea shows very complicated physics and requires a three dimensional analysis with high resolution. To resolve the processes in the channels, horizontal resolution of less than the Rossby radius of deformation is required. The model used here – the time dependent 3–dimensional stratified Princeton model – has 12 layers in the vertical. This is necessary to resolve the internal dynamics of the stratified fluid. FENNEL et al. (1991) calculated Rossby radii for different seasons in various part of the Baltic Sea. In the Belt Sea they found maximum values during summer (about 4 km) and minumum values during autumn and winter (about 1.4 km). The horizontal resolution of 2.5 km of the model may be critical for the latter period.

1.1   Barotropic and Baroclinic Response to External Forcing

At midlatitudes the Rossby deformation radius is much larger than at high latitudes because of the stratification. Rotation can be more important at higher latitudes for the time-dependent flow in a channel. The barotropic Rossby radius which may be responsible for along-channel motions, is smaller at higher latitude. Because of this shelf waves are faster at higher latitudes than those at lower latitudes (HSIEH and GILL, 1984).

MAGAARD and KRAUSS (1966) computed energy and amplitude spectra from the sea level records along the Baltic coast and explained the energy concentration in the range of about 120 h with a standing wave forced by wind. Because of meteorological forcing, during most of the time barotropic processes dominate in the

Baltic Sea. However, KIELMANN et al. (1973) used mode decomposition and found that the major baroclinic mode contains 10 times the energy of the barotropic one near the inertial frequency. They also found the strongest baroclinicity in the period range from approximately $10h - 40h$. For periods longer than about 50 hours the energy becomes nearly independent on depth, which means that the Baltic responds mainly barotropically at low frequencies.

The barotropic and baroclinic response to barotropic forcing of a semi-enclosed basin are discussed by STIGEBRANDT (1980). He emphasized that the velocity at topographical features must be considered in order to study the baroclinic response to barotropic forcing which causes larger transport through the channel. Some examples for this situation were computed by using two-basin experiments and realistic topography in the present study.

1.2   Recent Progress in Strait Dynamics

Some authors have suggested that a major change in understanding the dynamics of flow through straits has occured over the last few years due to the development of two-layer hydraulic control models and their application to new observations in the Strait of Gibraltar. Recent hydraulic model studies on the two-layer exchange through the Strait of Gibraltar are done by BORMANS and GARRETT (1989), DALZIEL (1990), GARRETT et al. (1990) and BRYDEN and KINDER (1991b). HOGG (1983, 1985) developed a multi-layer hydraulic model and applied it to the Vema Channel and to the circulation in the Alboran Sea . ÜNLÜATA et al. (1990) applied a hydraulic control model to the Bosphorus Strait. Based on recent investigations they found that a major portion of the Mediterranean flow entering through the Dardanelles is transported back to the Agean Sea due to upward mixing induced by internal hydraulic adjustments of the exchange flow in the straits and by wind in the Sea of Marmara proper. The jet–like Bosphorus outflow in the exit region of the Marmara Sea also has a substantial contribution to the overall upward mixing. The reneval of water in the deep basins of the Baltic Sea are studied by STIGE-

4

BRANDT (1987a) and KRAUSS and BRÜGGE (1991). STIGEBRANDT (1987a) examined the dense water pool in the deepest parts of the Arkona Basin. He assummed that the leakage of this pool is controlled by the vertical stratification in the Arkona Basin together with the rotation (rotational baroclinic control). KRAUSS and BRÜGGE (1991) found from observations and model results that the saline oxygen rich water which penetrates into the Bornholm Basin is transported into the Gotland Basin as a result of the wind conditions (especially northerly and easterly winds). STIGEBRANDT (1987b) studied an entraining dense bottom current. In his study the dynamical balance in the dense bottom current is between the longitudinal pressure gradient force and the frictional forces. An important result of this study is the generation of internal waves over topography. He assumed that barotropic and baroclinic currents which interact with bottom topography generate internal waves. In the application part of the present study the generation of the internal waves will be shown.

BAINES et al. (1991), MIDDLETON (1991), MIDDLETON and VIERA (1991, hereafter MV) and HANNAH (1992) emphasized the importance of coastal–trapped waves (CTWs) in the Bass Strait. MIDDLETON (1991) gave an explanation for the generation of CTWs as a result of Kelvin and Poincaré waves. The model of MV further treats the coupling between an ocean and a strait and scattering of Kelvin waves at the ends of the Bass Strait. They found that the high frequency motion (period 80 h) is predominantly driven by local wind stress and the motion with a 240 h periodicity is driven by local wind and CTWs. In both studies (Middleton (1991) and MV) linear systems which consist of the Kelvin and Poincaré waves, were used. HANNAH (1992) critisized the concept of geostrophic control of the MV model. He meant that difficulties arise when variable topography is considered in the MV model. BAINES et al. (1991) also described the dynamical processes in the Bass Strait. CTWs are converted to Kelvin waves as they enter the Bass Strait. In their study a double Kelvin wave occurs due to the escarpment at the opening of the strait and forces a Kelvin wave which propagates along the coast in the initial direction of the incident deep–water Kelvin wave. This linear development breaks

down due to the singularities at the corners of the Bass Strait.

After these recent case studies some theoretical studies are mentioned which were recently published. GILL (1986) examined how the flow is modified over a step–like bottom topography. Double Kelvin waves, which propagate along the step, play an important role in the Rossby adjustment problem. KILLWORTH (1992b, 1992c) discussed conditions and properties of rotating, stratified hydraulics. He found that uni–directional flow permits more water to pass through the rectangular sill than bi–directional flow. His comment is that eddy–resolving models can handle the hydraulic problem if they resolve the deformation radius. Advantage of the hydraulic control hypothesis is a fairly accurate prediction of the transport through straits (PRATT, 1991). Time-dependent dynamics can not be explained using hydraulic models. It can be said that the occurence of hydraulic or geostrophic control depends on space and time. This means that they occur at specific times and locally in straits. In chapter two these control processes will be discussed further and also the interaction between Poincaré waves and double Kelvin waves. An interaction between Poincaré and double Kelvin waves was found also in the present study and will be presented in the application section, also a speculation about double Kelvin waves. Pure geostrophic steady state flow or pure hydraulic relations have not been found. In the system studied here nonlinearities and friction always exist.

Papers mentioned already above, emphasized the importance of topographic effects. JOHNSON and DAVEY (1990) and McDONALD (1993) examined also the topographic effects and the interraction between flow and escarpment. McDonald noticed that the escarpment plays an important role as a eddy production mechanism. The generated eddies can propagate over large distances.

Chapter 2

Theory

In this chapter we summarize basic concepts which are important for the flow in a strait. Hydraulic control theory was first introduced into physical oceanography by the papers of STOMMEL and FARMER (1952,1953).

The Rossby radius of deformation is important for straits. It is a scale that determines whether a channel is wide or narrow. The dynamics are different in wide and narrow channels. In laboratory experiments WHITEHEAD and MILLER (1979, here referred to as WM) found that if rotation is sufficiently rapid so that the Rossby Radius of deformation, r_i, is less than the width of the connecting channel, the flow will go violently unstable and develop small turbulent eddies. As a result there would be little transport from one basin to another. If rotation is less rapid so that r_i is greater than the width of the opening, light fresh water will flow into the dense basin as a narrow jet propagating along the right-hand wall. At some lower rate of rotation flow separates from the wall and a gyre is observed in the adjacent basin. At the bottom, the fluid flows into the opposite direction. In the experiment of WM the transport measurement is consistent with the hydraulic theory of WHITEHEAD et al. (1974). WANG (1985) confirms the study of WM, and states in addition that without rotation, the gravity current passes through two distinct phases. An initial adjustment phase in which the speed of the front is constant, and an eventual self similar phase in which the speed decreases with time. With rotation, the gravity current is confined to the right-hand wall, forming a coastal jet. GILL (1976) found analytically that first geostrophical adjustment and then the steady flow occurs in

7

channels. His results are described in terms of Poincaré and Kelvin waves. If the basin width is wider than the Rossby radius of deformation then the final state involves a current of that width which follows the left-hand boundary to the position of the initial discontinuity, then crosses the channel and continues downstream along the right-hand wall. He argues that the time development may help to resolve the question, whether steady solutions are possible as a final state. The solution considered applies to any mode in a channel of uniform depth, and for general initial conditions the complete solution can be found as a sum of normal modes. The method can not be applied when the depth varies. Gill pointed out that the solution would be expected to have the same character in a real ocean basin since long trapped waves on sloping boundaries also propagate in one direction only. Results of the present study confirm some aspect of his solution during the linear adjustment phase of the model, but the topographic effects and the nonlinearities in a channel cannot be treated with his theory.

GILL (1977) assumed uniform potential vorticity for the homogeneous, inviscid fluid. Using his hydraulic relation it is possible to specify the upstream flow with three parameters ,i.e. the width and depth of the channel and the flow rate. He found that there always exist long-wave disturbances with zero phase speed. However, the assumption of uniform potential vorticity is valid only during the first stage in the channel adjustment processes. The uniform potential vorticity concept cannot explain recirculation of the flow. PRATT and ARMI (1987) tried to solve the same problem using nonuniform potential vorticity. They found two possible solutions, one of them yields potential vorticity waves with only one critical steady state, and the other solution is controlled by a gravity mode, having multiple critical steady states and allowing current reversal. The hydraulic solution is a special solution. It has no time dependence and it cannot be responsible for another physical process, i.e. flow separation from the boundary in the channel. The results obtained in the present study show nonlinear interractions in the exchange of kinetic energy.

The Coriolis acceleration and the frictional terms cannot be ignored. Of particular interest is that on the inertial time scale the system goes from an initially motionless

state to one in which the fluid is in motion. During that time there is a discrepancy between the total final energy and the initial one. KILLWORTH (1992a) argued that wave radiation cannot be responsible for this discrepancy in some cases. He examined the wave-breaking events (as a part of a convective chimney), which can act as a mechanism to remove the energy deficit on short (i.e. inertial) time scales. Wave–breaking can play an important role in field and in laboratory experiments. However it is impossible to make a model that covers the wave–breaking phenemenon. Some processes which cause the same results (convective chimney) can be parametrized in a model (MAROTZKE, 1991). Confirmation for the existence of these chimneys is given in the two-basin experiments.

2.1   The Processes in Straits

BRYDEN and KINDER (1991a) reviewed the recent progress in strait dynamics, focusing on flow through the Strait of Gibraltar within the context of hydraulic theory. PRATT (1991) compared the theories of hydraulic control and geostrophic control and concluded that the transport given by geostrophic control does not put any bound on the exchange predicted by hydraulic theory. The agreement between transport estimates resulting from hydraulic theory and recent observations in straits encouraged many further studies on hydraulic theory. Thus the discussion on the dominance of hydraulic control or geostrophic control in straits will continue. In the study presented here it is found that both types of control are possible in strait dynamics. However, in the present study the "pure" hydraulic relation could not be found, where nonlinear acceleration balances the pressure gradient. On the other side the residual terms in the exchange of energy point towards an occurence of convection. This leads to a dome–up in the two–basin experiments. Hydraulic control takes place between the dome and the sill. Which procceses are dominant depends on the geometry of the channel, the driving forces and the properties of the water masses involved. Homogeneous and stratified fluids have different properties with respect to vertical propagation. Results of the presented study cover most of the

important processes in channels. These are, for example, bore formation, reservoir effects, the existence of a rotating cylinder (chimney), the secondary circulation in boundary mixing, nonlinear interactions, amphidromies and both kinds of control. Some of the processes mentioned will be later explained in details. The results will be presented in the section on the application of the model.

2.1.1 Geostrophic Control

GILL (1976) described his linear adjustment process in terms of Poincaré and Kelvin waves. In his application, if the Rossby deformation radius r_i is less than the basin width, then the final state involves a current of scale r_i which follows the left-hand boundary to the position of the initial discontinuity, then crosses the channel and continues downstream along the right-hand wall.

WRIGHT (1987) states that the geostrophic control is not possible for basins of finite area. However WHITEHEAD (1986) has performed an experiment that seems to verify geostrophic control in a laboratory strait connecting two finite basins. At the same time Wright has pointed out that when dissipation of the cyclonically propagating waves in the basins is significant, even for finite basins the idea of geostrophic control can be important. MIDDLETON (1991), MIDDLETON and VIERA (1991), BAINES (1991) and HANNAH (1992) found a geostrophic control in the Bass Strait.

PRATT (1991) compared the hydraulic flow with geostrophic flow and gave some initial conditions and a number of restrictions for both controls. Geostrophic control breaks down when the Kelvin waves and the associated boundary current have passed the channel. The second limitation is that the system must be restricted to small amplitude motions. It means that the difference between the surface elevations in the two basins or the isopycnal levels must be smaller than the depth of the channel by an order of magnitude. The third restriction is that the ratio between channel width and basin width must be large enough that the effect of rotation may not be ignored.

Channel transports obtained by field observations and tank experiments in the la-

boratory cannot be predicted using geostrophic control theory. Flow determined by geostrophic control has generally an asymmetry, especially at the downstream side of the channel. The asymmetric shape does not always occur.

2.1.2 Hydraulic Control

The title of this section is hydraulic control, but it would be preferable to talk about the hydraulic character of the flow. The inviscid, rotationless fluid can have a steady state, in which the nonlinear acceleration balances the pressure gradient. Under these conditions internal hydraulic control arises in a system with two homogeneous layers. Long wave disturbances can have zero phase speed at the control section.

After STOMMEL and FARMER (1952, 1953) other papers have been published on hydraulic control. Some of these have already been mentioned. GILL (1977), used unifom finite potential vorticity and showed that the flow is confined to boundary layers on each side wall. He also showed that the principle of maximum transport is equivalent to linear Kelvin waves having zero phase speed at the control section.

PRATT and ARMI (1987) considered nonuniform potential vorticity with the distribution $G = G_0 - \alpha\psi$, where ψ is a stream function, G_0 and α constants. For positive α they found that the potential vorticity waves are propagating against the flow and suggested that the solution is controlled by the gravity mode. If α is negative then potential vorticity waves move in the same direction as the mass transport. The only wave which can become stationary in the flow is the gravity mode (one critical steady state).

PRATT (1987) pointed out that no example of hydraulically critical, separated flow has been produced in the laboratory. In theory one should need very high rates of rotation for the separation of supercritical flow, but the critical flow at the sill remained attached for all rotation rates. Among other points to be discussed is the fact that time dependent overflow cannot be analysed using hydraulic theory. The time-dependence must be weak, but not too weak. Another point to note is the communication between parallel walls of the channel. Cross current is not allowed

in hydraulic theory, it admits only Kelvin wave dynamics. In the paper of GILL (1977) Kelvin waves play a similiar role as long gravity waves in classical hydraulics, at least when the fluid flows along both side walls. Hydraulically driven flow is found by field observations in many straits, e.g. in the Denmark Strait, Strait of Gibraltar, Vema Channel, Bornholm Channel and Bosphorus.

The controls in a channel, geostrophic and hydraulic, depend on some conditions in space and time (HERMANN et al., 1989 and PRATT, 1991). For hydraulic control these are the following: First, hydraulic control begins after linear geostrophic adjustment and before the frictional time scale dominates. The second condition is that hydraulic control is generally associated with narrow channels whose width is smaller than the internal Rosbby radius, or at least of the same order of magnitude. The ratio of channel width to basin width plays also an important role. In this case, the Rossby number, which is responsible for the scale of rotation can be O(1). This means that the rotation looses its effect on the system. Another important condition is the ratio between $\nabla \eta$ (the change in surface elevation or level of isopycnals), and the water depth H, which can be O(1) and the corresponding flows can be hydraulically controlled.

Both control mechanisms have difficulties to describe the circulation in the channel. This can be explained by an examination of how the sill regulates the flow.

2.2 Linear System

We begin our discussion with the long wave approximation. The equations of motion and continuity are

$$u_t - fv = -g\eta_x \tag{2.1}$$

$$v_t + fu = -g\eta_y \tag{2.2}$$

$$\eta_t + (uH)_x + (vH)_y = 0 \tag{2.3}$$

Here u and v are horizontal velocities, g is gravity ,η or p_n is surface elevation or pressure, respectively, H or h_n are the total depth for the homogeneous case or the

eqivalent depths ($n = 0, 1, 2, ...$) for the stratified case. Most of the literature on long-wave oscillations in rectangular basins deals with barotropic motions; for this case, $n = 0$ and $h_0 = H$. In the baroclinic case the presure p_n replaces η, the free surface elevation. This system of equations has been analysed with different boundary conditions in a large number of textbooks and papers. They describe a broad spectrum of solutions. The related eigenvalue problem consists of the Kelvin mode, the Poincaré modes and the geostrophic mode (PEDLOSKY, 1979). KRAUSS (1973) presented solutions of these equations for different geometries and discussed the reflection at the end of a channel. DEFANT (1961) has shown that in an infinitely long channel an amphidromic system exists which results from two Kelvin waves travelling in opposite directions. For a homogeneous case in which $\omega < f$ and where two circular basins are linked by a channel of uniform width, HUTHNANCE (1980) obtained as a solution in form of modified Bessel functions. He noted that for large basins the normal modes correspond to Kelvin waves. GILL (1976) described his steady state solution in terms of Poincaré and Kelvin waves.

If we solve the system (2.1), (2.2) and (2.3) for η and use $e^{i\omega t}$ for the time dependent part, we get for H constant

$$\eta_{xx} + \eta_{yy} - \frac{f^2 - \omega^2}{gH}\eta = 0 \tag{2.4}$$

LeBLOND and MYSAK (1978, hereafter LM) reviewed waves in a closed basin. They based their analysis on this Helmholtz equation (2.4), which represents a boundary-value problem for the eigenfrequency ω and eigenfunction η or (p_n) in a rectangular domain. For the barotropic and nonrotating case ($f = 0$) the solution gives Merian's formula for the period and for the first mode,

$$\tau = \frac{2L}{(gH)^{\frac{1}{2}}}$$

(DEFANT, 1961). In order to test the rotation effect an experiment was conducted for this case. The dimensions of the rectangular basins used are shown in Figure 2.1. Figures 2.2-4 summarize the barotropic case, demonstrating that the period of free
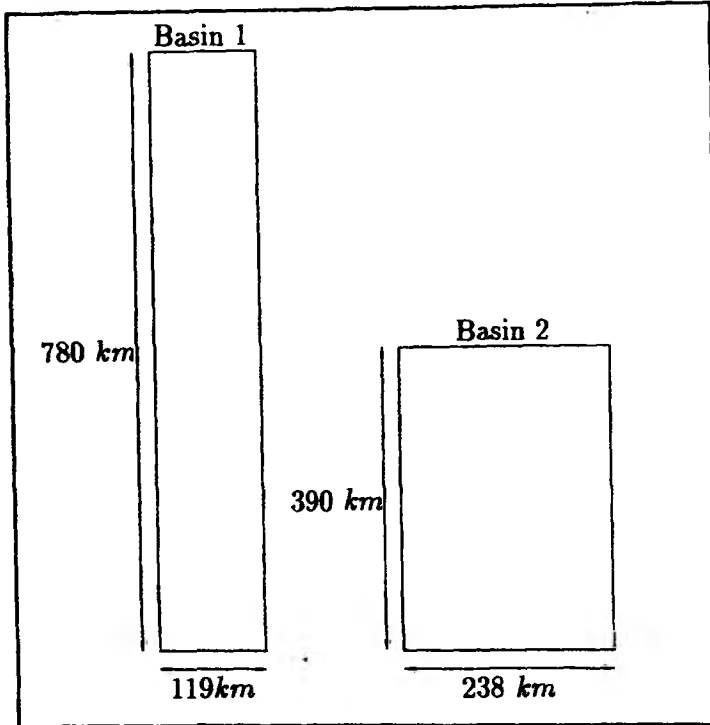
13

Figure 2.1: *The dimension of the chosen rectangular basins a) Basin 1 b) Basin 2.*

surface oscillations in a rectangular basin can be calculated almost accurately for the case $f = \epsilon f_0$ (where $\epsilon = 0.01$ and $f_0 = 2\Omega \sin\theta$, Ω is the angular velocity of the earth and θ is the latitude). This is also true for the case $f = f_0$ in a narrow channel i.e., the width of the basin is smaller than the external Rossby radius, r_e. Otherwise, when the width of the basin is larger than the external Rossby radius then the effects of rotation influence the basin oscillations (Fig.2.2d). Figure 2.2 shows the kinetic energy. Kinetic energy of standing waves is proportional $\sim cos^2\omega t \sim cos(2\omega t)$. This means that the period in kinetic energy curves is not given by Merian's relation but is two times the period of the oscillations. The corresponding surface elevation patterns are shown in Figure 2.3 for the case $f = \epsilon f_0$. For the same basin an amphidromic system exists for $f = f_0$. It rotates in a clockwise direction (Fig. 2.4). LM have pointed out that when $f \neq 0$, the solution consists of a complex mixture of Kelvin- and Poincaré-type waves that propagate around the basin in a positive or negative sense. They note that there are two modes, one of them is symmetric and the other antisymmetric. Our aim is not to solve the differential equation (2.4), but to discuss
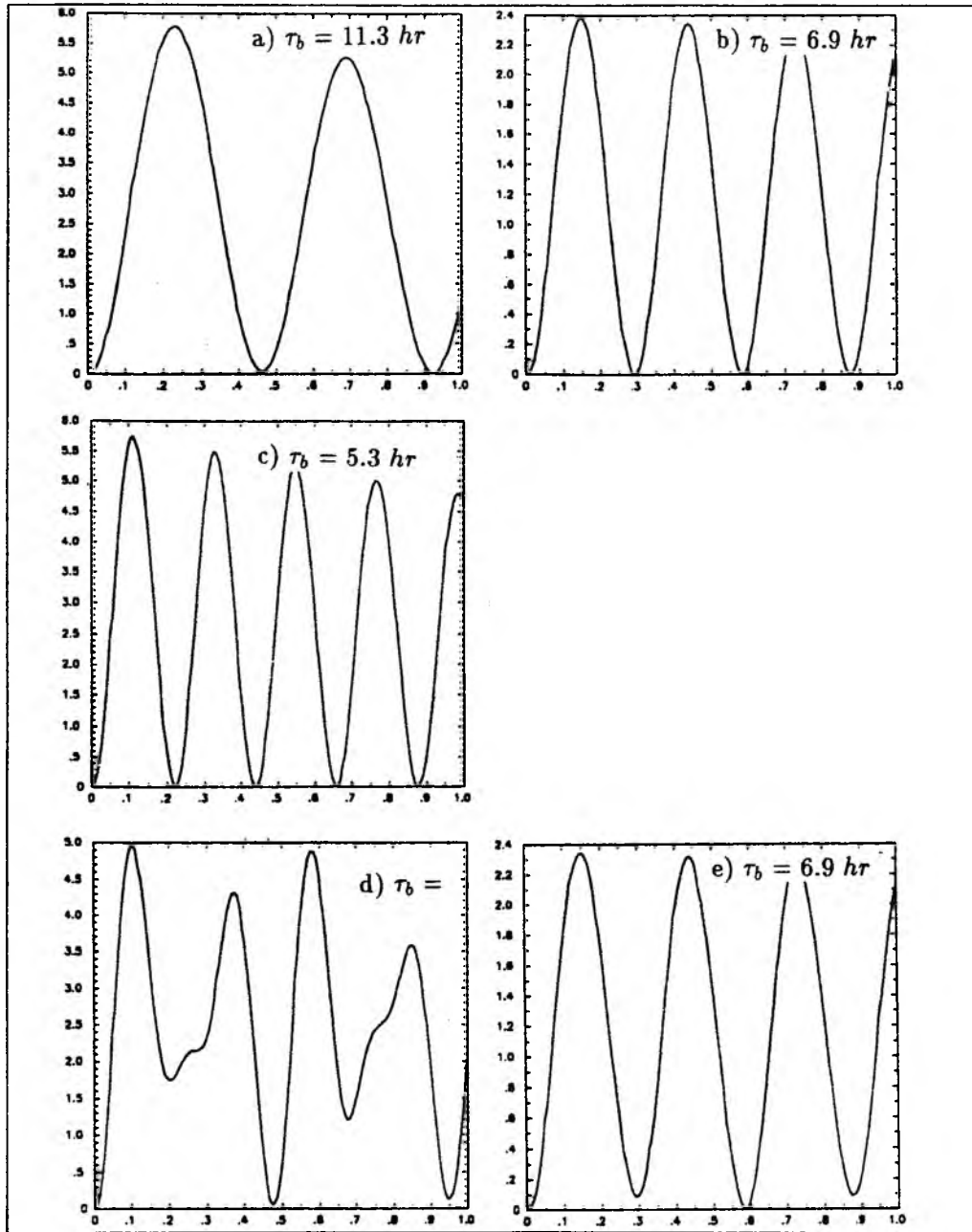
Figure 2.2: *The long wave kinetic energy in a rectangular basin. The pictures on the left show oscillations in a basin of 40 m depth , the one on the right hand those for H = 100 m. The values of the period τ_b are the time span between two successive maxima. a) Basin 1 from Fig.2.1, H = 40 m, f = ϵf_0, calculated period τ = 21.9 hr, b) Basin 1, 100 m, f = ϵf_0, τ = 13.8 hr, c) Basin 2, 40 m, f = ϵf_0, τ = 10.9 hr.d) Basin 2, H = 40 m, f = f_0, τ = 10.7 hr, r_e = 198.1 km. The effect of rotation can clearly be seen, because W > r_e. e) Basin 1, H = 100 m, f = f_0, τ = 13.8 hr, r_e = 313.2 km, no rotation effect, W < r_e.*

15
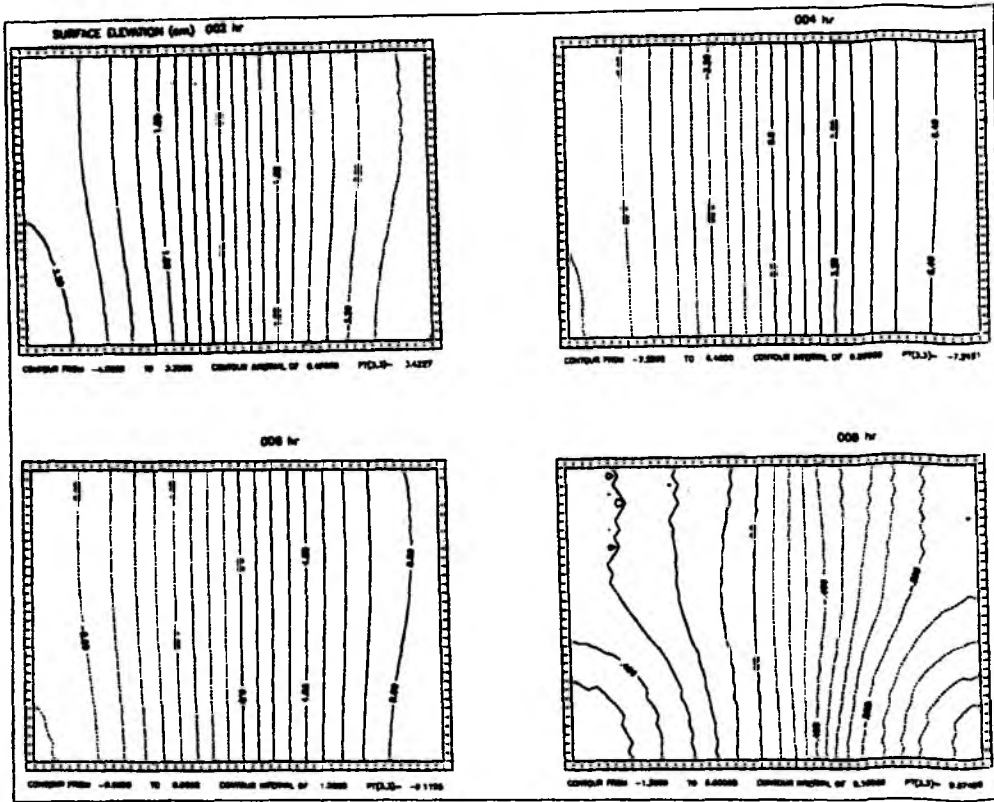
Figure 2.3: *The patterns of surface elevation at time* $t = 2, 4, 6, 8$ *hr for the case* $f = \epsilon f_0$.

if there are explanations that help us to determine what kind of solution might be expected. The expectation is to find Kelvin- and Poincaré-type solution as LM did, the Kelvin-type solution being perhaps more likely.

The eigenvalue relations for Kelvin (ω_k) and Poincaré (ω_p) waves are given in LM (1978):

$$\omega_k^2 = gh_n l^2 \tag{2.5}$$

$$\omega_p^2 \geq f^2 + \frac{m^2 \pi^2 gh_n}{W^2} \equiv \omega_c. \tag{2.6}$$

It should be noted that when the channel is wider than the Rossby radius of deformation stratified long waves give approximately $\omega \sim f$ according to (2.6). GILL (1982) pointed out that in this limit fluid particles move under their own inertia. The phase velocity and group velocity of Poincaré waves are the following

$$c^2 = gh_n + \frac{f^2}{l^2} + \frac{m^2 \pi^2 gh_n}{W^2 l^2} \tag{2.7}$$

16
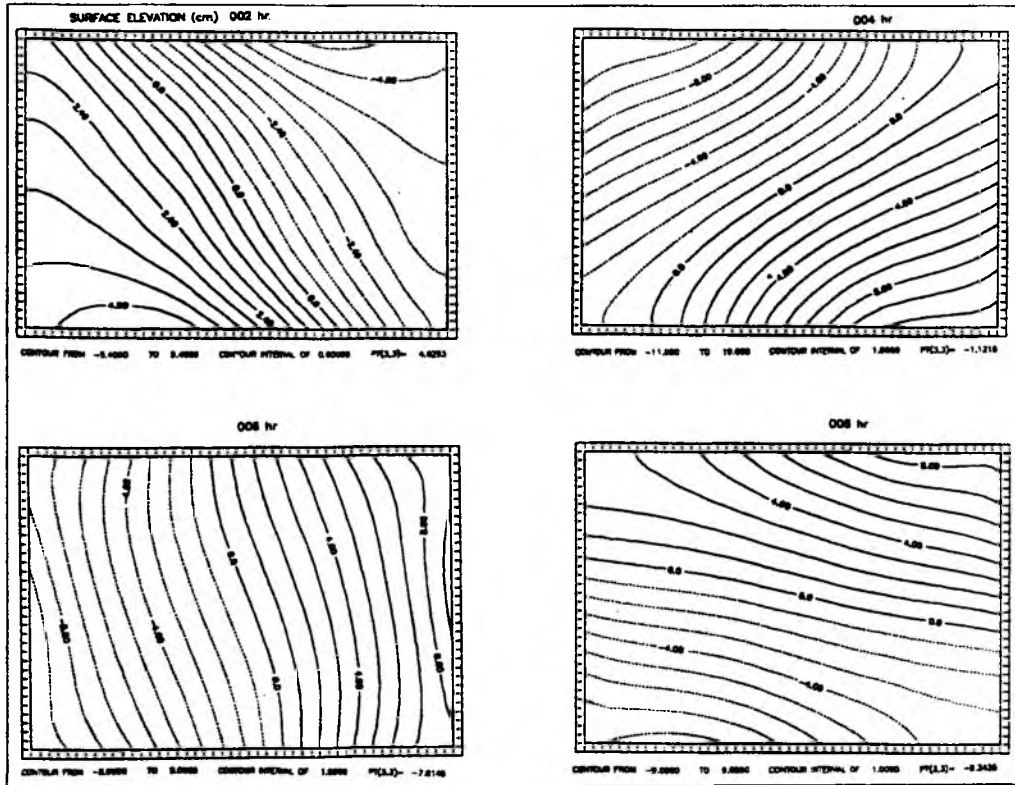
Figure 2.4: *same as Figure 2.3, for the case $f = f_0$.*

$$c_g = \frac{gh_n}{c}.$$
(2.8)

When $l^2 \to 0$, $\omega = \omega_c$. In this case, (2.7) and (2.8) give $c = \infty$ and $c_g = 0$. This type of geometric dispersion is a common property of waveguides (LM, 1978). The two boundaries have the effect of confining wave energy to a region of finite vertical extent, so the water can be considered as a waveguide that causes energy to propagate horizontally, provided the system is in resonance. These waves have the property that the solution that satisfies the boundary conditions exists only for particular values (eigenvalues) ω, for each of which there is a corresponding waveguide mode or eigenfunction (GILL ,1982). In general these have a different structure for each different wavenumber. In the long-wave limit the eigenfunctions are called *normal modes* each of which has a fixed vertical structure. There is no definite wavenumber which corresponds to each mode for the forced case (KIELMANN et al., 1973). These resonant modes are identical with the modes that can exist in the absence

17

of forcing (Gill, 1982). The energy carried horizontally without loss is trapped in a region that is called a *waveguide* or a *duct*. In this study we try to find the reasons and properties of this type of phenomenon. The waveguide process cannot be explained using only a linear system; friction, nonlinearities and instabilities play important roles. In the section on model application this statement will be confirmed by the analysis of the model results. The topographic effect has to be included in the analysis. Finding a solution for varying bottom topography is not straight forward, compared to the flat bottom case, because the technique of separation of variables cannot be applied without consideration of the boundary conditions to be satisfied at the bottom. A semi-spectral model was developed by KRAUSS (1979a), in which a sum of free waves is used to force the solutions in such a way that the sum of all Fourier components fulfills the boundary condition at the bottom. ORVIK and MORK (1993) have also used a spectral model to analyse topographic effects in stratified flows. They concluded that topographic effects are of great importance and that the flow is dominated by topographic waves.

2.3   Instabilities and Nonlinear Effects

Which processes play an important role for removing energy from the system and causing turbulence? There are three candidates, instabilities, hydraulics or the boundary mixing at the sloping bottom. The cylinder collapse occurs on inertial time scales (KILLWORTH, 1992a). Friction and dissipative effects will also play a role but they take more time to occur. Kelvin-Helmholz instabilities need approximately 8-10 inertial periods to grow (KILLWORTH, 1992a). LM (1978) concluded that stratified shear flow instability may not be the most effective turbulence producing mechanism if the growth rates are very slow or if the amplitudes of the growing perturbations are severly limited by dissipation or nonlinearities. BAINES and GRANEK (1990) emphasized that the flow over topography is very sensitive to stratification. If the value of

$$\frac{N h_m}{U}$$

is small, they found that internal energy generated by topography propagates horizontally in discrete modes with a well-defined vertical structure and there is little or no motion in the upper levels. They meant that if the value is increased, the flow will have a hydraulic character. LILLY and KLEMP (1979) define this relation as the inverse of the Froude number F. The critical value is $F \sim 0.85$. In their study, for larger values of h_m a rotor forms behind the sill. They claimed that any further tilt of the isopycnals would cause heavy fluid to overlay light fluid, thus producing rapid mixing. In this limit the drag might change significantly depending on whether or not flow separation occurs.

The inverse Froude number F^{-1} is proportional to the square root of the bulk Richardson number R_i. For weakly stratified fluid, R_i is a measure of the stability of the fluid. Almost complete mixing occurs for the critical value of R_i, ($R_i \ll 1$, if $F^2 \gg 1$). If ($F^2 \leq 1$), the flow is said to satisfy Long's stability criterion for long internal waves (LAWRENCE, 1990).

GRIFFITHS and HOPFINGER (1983) in their laboratory experiment determined many developing billows near the nose of currents. Wavelength, maximum amplitude and growth rate of these billows indicate that they are the result of a Kelvin-Helmholtz instability that is little influenced by rotation. They stated that intrusions and turbulent motions represent a forcing to the lower layer that produces vortex and wave-like motions which penetrate deep into the lower layer. Inertial waves and Taylor columns can occur in the lower layer depending on a parameter F which they defined as $F = hR_o/D$, (where R_o is Rossby number, h upper layer thickness and D total depth of fluid). They reported also the appearance of baroclinic waves. Unlike the Kelvin-Helmholtz billows, these waves break the constraint of rotation, and at large amplitude cause a large horizontal spreading of the buoyant fluid. However, they require times of the order of 10 rotation periods to grow to a visible amplitude. Kelvin-Helmholtz instability may not be the most effective turbulence-producing mechanism if the growth rates are very slow or if the amplitudes of the growing perturbations are severely limited by dissipation or nonlinearities. There is another possibility, dynamic gravitational instability in which the vertical density gradient

associated with large-amplitude internal waves becomes positive. This is a nonlinear instability that occurs when the particle velocity of the wave motion exceeds the wave phase velocity. The result is convective overturning (LM, 1978). This process is a more likely candidate than Kelvin-Helmholtz instability for removing energy from the system. The static stability was checked in the two-basin experiments of the presented study and instable layers were determined confirming the above mentioned nonlinear instability process at the begining of the integration.

2.3.1 Time Dependence and Nonlinear Interactions

PIERRINI (1989), HELFRICH and MELWILLE (1990) and SHEN (1992) studied long waves which are nonlinear and dispersive. They used the Korteweg-de Vries (KdV) equation to analyse fluid in the region between nonlinear and dispersive regime analytically. They obtain as a common result that internal solitary waves which were observed in different field studies are dispersive. Pierrini's starting point was that horizontally propagating internal waves in the oceanic waveguide are nonlinear and dispersive. It was emphasized that the dispersion explains the observed connection between the weakening of the Atlantic water jet and the appearance of energetic internal solitary waves. Helfrich and Melwille obtained a steady transcritical flow ($F \sim 1$) over topography as a result of the forced KdV equation and found that the Kelvin wave is unstable if in resonance with Poincaré waves. This solution showed that time-dependent strait flows which pass through the transcritical regime may be inadequately described by hydraulic theory because the time scale for generation of a solitary wave is less than the tidal period. These studies demonstrate that dispersion and nonlinearities are important (weak nonlinearity and weak dispersion) to describe wave evolution in rotating channels. Mälkki and Tamsalu (1985) stated that the soliton type internal waves may produce a shear instability, thus regulating the exchange processes between the upper and lower layers. In the study presented here solitary waves occured in the two-basin experiments. But any resonance interactions between Poincaré and Kelvin waves were not determined.

Chapter 3

The Free Surface Princeton Model and Applications

As outlined in the preceeding sections several possible mechanisms of channel dynamics are presently under discussion. Some questions are, for example, which type of control determines the dynamics in straits and which one gives the best prediction of the transport through a channel? Is the Rossby deformation radius important? Do barotropic and baroclinic processes play an important role? What are the effects of instabilities and turbulence from the point of view of energy propagation? Is it possible to see time dependent cylinders of rotating fluid in the system? Some of these questions can be answered by analytical theories, for others numerical studies are required. For this reason three experiments were done.

The first one is a two–basin experiment. Two equal basins are separated by a channel. The channel dimension is approximately the same as that of the Belt. In most of the experiments a simple topography is prescribed in the middle of the channel (Fig.3.1). The results are described in section 3.2. Effects of rotation, topography, friction, different stratification and barotropic forcing were studied to analyse the water exchange and the control between the two basins. The flow has two distinct phases, one of them being the linear adjustment, in which Kelvin and Poincaré dynamics set up the boundary interior circulations, and second being the nonlinear phase, in which topographic effects and stratification play an important role and instabilities can occur.

The second experiment is performed to determine the effects of barotropic forcing on the stratified Baltic. The resulting circulation with and without barotropic forcing both show expected, realistic patterns. The thermohaline circulation looses its two–layer character with barotropic forcing which is given as a prescribed surface elevation at the boundaries of the model region. Uni–directional flow permits larger transport of volume and salt than bi–directional flow in a channel. Sea level slopes along the straits induce barotropic currents while the density field induces baroclinic currents. According to observations inflow occurs mainly through the Belt (75 %) and the Sound (25 %). This observed transport relation is also obtained in these Baltic experiments.

However, the model region does not include the northern and eastern Baltic. Therefore, in this finite model–basin incorrect seiches periods do occur. As is to be expected currents over variable topography cause barotropic-baroclinic interaction. This interaction is responsible for the spreading of isopycnals.

In the third experiment observed data were used. Temperature and salinity distribution were prescribed as initial conditions, surface elevation (at both ends of the channel) and wind data were specified for the months of January, July, September and November. The model surface elevations are highly correlated with observations. The velocities in the Fehmarnbelt show good agreement with observed velocities only in situations with strong winds. The sea surface slope provides the dominant driving force except during periods when the wind stress and the horizontal density gradient become important. However when the barotropic component is weak, the baroclinic circulation is observed as a bi–directional flow with the fresh layer moving north above the southward flowing deeper layer.

The model results are suited for comparison with laboratory and field studies. Particularly the dense rotating water in the Bornholm basin can be explained by the processes over a sill.

3.1 The Free Surface Princeton Model

The free surface version of the Princeton model is a modification of the Bryan-Cox-Semtner numerical ocean general circulation model which has been adapted to include a free surface (KILLWORTH et al., 1989c). The time necessary to obtain the stream function by relaxation in the Cox model is similar to the time taken by the Killworth model to calculate the barotropic part using a number of short time steps.

A detailed describtion of the free surface model will not be given because there is a lot of literature on this model and the original Princeton code (BRYAN, 1969, 1989; COX, 1984; SEMTNER, 1974 and KILLWORTH et al., 1989c). In the following section a brief description of the equations and some important properties of the model will be given.

The basic equations of the model are the following. The momentum equations read

$$u_t + \Gamma(u) - fv = -ma^{-1}(\frac{p}{\rho_0})_\lambda + F^u \tag{3.1}$$

$$v_t + \Gamma(v) + fv = -a^{-1}(\frac{p}{\rho_0})_\phi + F^v \tag{3.2}$$

where ϕ is latitude, λ is longitude, and a is the radius of the earth. The velocity field is given by (u:east, v:north,w:up). ρ_0 is a reference density, F^u,F^v represent effects of horizontal turbulence as detailed by COX (1984). The continuity equation is given by

$$\Gamma(1) = 0. \tag{3.3}$$

Here the operator Γ is an advective operator, defined by

$$\Gamma(\mu) = ma^{-1}[(u\mu)_\lambda + (v\mu m^{-1})_\phi] + (w\mu)_z \tag{3.4}$$

and μ represents any scalar quantity.

$$m = \sec\phi$$

$$f = 2\Omega\sin\phi$$

23

$$u = \frac{a\dot{\lambda}}{m}$$

$$v = a\dot{\phi} \tag{3.5}$$

The local pressure p is given by the hydrostatic relation

$$p = p_s + \int_z^0 g\rho \, dz \tag{3.6}$$

where p_s is the pressure at $z = 0$. It is defined as

$$p_s = \rho_0 g \eta(\lambda, \phi, t) \tag{3.7}$$

where η is the free-surface elevation. The conservation of a tracer T is

$$T_t + \Gamma(T) = F^T \tag{3.8}$$

where F^T represents diffusive and other effects acting on T. The equation of state is

$$\rho = \rho(\theta, S, z) \tag{3.9}$$

where θ is potential temperature and S is salinity. A polynomial fit is used for (3.9). The lateral boundary conditions are

$$u = v = T_n = 0 \tag{3.10}$$

where n is a coordinate normal to the wall. Kinematic boundary conditions are required at the surface and at the bottom, respectively

$$w = \eta_t + uma^{-1}\eta_\lambda + va^{-1}\eta_\phi, \qquad z = 0 \tag{3.11}$$

$$w = -mua^{-1}H_\lambda - va^{-1}H_\phi, \qquad z = -H. \tag{3.12}$$

The barotropic mode is defined by

$$u = \frac{U}{H} + u' \qquad v = \frac{V}{H} + v' \tag{3.13}$$

where (U,V) is the vertically integrated (barotropic) mass flux

$$U = \int_{-H}^z u \, dz \qquad V = \int_{-H}^z v \, dz \tag{3.14}$$

and (u', v') is the baroclinic flow which has no depth average.

$$\int_{-H}^{z} u' \, dz \;=\; 0 \qquad \int_{-H}^{z} v' \, dz \;=\; 0 \tag{3.15}$$

Integration of the continuity equation (3.7) with respect to z from $-H$ to η together with the kinematic boundary conditions and the approximation $\eta \ll H$ gives

$$\eta_t + a^{-1}[mU_\lambda + m(Vm^{-1})_\phi] \;=\; 0. \tag{3.16}$$

This equation yields a prognostic equation for η. If the momentum equations (3.1) and (3.2) are integrated with respect to z from $-H$ to η and applying the boundary condition on w, one obtains

$$U_t - fV \;=\; -ma^{-1}gH\eta_\lambda + X \tag{3.17}$$

$$V_t + fU \;=\; -a^{-1}gH\eta_\phi + Y \tag{3.18}$$

These equations are familiar from forced linear gravity wave theory, where (X,Y) are the forcing or residual forcing terms (described by KILLWORTH et al., 1989c). They contain baroclinic and barotropic information during the integration in time. Because of this these terms play an important role in baroclinic–barotropic ,barotropic–barotropic and baroclinic–baroclinic interractions. More details on the model can be found in KILLWORTH et al. (1989c and 1991). Two final remarks have to be made about the model: The first is that topographical features are well handled in this code, and so momentum can be completely conserved over topography. The second is that the new code damps the long-period waves only slightly whereas it damps short-periodic oscillations associated with small spatial scales very efficiently . The steady geostrophic flow is left unaffected.

3.2 The Two-Basin Experiment

We consider the basins shown in figure 3.1, where a sill separates initially two fluids of different density ρ_1 and ρ_2. We are interested in the development of currents and stratification with time. Linear theory cannot be used for strait problems because the processes are nonlinear. On the other hand hydraulic theory is not sufficient to explain the time-dependence of the processes. An open question is which role instabilities, convection, double diffusion, wave-wave and wave-shear interaction and boundary layer mixing plays during the overflow. The numerical model does not allow double diffusion explicitely. The physics of the boundary mixing are similar as those in studies done by PHILLIPS et al. (1986), GARRETT (1991) and Mac-CREADY and RHINES (1993).
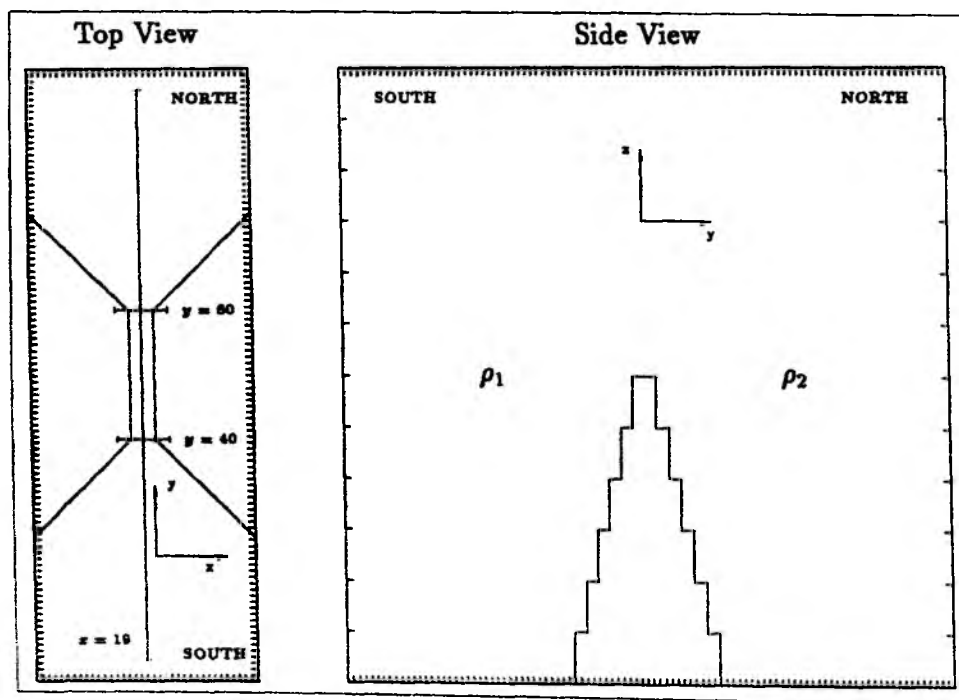
Figure 3.1: *Top and side view of the model basin. There are $36 \times 100 \times 13$ grid points in the x, y and z directions. Horizontal and vertical resolution is 2.5 km and 4 m respectively. The basin is 250 km long, 90 km wide and 52 m deep. The central line shows the position of the vertical section along the channel. $\rho_2 > \rho_1$.*

The heavy fluid above the topography prefers to flow on the right side of the channel in the negative y-direction (due to internal Kelvin wave dynamics at the upstream end). Upstream is defined as the region where lighter fluid exists initially in the south of the basin. The heavy fluid causes buoyancy forces to be stronger at the right hand side due to the downward flow of the denser fluid there. Therefore the net bouyancy force is from right to left across (if we look in south direction) the sill and balanced by viscous forces. A consequence of this mechanism is that the mixed layer will be further mixed and thickens. This buoyancy flow causes that dense fluid flows to the left side and it leads a downwelling at the right side. From the left side less dense fluid flows to the rigth due to the Coriolis force and overlays the above mentioned heavy fluid. This means that near the sill the flow will become bi–directional across the channel in the south (PHILLIPS et al., 1986). The so produced mixed layer has the effect that the upper fluid is little affected by the boundaries and becomes more inviscid. At the same time the effect of rotation decreases due to the bi–directional flow in the mixed layer, and an decrease in wavenumber of motion will be observed. A similar small wavenumber is valid for solitary waves. The heavy fluid near and over the escarpment returns from the left side due to double Kelvin wave–dynamics and flows again down the sill at the right hand side. This process repeats for every escarpment again. Isopycnals that do not cross the escarpment of the channel remain undistorted. The combination of both the boundary layer effect and the buoyancy forces causes isopycnals to spread near the escarpment and to shift away from the topography. At this stage the basin scale becomes important and the Rossby number becomes smaller relative to its magnitude in the channel. This means that rotation will dominate. This rotation and the recirculation in the basin cause eddy formation there. Of course potential vorticity flow is also important for the generation of eddies. This potential vorticity, however, is not the initial one due to recirculation and depth discontinuities. The shifting of isopycnals cannot be described by linear theory, which, in contrary, predicts that fluid does not spread along the escarpment but accumulates upstream (McDONALD, 1993). The steady state flow discussed

above shows different characters for the forced case and the nonforced one. These differencies will be outlined below.

Two cases will be discussed in detail, one of them is the density driven circulation, the other one is the forced case. A summary of the results of other experiments will be given in addition.

Figure 3.2 shows density fields of three different density driven circulations. The propagation of the density front becomes faster if the density difference is increased. In the beginning two Kelvin waves propagate in opposite directions keeping the shallow water on their right. Because of the barotropic force due to the surface elevation difference between the two basins we can see only one Kelvin wave propagating to the north. Poincaré waves are responsible for the communication of the walls with
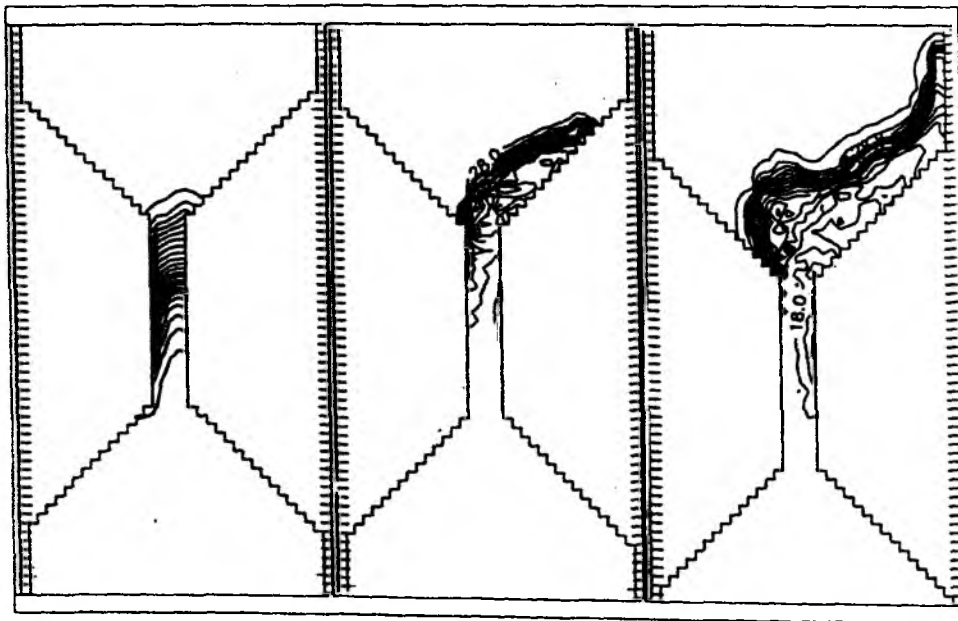
Figure 3.2: *Three different density patterns. The density difference between the two basins is smallest ($\Delta S = 6.$ [psu]) in the left (contour interval, $ci=0.2$, contours from 22.2 to 26.8), largest in the right picture ($\Delta S = 16.$, $ci=0.9$, contours from 15.3 to 30.6). In the middle the values are $\Delta S = 10.$ $ci=0.5$, contours from 20.0 to 28.0. Temperature is constant ($T = 15^0$ C) for all three cases.*

28
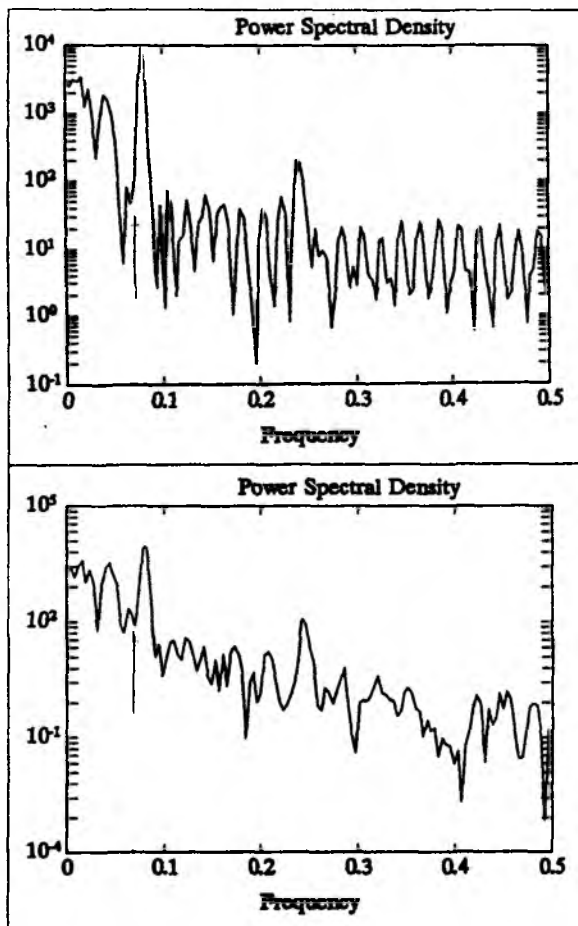
Figure 3.3: *The frequency response of the density driven circulation for the first 12 days at the middle of the sections y = 40 and x = 19. Three clear peaks can be distinguished, one of them at a frequency of 0.08 cph, second 0.25 cph and third 0.037 cph. Inertial frequncy is indicated with an arrow in the figures.*

each other in the channel. Figure 3.3 shows the spectrum of the velocities (v–component) at the middle of the section at $y = 40$ and $x = 19$. The frequency peaks corresponding to internal Poincaré waves (crossoscillations), inertial waves and bottom trapped waves can be seen in both spectra. The same spectral peaks are also seen in the Baltic experiments described in section 5. Two peaks occur near the inertial frequency 0.069 *cph* and another one is at frequency 0.25 *cph*. The peak at the frequency which is slightly lower than inertial one is due to bottom trapped

29

waves; that one which is slightly higher (0.08 *cph*) is due to inertial waves (shifted from inertial frequency). The last one at 0.25 *cph* is due to Poincaré waves. KRAUSS (1979) using a semi–spectral model examined also Poincaré and bottom trapped waves. From the dispersion relation he estimated the period of the Poincaré waves to be less than 5 hours for a channel which is wider than the channel used in this presented experiment. According to the dispersion relation the period of Poincaré waves is expected to be 2.2 *h*. This is in good agreement with the peak at 2.5 *h* in the spectra (Fig.3.3). It results from crossoscillations in the channel.

The internal waves may be generated by topographic scattering of the Kelvin waves over variable topography (Pratt, 1987). MÜLLER and XU (1992) stated that scattering might be equally or more efficient than reflection, causing high shears and mixing near the bottom. KRAUSS and MAGAARD (1961) analysed internal waves in the Baltic. For the Arkona Basin they obtained long periodic waves (due to wind) which have periods of 14.5 *h* and also the waves with periods of $5-6$ *h*. They found the same periods also for Darßer Sill. Additionally, periods of 4 *h* were found in that area. The most energetic waves of the Darßer sill had a period of $T = 13.7$ (with 1.4 standard deviation). They assumed that the waves which have periods of $5-6$ *h* are due to crossoscillations.

Kelvin and Poincaré dynamics set up boundary and interior flows during the linear regime. After this linear adjustment quasi-steady flow dominates in the south of the channel (y=40). Advection and recirculation in the channel cause a rearrangement of the initial potential vorticity distribution during this nonlinear regime (HERMANN et al., 1989). McDONALD (1993) has defined these two phases as fast geostrophic and slow topographic adjustment.

Kelvin-like circulations are seen in both basins (Fig.3.4). Kelvin-like waves at the surface propagate counter-clockwise around the northern basin and set up an anticyclonic gyre before being trapped at the coast. South of the channel counter-clockwise propagation takes place in the bottom layers and at the upstream end near the topography a cyclonic eddy reaches almost from surface to bottom. As expected, surface horizontal velocities have greater values than the velocities in the
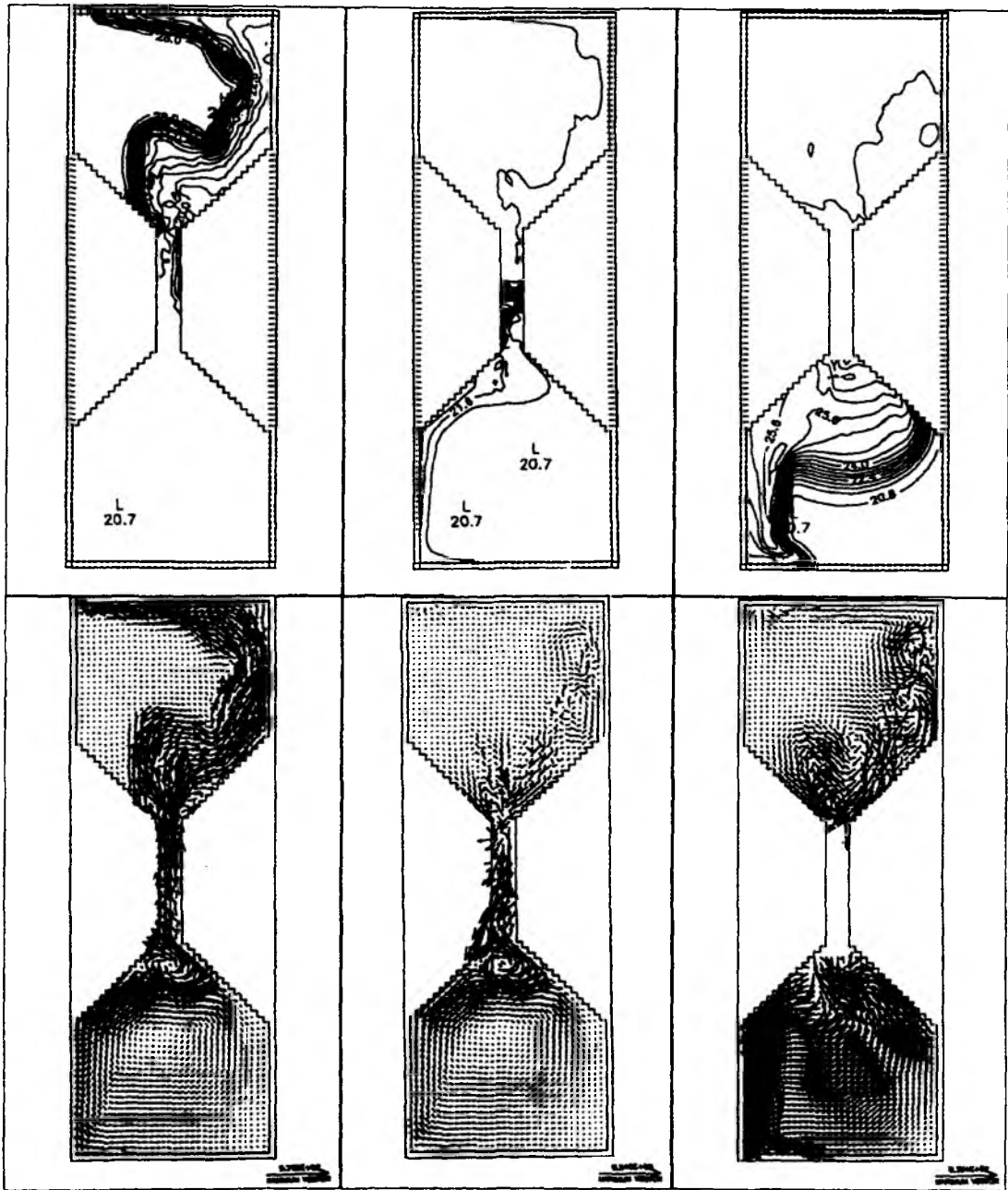
Figure 3.4: *The density fields and their respective velocities for the layers 1,7 and 13 for the density driven circulation from left to right. Maximum vector is 0.9cm (78.3 cm/s for layer 1, 34.8 cm/s for layer 7, 30.4 cm/s for layer 13) for three velocity fields.*

bottom layers, because of the conservation of mass. The Coriolis force deflects the fresh water and hence the current to the right in the downstream direction. In the mid–layer over the topography (layer 7) flow separates from the left wall in the channel (in the south direction). This can be seen in the current and the density fields in the figure 3.4. It can be assumed that double Kelvin waves are forced by
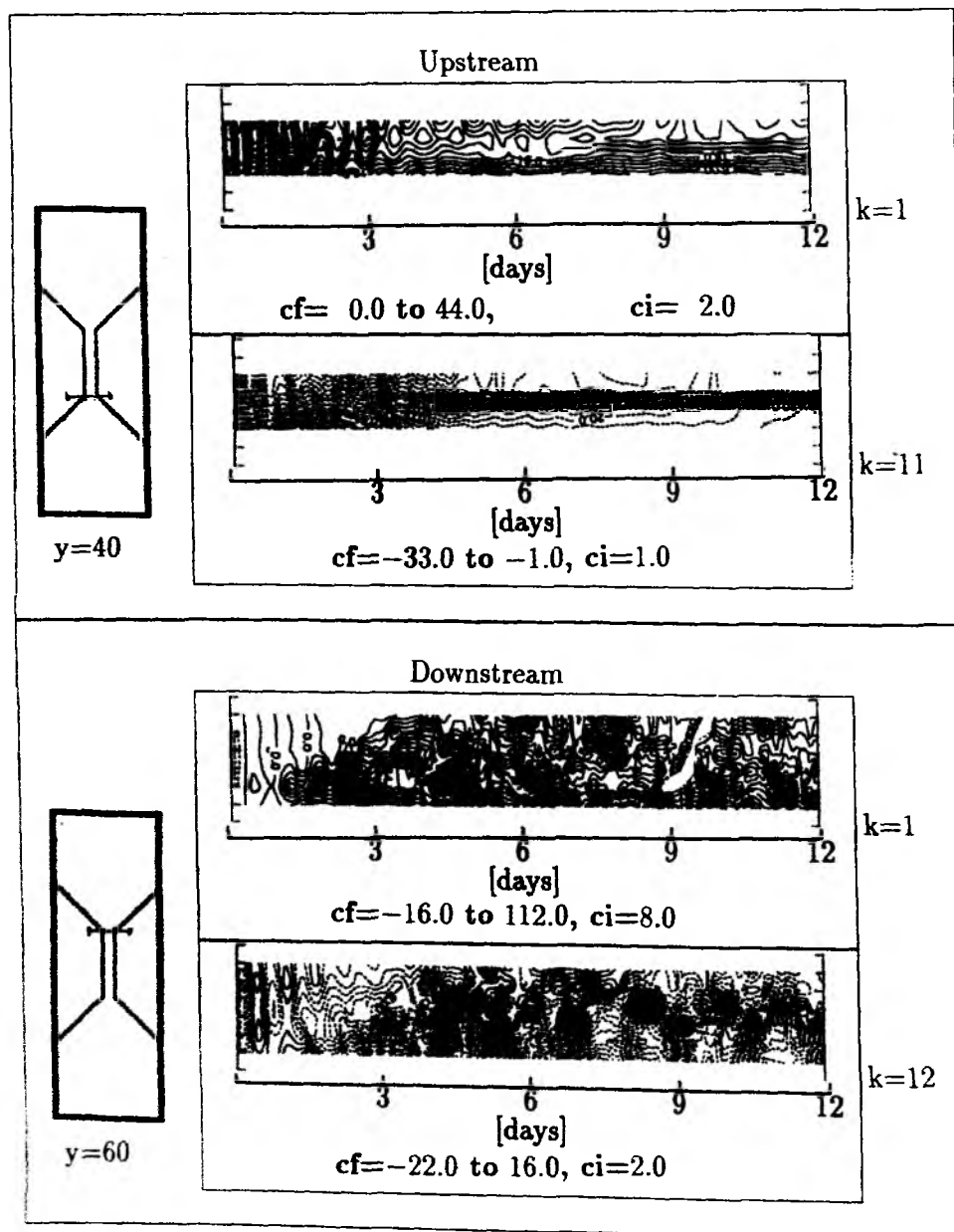
Figure 3.5: *Space-time contour plots of the v–component at an upstream and downstream cross–section in the upper k=1 and lower layers k=11 and k=12 (cf–contour from, ci–contour interval).*

the Poincaré waves over the topography (current or pressure variations can exite Poincaré as well as Kelvin waves, LM, 1978). In the bottom layer the dense water flows into the connected basin. Away from the topography the flow is deflected to the right due to rotational effects and becomes trapped to the coast.

Space–time contour plots (Fig.3.5) show the different phases in the channel. Surface velocities (v–component) in the north show that after one inertial period the fluid is in motion. The flow is asymmetric at the beginning with light fluid on the right. After the quasi-steady state is reached the upstream flow becomes more or less symmetric (due to advection of the potential vorticity front, Fig.3.5). Finally, Bernoulli flow can take place on the upstream side of the sill (explained in STIGEBRANDT, 1980, as nonlinear regime), at $y = 40$. The oscillations which are part of the adjustment process are seen at the downstream side, at $y = 60$.

The coastally trapped waves propagate with the same phase speed of $\sim 30 cm\ s^{-1}$ in the upper and in the lower layer of the basin in the north (Fig.3.6). There and in the channel maximum upper layer velocities are 109 $cm\ s^{-1}$ (Fig.3.6) and 112 $cm\ s^{-1}$ (Fig.3.5) respectively. They are consistent with the sum of the barotropic and baroclinic first mode velocities for the upper layer. On the other hand they correspond to the speed of long waves in the channel, $c = (g'h_{eq})^{1/2}$ (here h_{eq} is the equivalent depth for the first baroclinic mode), $\sim 109\ cms^{-1}$. In the lower layer however the maximum velocities decrease to values of 22 $cm\ s^{-1}$ in the channel and of $19 cm\ s^{-1}$ near the boundary because the barotropic and baroclinic modes cancel each other partially.

The propagation of solitary Kelvin waves to the north has been analysed for the lower layer near the boundary. These solitary waves can be considered as resulting from interactions between double Kelvin waves and Poincaré waves. The topographic waves have a wavelength of approximately $35 - 40\ km$ in the north and $50 - 60\ km$ in the south of the channel. The frequency is $\omega \sim f/2$ in the north. HSIEH and GILL (1984) interpret this frequency with the transfer of energy at near-inertial frequency from internal Poincaré waves to subharmonic shelf-waves with $\omega \sim f/2$.

cf=0.0 to 108.0, ci=6.0
upper layer (k=1)

cf=−19.0 to 5.0, ci=1.0
lower layer (k=13)

x=35
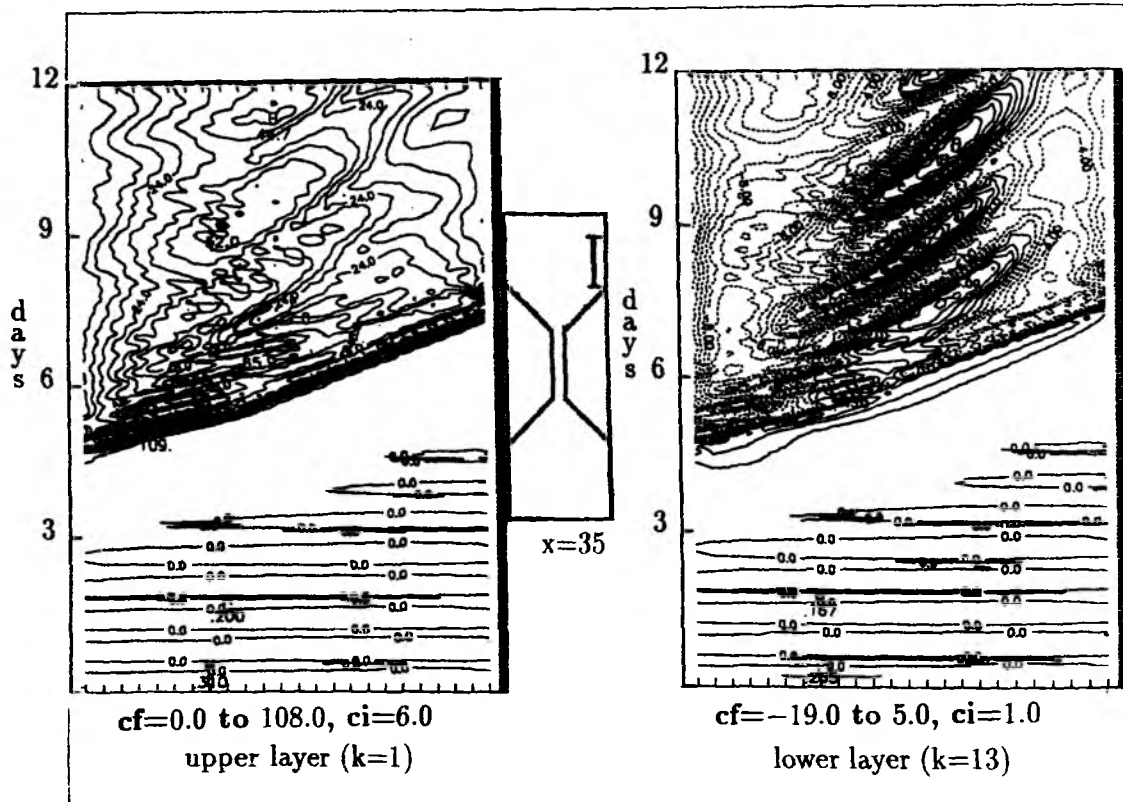
Figure 3.6: *Space-time contour plots of the upper and lower layer velocities (v-component) near the right boundary in the north.*

The frequency of these oscillations is lower in the south than in the north of the channel. The phase plot shows the topographic effects on 'he v-component of the velocity in the lower layer (Fig.3.7). It demonstrates th .t the length scale of the current is increased there (decrease in wavenumber of the motion). Nonlinearities start to play an important role when dense water flows over the topography into the other basin.

The energy cycle from the study of BÖNING (1989) is used to interpret the energy transfer and the interactions between the internal mode and the external mode. Figure 3.8 shows values of the energy transfer terms and of the kinetic energy of internal (K_i) and external modes (K_e). Internal kinetic energy amounts to 57.5 % of the total kinetic energy, the remaining 42.5 % is external kinetic energy. In figure 3.8 NL is the sum of the nonlinear transfer terms, LF lateral friction, BF bottom

34
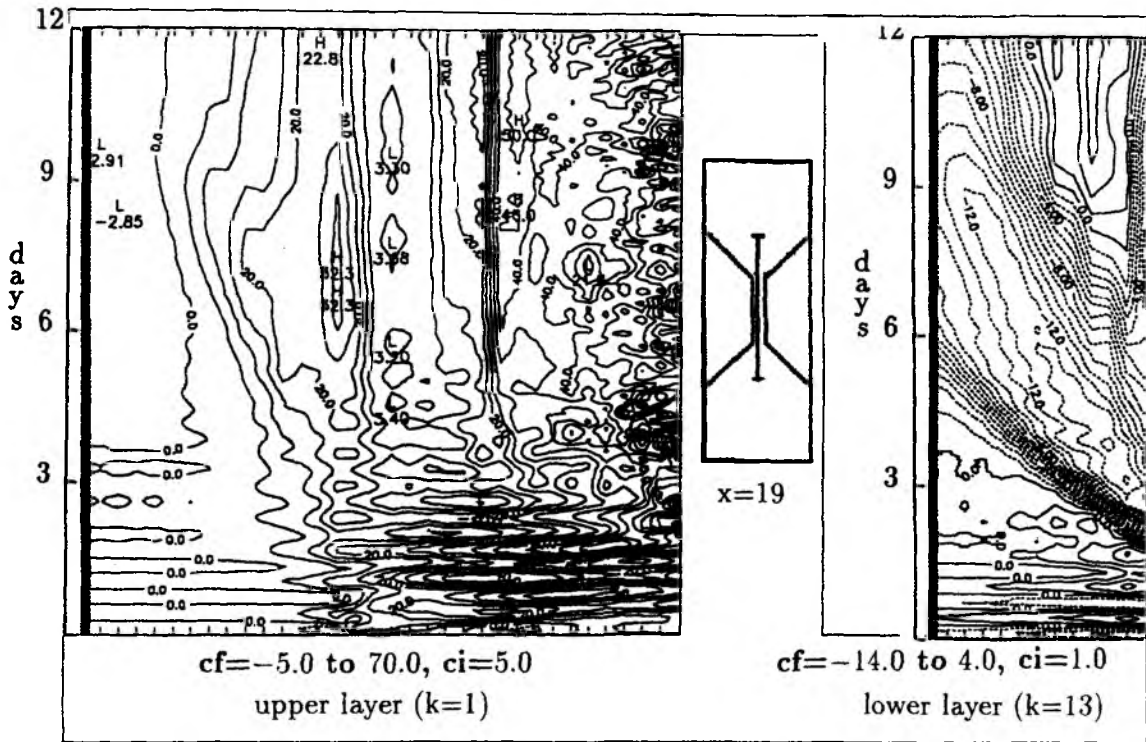
Figure 3.7: *Space-time contour plots of the upper and lower layer velocities (v–component) along the channel. In the right–hand figure the velocities (v–component) are shown only for the southern part of the section at x = 19 .*

friction, PF pressure forces and R residual terms. More information about these terms are found in the study of Böning, 1989. The nonlinear terms provide an exchange between the internal and external components of the flow. If the Reynolds stresses (NL) which feed the external mode, increases then a barotropic instability is favourable. The pressure terms (PFs) provide the link between potential and kinetic energy. Both these terms show strong baroclinic contributions. This means that the coupling of surface and deep layers is strong. The term R is very important in the analysis of the channel dynamics. This term represents the change of potential energy by diffusion and convection. In Fig 3.9b convection processes are seen in the left (southern) basin, where the isopycnal dome is located. The separation of isopycnals is due to convection. In the free surface Bryan–Cox–Semtner model the
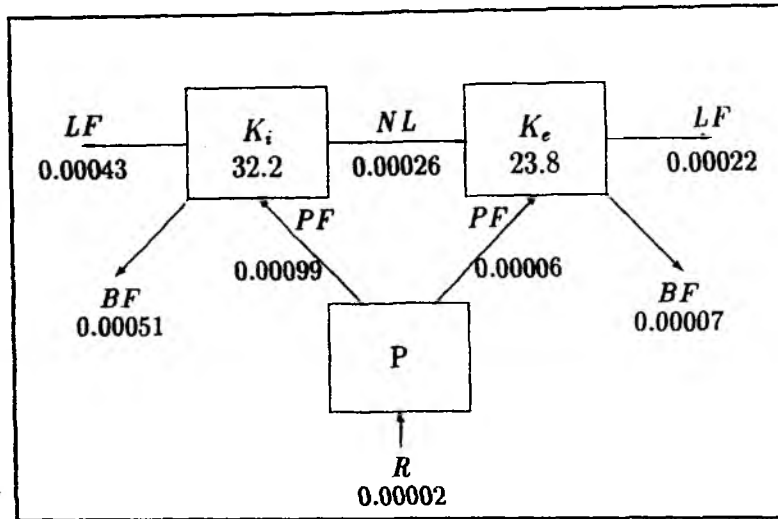
Figure 3.8: *Energy cycle for the density driven case. The directions of the energy transfers are indicated by the arrows. (Units in $ergcm^{-3}s^{-1}$).*

depth integrated flow is not precisely the barotropic mode. Because of this the energy cycle can not give accurate results. A leakage of energy and information between barotropic and baroclinic modes is possible.

The vertical sections of density and vertical velocity along the channel at $x = 19$ show regions of upwelling and downwelling (Fig.3.9). The downwelling is stronger behind the head of the flow at the downstream side and upwelling dominates at the upstream side of the channel. The downwelling tendency related to the Coriolis acceleration dominates over the upwelling tendency due to upward entrainment at the downstream side. Vice verca, detrainment causes that downwelling dominates over the upwelling due to Coriolis acceleration at the upstream end of the channel (CHAO, 1988). In figure 3.9 the vertical velocities show also the existence of waveguide modes. It is not only the waveguide mode but a superposition of both discrete waveguide modes and sinusoidal modes.

Upwelling and downwelling situation can be seen in cross-channel sections of density at the downstream and upstream side of the channel. The density field has an "S" shape (typical shape, CHAO and BOICOURT, 1986), and the isopycnals are inclined

cf=19.8 to 30.6, ci=0.6
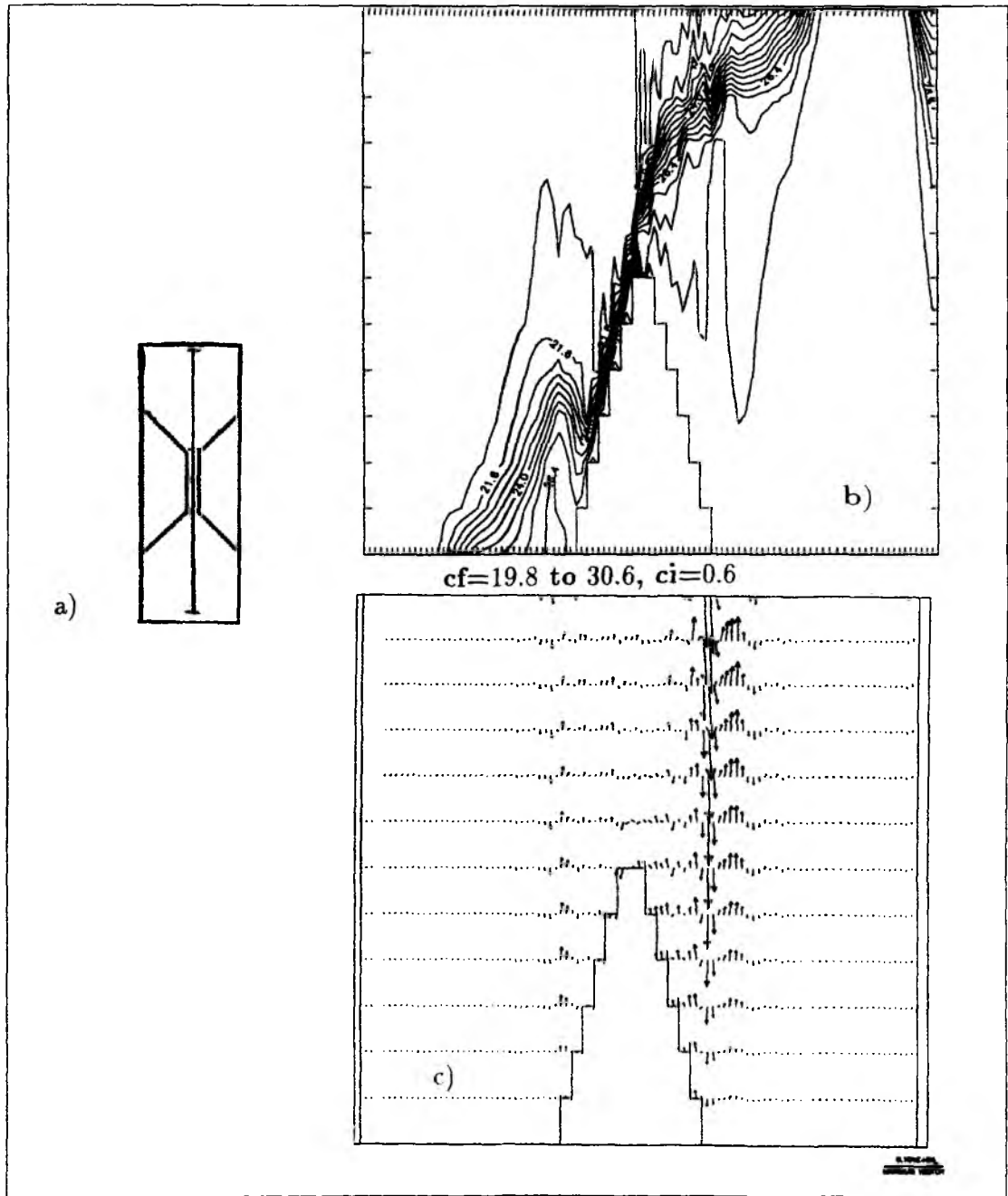
Figure 3.9: *a) Location of the vertical section at $x = 19$ along the channel b) Density field along $x = 19$ c) Vector plot of velocities, vertical component of velocity is multiplied by 5000. Maximum velocity vector is 0.9 cm and 0.2 cm/s.*

37
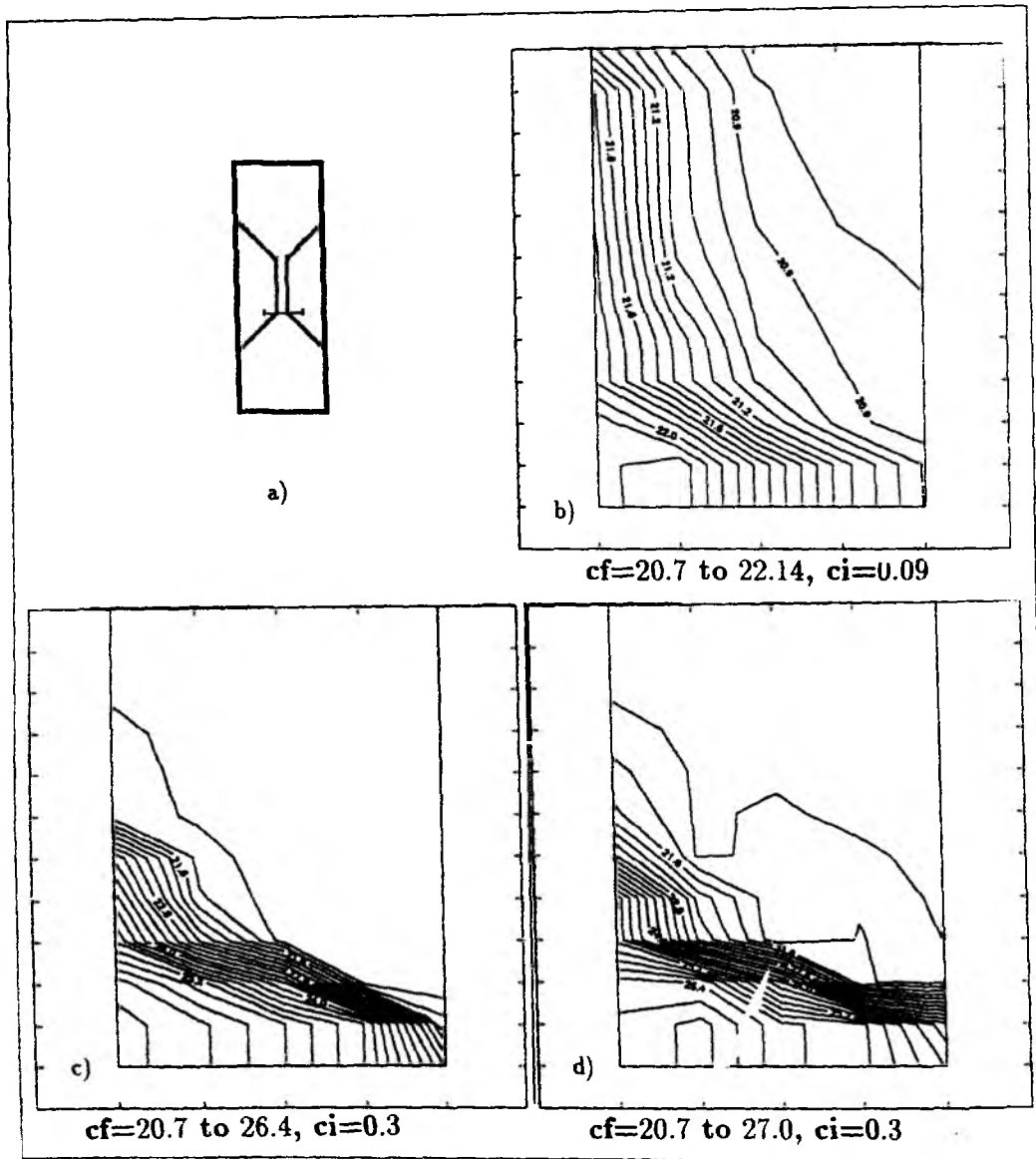
Figure 3.10: *a) Position of the vertical section across the channel (at y = 40, upstream) b) Density field after 1 day c) after 4 days d) after 12 days. (cf, contour from and ci, contour interval)*

between surface and bottom after 1 day (Fig.3.10-11). Less dense fluid is on the right side of the surface layer and denser fluid is on the left side of the bottom layer (looking in north direction) at both $y = 40$ and $y = 60$. Bottom intensification of dense flow at the upstream side (due to downwelling) and surface intensification at the downstream side of the channel (due to upwelling) can be distinguished at days 4 and 12 (Fig.3.10). Surface intensified less dense flow takes place on the downstream

38
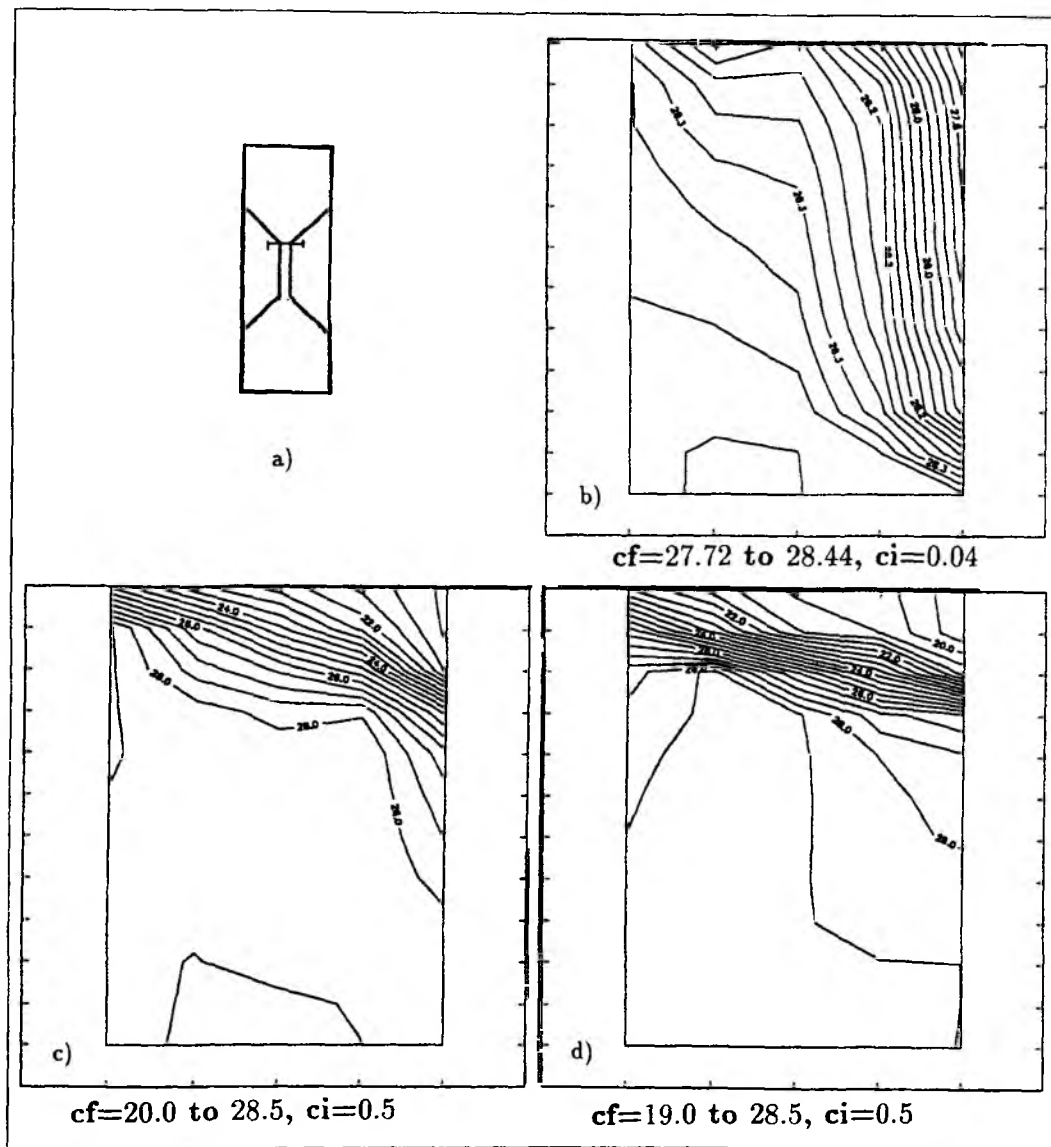
Figure 3.11: *a) Position of the vertical section across the channel (at $y = 40$, down-stream) b) Density field after 1 day c) after 4 days d) after 12 days. (cf, contour from and ci, contour interval)*

side. Because of the topographic effects in the lower layer at the upstream side, the Coriolis acceleration dominates only at the downstream side of the channel. The model's vertical resolution limits the boundary mixed layer to approximately 4 m. The horizontal velocities in the x-direction produce a secondary circulation. Clearly, the boundary layer has already formed before a secondary circulation develops.

39
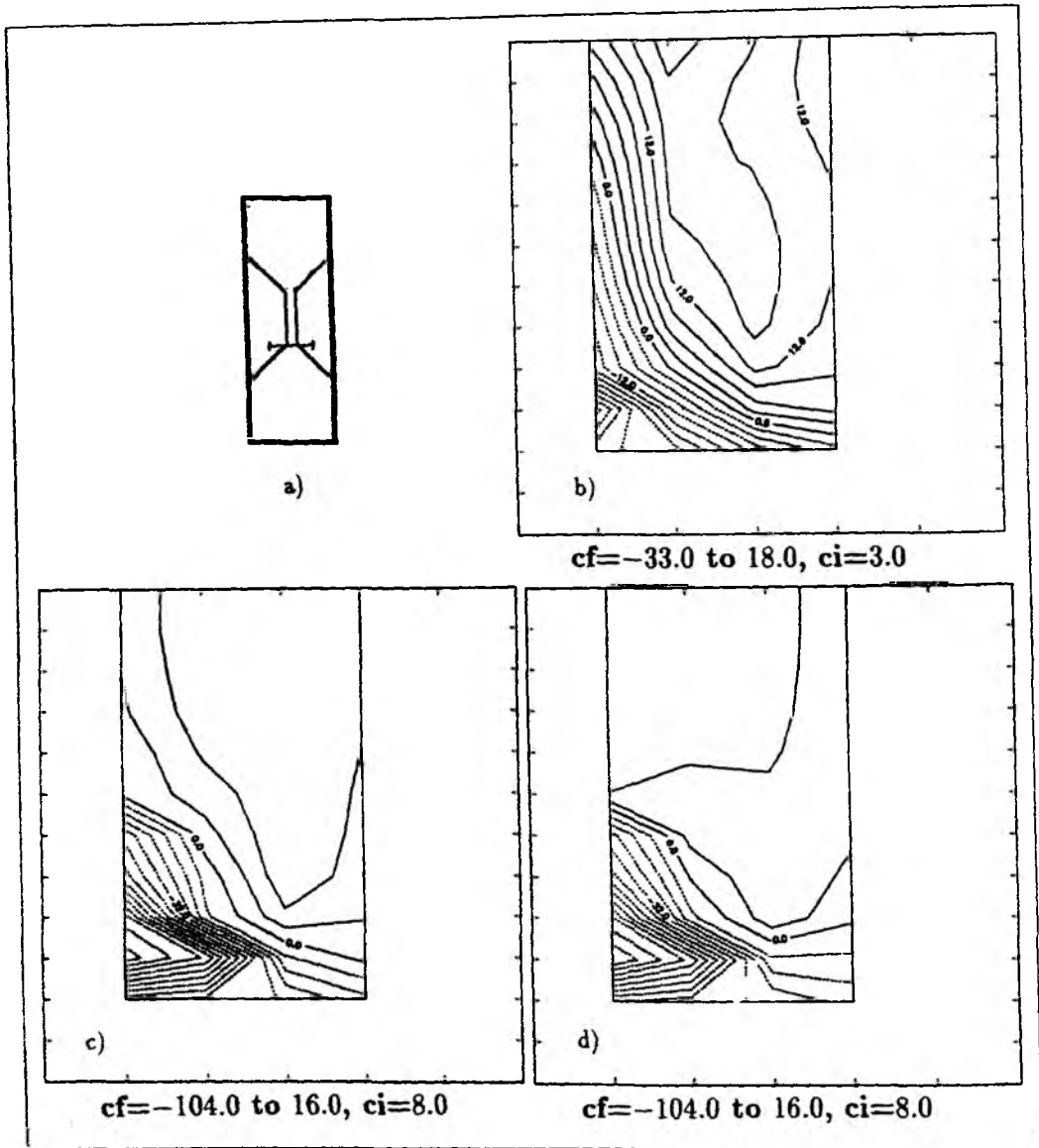
Figure 3.12: *a) Position of the vertical section (at y = 40, upstream). V-component of the horizontal velocities b) after 1 day c) after 4 days d) after 12 days.*

As a result of this mechanism the bottom intensification process at the upstream side dominates over the surface intensification after several inertial periods (depending on when the fluid comes into contact with the sloping boundary) and the velocities will increase in the lower layer above the topography at the upstream side of the channel (Fig.3.12). Because of increasing vertical shear (thermal wind relation) baroclinic instabilities occur, which lead to the development of a cyclonic eddy in

40
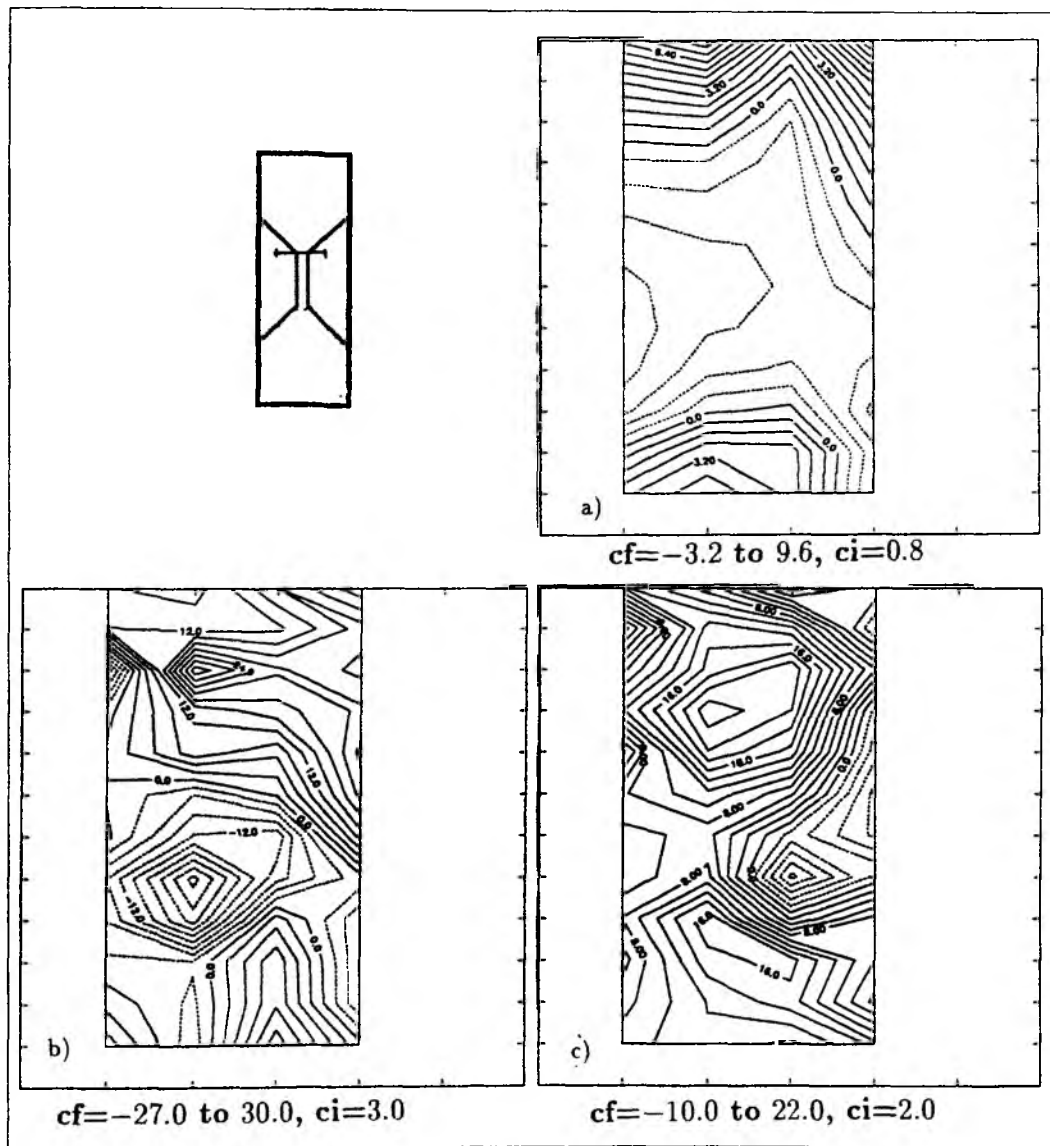
Figure 3.13: *a) Position of the vertical section (at y = 60, downstream). V–component of the horizontal velocities b) after 1 day c) after 4 days d) after 12 days.*

the bottom layer. The upwelling- or downwelling-favourable tendency and the regions in which that eddy forms depend on the distribution of sinks and sources. The v–component of the horizontal velocities has a two-layer character in the channel (Fig.3.12-13).
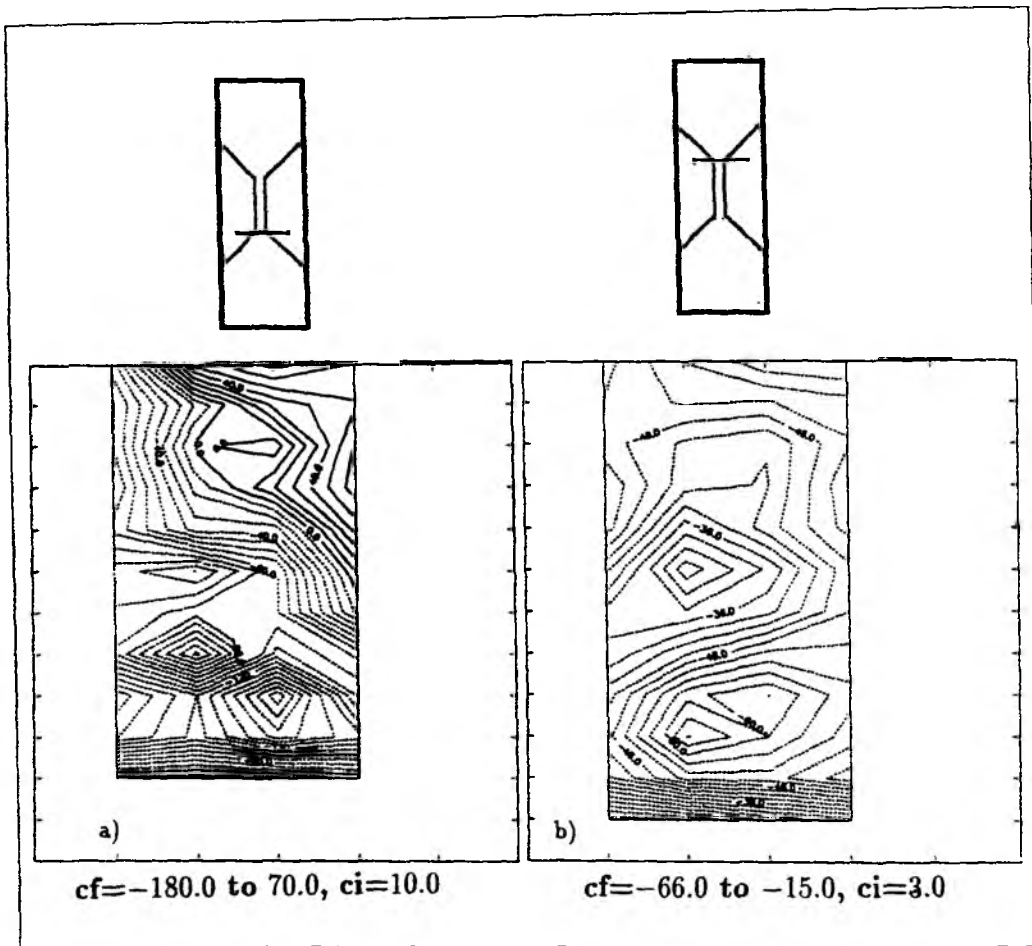
Figure 3.14: *v–component of the horizontal velocity field for the forced case. Small figures show the chosen vertical sections in a) the south b) the north of the channel.*

Dense water flowing over the topography accumulates at the upstream side (Fig.3.9). This scenario changes when a barotropic force is applied as source or sink, respectively, at the two ends of the channel. The surface displacements which are prescribed, change linearly with increasing distance from the ends of the basin and take self adjusted values in the interior of the channel. They are given as

$$\eta = \begin{cases} -\eta_0 & y < 10 \\ \eta_0 & y > 90 \end{cases}$$

The differences to the density driven case are

- Instead of a bidirectional, now a unidirectional flow is established along the channel. The back flow that corresponds to the density driven current can be seen at the upstream side of the channel (Fig.3.14).

42
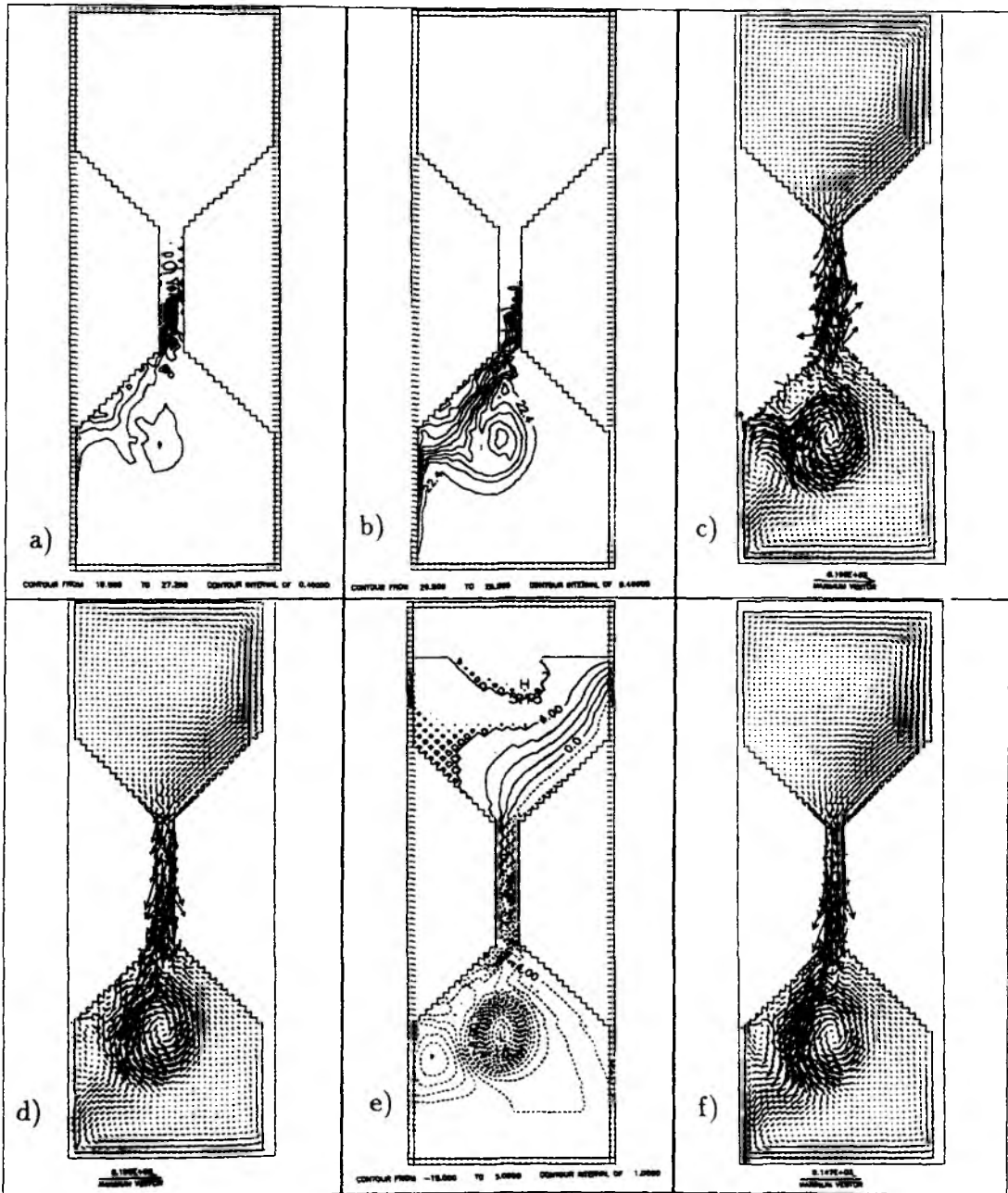
Figure 3.15: *The density fields of the forced case for the layers k=1 and k=5 a) and b). Their velocities c) and d). e) Surface elevation pattern f) Barotropic velocity field. Maximum vector is 0.9cm (166.0 cm/s for layer 1; 130.0 cm/s for layer 5; 147.0 cm/s for barotropic velocity) .*

• Kinetic and potential energies have increased relative to the previous experiment. Most of the initial kinetic energy is used for the rapid eddy formation in approximately one inertial period. Figure 3.15 shows the cyclonic eddy at the upstream side. Especially in the lower layer the velocities have increased, because the barotropic mode and the first baroclinic mode of the density driven current are overwhelmed by the barotropic forcing in the upper layer.
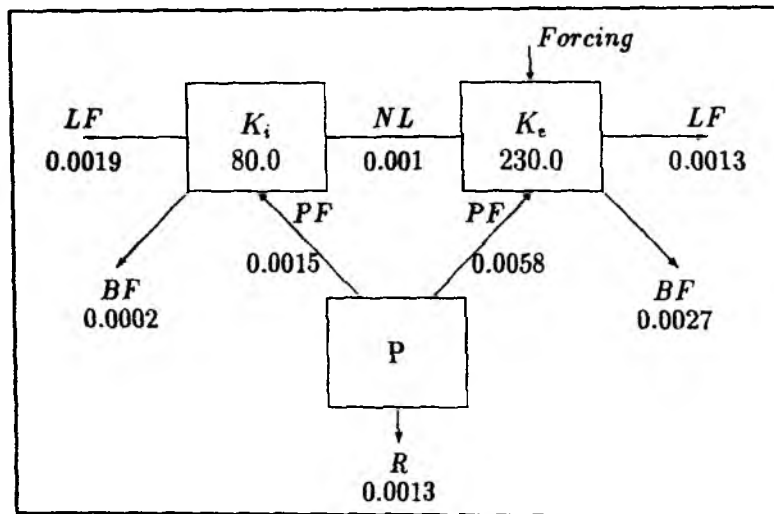
Figure 3.16: *Energy cycle for the forced case. The directions of the energy transfers are indicated by the arrows. (Units in* $ergcm^{-3}s^{-1}$*)*.

• The energy cycle (Fig.3.16) shows that the external kinetic energy is dominant and amounts to 74.2 % of the total kinetic energy. The terms in figure 3.16 have similar meaning as the terms described in the density–driven case (figure 3.8). The bottom convection is stronger in comparison to the density–driven case (term R in figure 3.16). When the pressure force which transfers energy in the direction from potential energy to external kinetic energy, increases, then decoupling of surface and deep layers increases and this can cause baroclinic instability. This term represents at the same time work done by the eddy buoyancy. The direction of energy transfer between internal kinetic energy and external kinetic energy is opposite compared to the density–driven case.

44
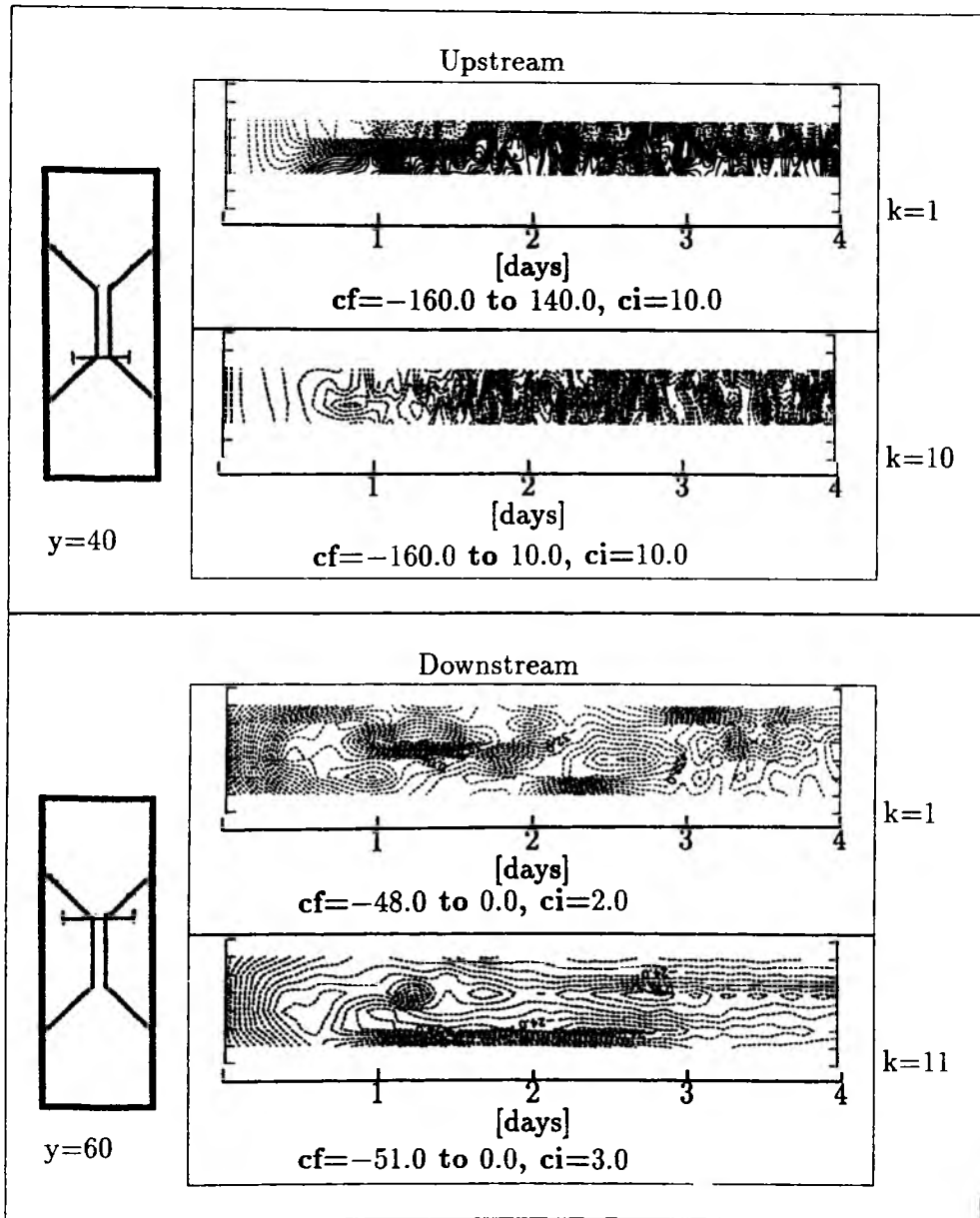
Figure 3.17: *Space-time contour plots of the velocities (v-component) in the upper and lower layers. Locations of the vertical sections in the south and in the north, respectively.*

- In this experiment a steady geostrophic flow can be found in the northern basin. It has constant barotropic velocity in the negative y-direction (max.~ $38cm \ s^{-1}$) (Fig.3.18). Space–time contour plots of the v-component are shown in figure 3.17 for the upstream and the downstream location. Con-

tours which represent oscillations are in both openings of the channel more ellipsoidal as compared to the density–driven case. Space-time contour plots of surface elevations (Fig.3.20) for the forced case show that forced waves propagate with 40 cm s^{-1} phase speed in south of the channel (consistent with the velocities shown in Fig.3.19). On the other hand, in the density driven case barotropic waves propagate in the same region with only 20 cm s^{-1} phase speed. In the forced case, in both layers velocities reach approximately 40 cm s^{-1} (Fig.3.19). Figure 3.20 shows that it takes 7–8 inertial periods until the oscillations loose their strength and the system goes into a quasi–steady state for the density–driven case. A steady state can be determined at the north of the channel for the forced case.
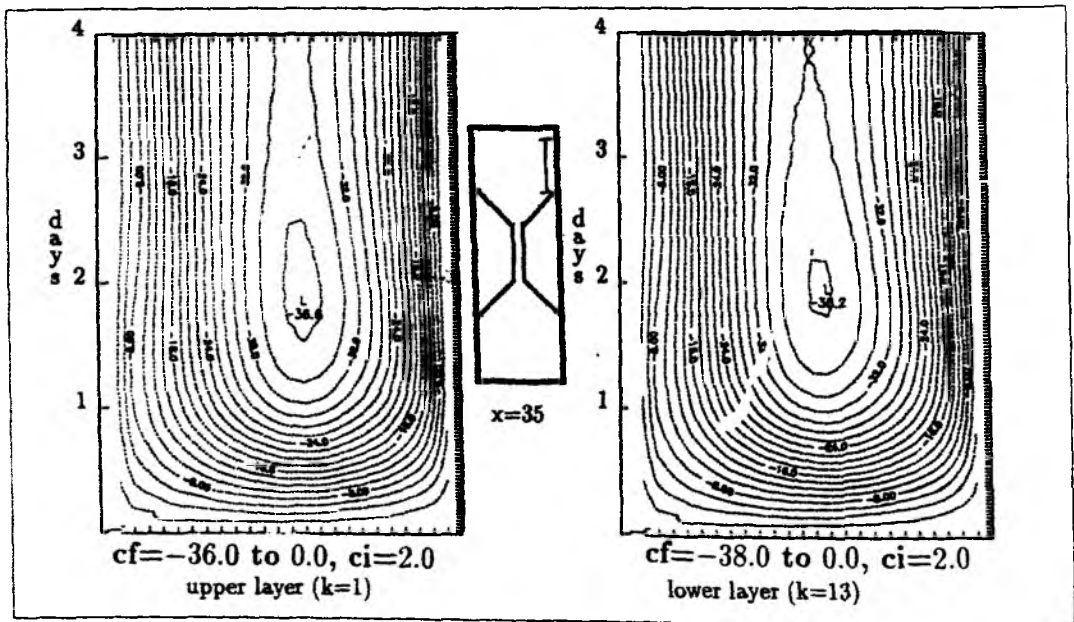
Figure 3.18: *Space-time contour plots of the upper and lower layer velocities (v–component) near the right boundary in the north.*

- Volume and salt transport increase with barotropic forcing (Fig.3.21). The net volume transport is almost zero at the upstream as well as at the downstream side of the channel for the density driven case. The values of volume and salt transport are given in Table 3.1 for both experiments at the upstream and at

the downstream end of the channel. Table 3.6 shows the effects of barotropic forcing on the transports.

• Downwelling is found also in this case at the righthand side in the upstream region (looking to the negative y-direction, at $y = 40$). The difference to the first experiment is that no homogenization of water occurs in the upper layer or a stratification in the lower layer during the downwelling (Fig.3.22). The boundary layer is thicker in the second experiment in comparison with the first one. Armi (1978) suggested that the boundary layer thickness is controlled by the instability of the mean flow which causes the formation of roll waves. He stated that if the internal Froude number is larger than the critical value for the formation of roll waves, then the intermittent surges and bores can be formed. The bore formation will be explained in details in the Baltic experiments.

cf=-160.0 to 130.0, ci=10.0 cf=-110.0 to 50.0, ci=10.0
upper layer (k=1)   lower layer (k=13)
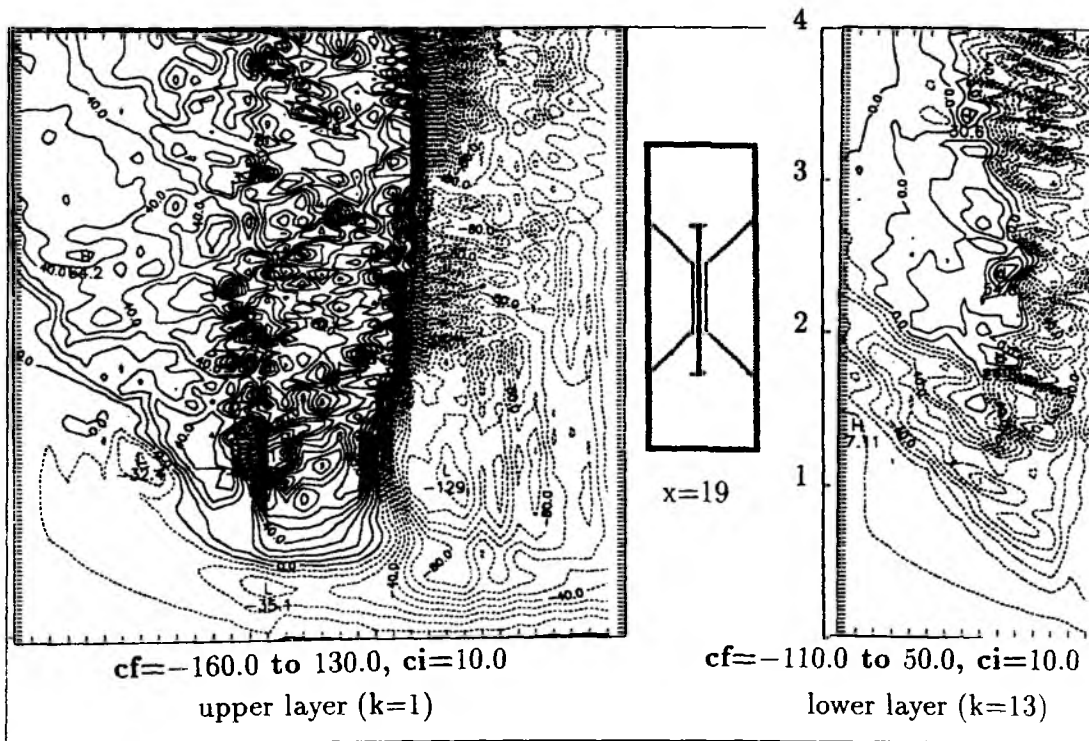
Figure 3.19: *Space-time contour plots of the upper and lower layer velocities (v-component) along the channel. In the right-hand figure the velocities (v-component) are shown only for the southern part of the section at $x = 19$.*

47

$x = 19$

cf=−12.0 to 12.0, ci=1.0

cf=−17.0 to 7.0, ci=1.0
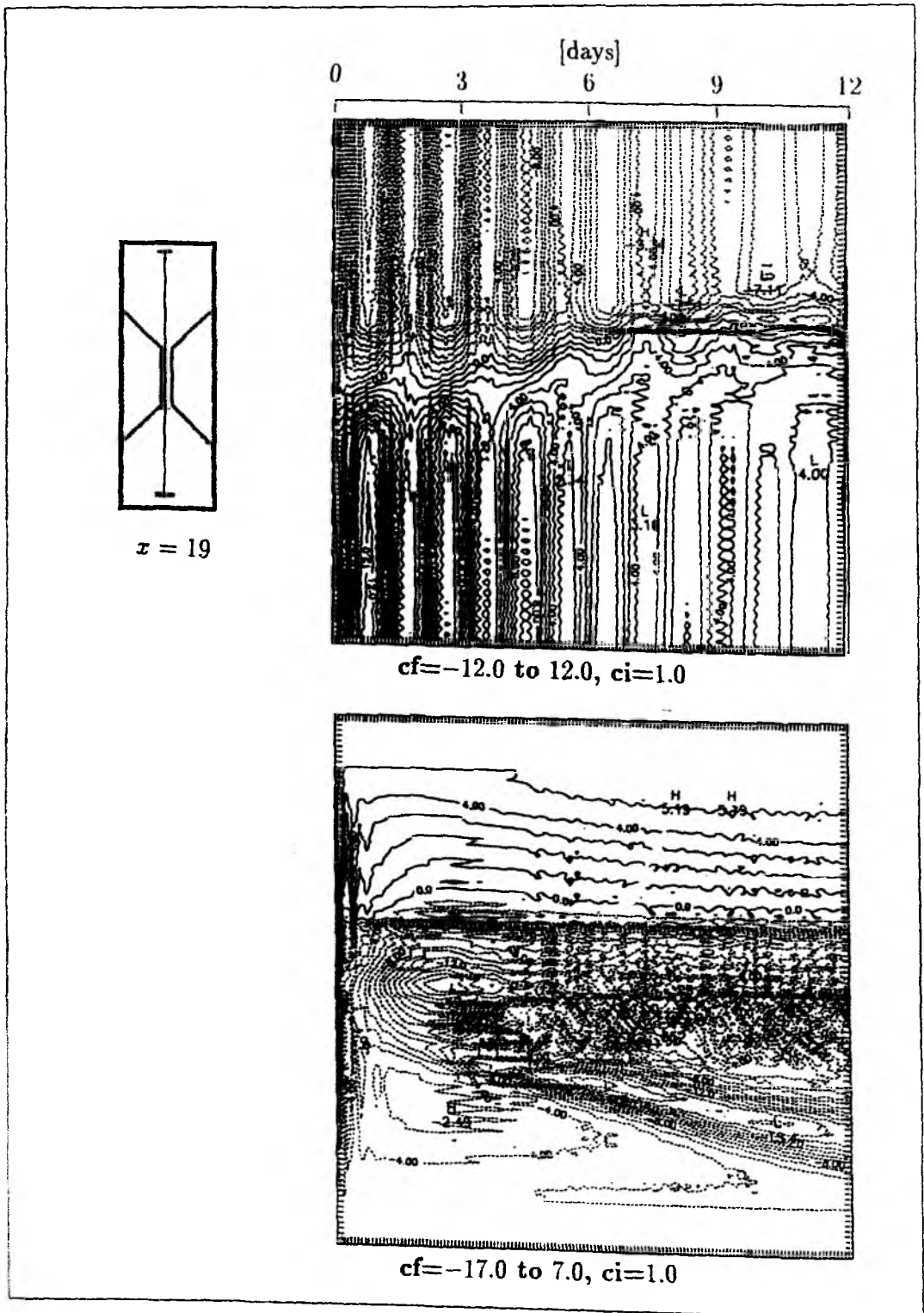
Figure 3.20: *Space-time contour plots of surface displacements at $x = 19$ a) density-driven case b) forced case.*

48

- An important difference is that the cyclonic eddy which is formed near the topography in the lower layer south of the channel is advected away from the topography in the forced case. GILL (1977) defined this accumulation of water near topography as a *dome–shape* and states that if the fluid is inviscid, outflow will not occur until the *dome* has become so large that its effective Rossby radius is comparable with the basin width and the skirts of the *dome* reach the channel exit. In this case, it may be possible to find a solution where friction is important in the basin, but not in the immediate neighbourhood of the sill, where hydraulic control takes place.
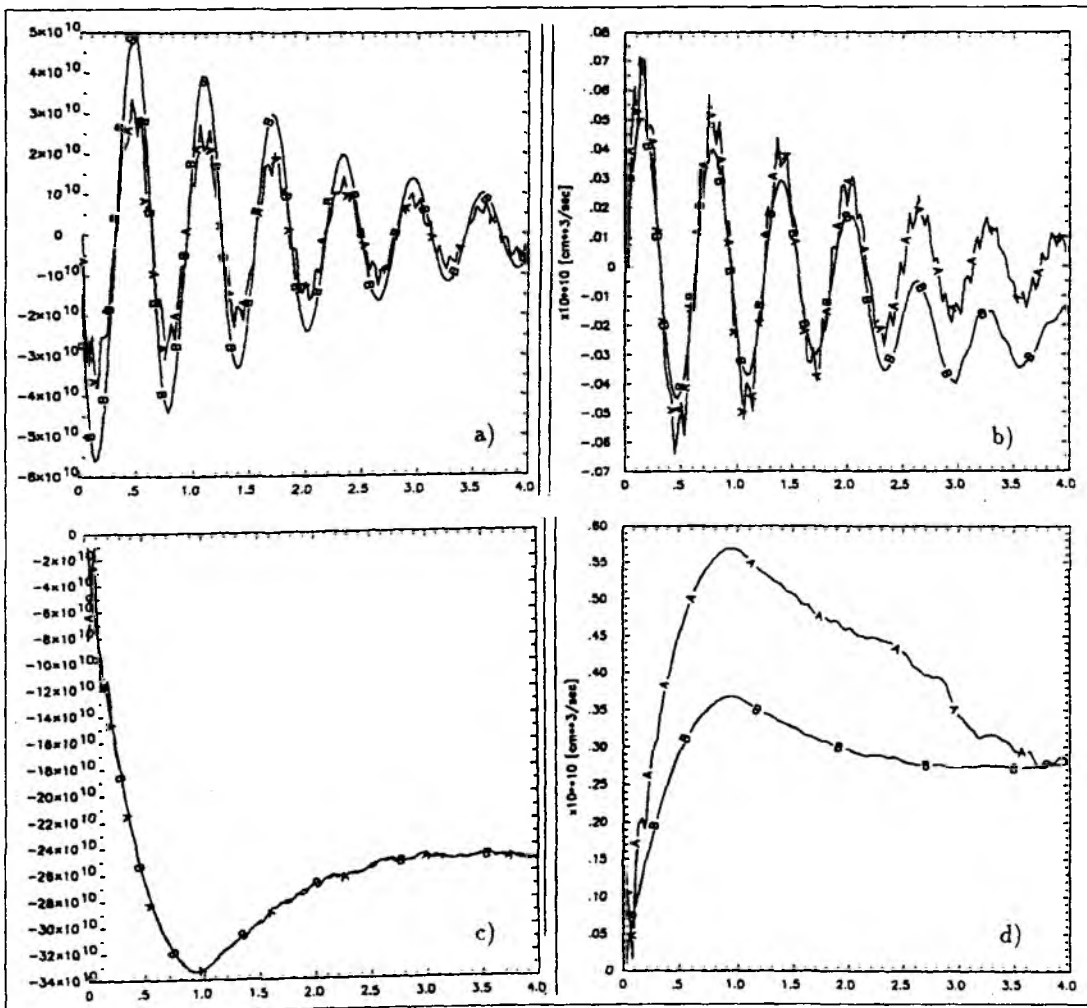
Figure 3.21: *a) Volume and b) Salt transport for the density–driven case. c) Volume and d) Salt transport for the forced case. A - Location in the south and B - in the north.*

The other results of the experiments are the following:

- The volume and salt transport decrease with increasing topographic obstacle height with or without barotropic forcing. (Table 3.1-4)

cf=20.5 to 0.0, ci=2.0   cf=26.510 to 26.895, ci=0.005
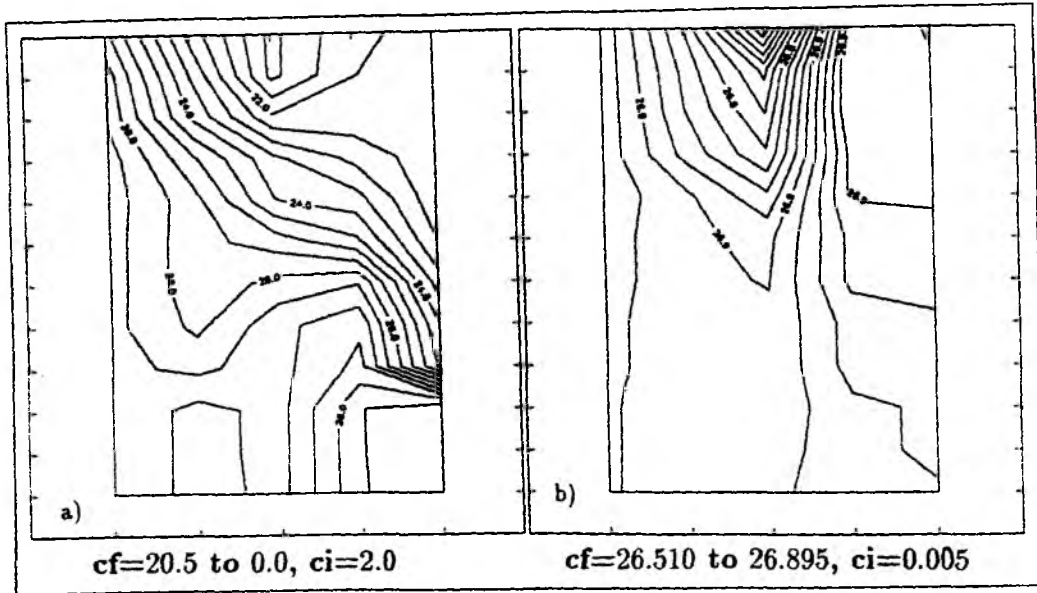
Figure 3.22: *Vertical sections of the density fields a) in the south (y = 40) and b) in the north (y = 60) of the channel. Location of the sections as in figure 3.17.*

Table 3.1: Volume and salt transport ($\times 10^{10}$ cm^3 s^{-1}) for the density driven and forced experiments, (* shows rms values)

	density–driven		forced	
	volume	salt	volume	salt
south of the channel	1.33*	0.0251*	28.	.40
north of the channel	1.91*	0.0097*	28.	.31

Table 3.2: Effect of topography on the volume and salt transport in the channel without barotropic forcing. Transport values ($\times 10^{10}$ cm^3 s^{-1}) (* shows rms values)

	with topography		without	
	volume	salt	volume	salt
south of the channel	0.93*	0.0162*	1.54*	0.0286*
north of the channel	1.40*	0.0158*	2.29*	0.0168*

50

cf=20.8 to 28.8, ci=0.4
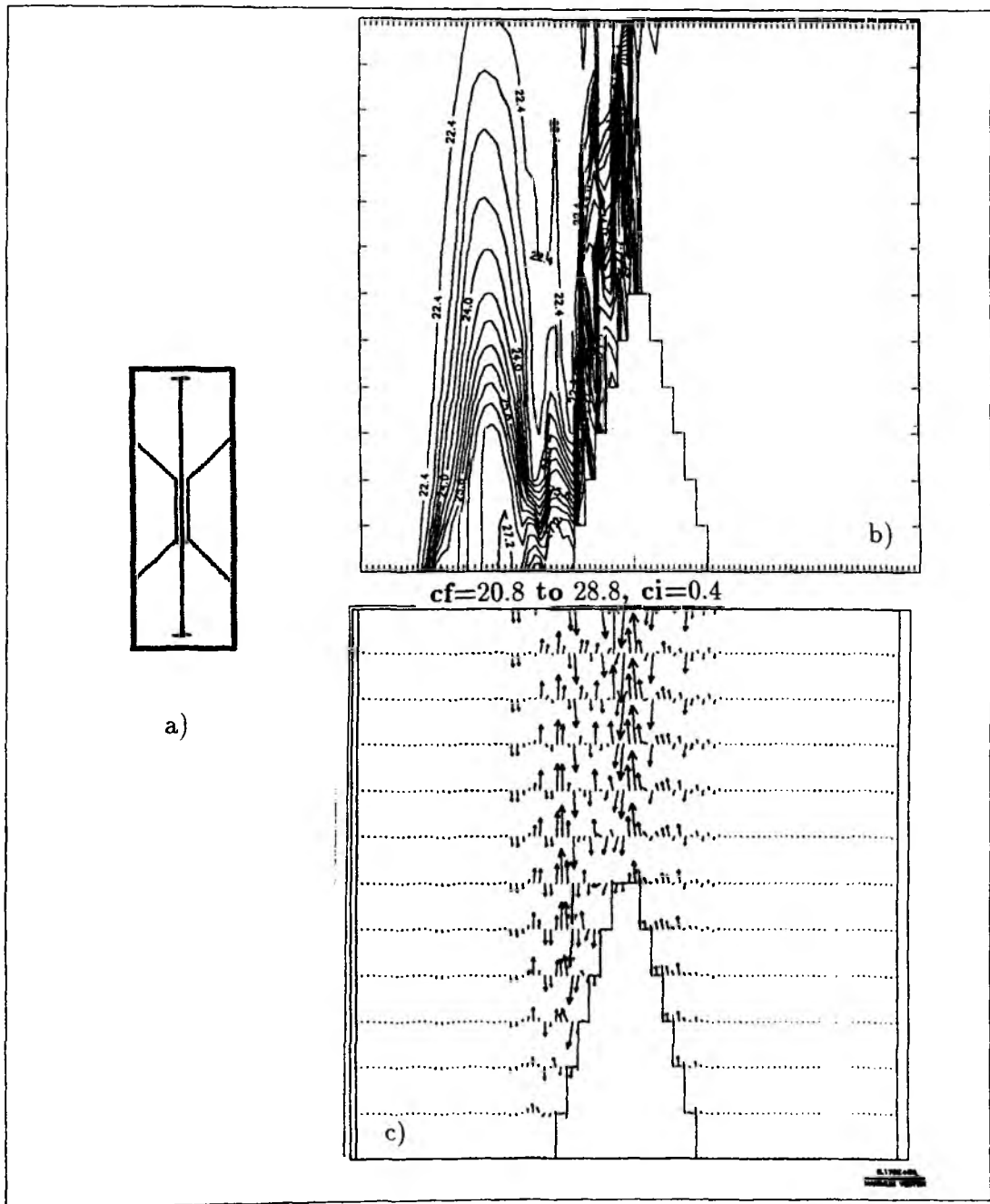
Figure 3.23: *a) Location of the vertical section at x = 19 along the channel b) Density field along x = 19 c) Vector plot of velocities, vertical component of velocity is multiplied by 5000. Maximum velocity vector is 0.9 cm and 0.36 cm/s.*

51

Table 3.3: Effect of topography on the volume and salt transport in the channel with barotropic forcing and two different topographic obstacles T_2 and T_1. The sill height from the bottom is higher for T_2 than for T_1. Transport values ($\times\ 10^{10}\ cm^3\ s^{-1}$)

	topography T_2		topography T_1	
	volume	salt	volume	salt
south of the channel	6.63	0.090	25.24	0.28
north of the channel	6.63	0.090	25.24	0.28

- The rotational effect on volume and salt transport is shown in Table 3.5. Increasing the rotation results in smaller volume and salt transport.

Table 3.4: Effect of rotation (Coriolis acceleration) on the volume and salt transport in the channel. Transport values ($\times\ 10^{10}\ cm^3\ s^{-1}$)

	with Coriolis force		without	
	volume	salt	volume	salt
south of the channel	4.01	0.070	9.00	0.129
north of the channel	4.01	0.060	9.00	0.0130

- As expected lateral friction reduces both transport values (Table 3.6). It would be more relevant to test if vertical friction changes the transport relations. This was done by CHAO (1991). He used Richardson number–dependent mixing coefficients in his model. The results was that grid noise dissapeared and topographic control of the density current weakened. Additionally, the transport decreased.

Table 3.5: Effect of lateral friction on the volume and salt transport in the channel with two different lateral friction coefficients for momentum, $A_1 = 4.0\ 10^5\ cm^2\ s^{-1}$, $A_2 = 4.0\ 10^5\ cm^2\ s^{-1}$. Transport values ($\times\ 10^{10}\ cm^3\ s^{-1}$)

	friction A_1		friction A_2	
	volume	salt	volume	salt
south of the channel	4.01	0.070	4.00	0.067
north of the channel	4.01	0.060	4.00	0.056

Table 3.6: Effect of barotropic forcing on the volume and salt transport in the channel with and without forcing. Transport values ($\times 10^{10}$ cm^3 s^{-1}) (* shows rms values)

	with forcing		without	
	volume	salt	volume	salt
south of the channel	4.01	0.07	0.93*	0.0162*
north of the channel	4.01	0.06	1.40*	0.0158*

- The density stratification influences the results. When the system has no driving external force, the volume and salt transport increase if the density gradient between the two basins is stronger (Table 3.7). With barotropic forcing a stronger density gradient yields less water and salt flow through the channel (Table 3.8).

Table 3.7: Effect of density stratification on the volume and salt transport in the channel with two different density gradients, $D_1 = 5.2$ sigma–t and $D_2 = 8$ sigma–t, without barotropic forcing. Transport values ($\times 10^{10}$ cm^3 s^{-1}) (* shows rms values)

	gradient D_1		gradient D_2	
	volume	salt	volume	salt
south of the channel	0.93*	0.0162*	1.33*	0.0251*
north of the channel	1.40*	0.0158*	1.91*	0.0097*

Table 3.8: Effect of density stratification on the volume and salt transport in the channel with barotropic forcing and with two different density gradients, $D_1 = 5.2$ sigma–t and $D_2 = 8$ sigma–t. Transport values ($\times 10^{10}$ cm^3 s^{-1})

	gradient D_1		gradient D_2	
	volume	salt	volume	salt
south of the channel	9.94	0.170	6.76	0.128
north of the channel	9.93	0.170	6.75	0.127

The results described here do not give a generalized transport relation. To obtain that more experiments are required. The volume transport in the Belt and its relationship to the surface elevation will be given in chapter 4.

Chapter 4

Baltic Experiment

Before the description of the Baltic Experiments, a comparison is made between results obtained for the density driven circulation and observations. It has been mentioned in chapter 3 that eddy formation begins at the bottom as rotation of the dense fluid. If no barotropic forcing is specified for the background field, this fluid will then be accumulated in the lower layer at the upstream side of the channel. If the system is forced then the dense fluid can spread away from the sill. This dense fluid is described as *dome-shaped* by GILL (1977) and as *convective chimney* by KILLWORTH (1992a). The experiment performed in chapter 3, using as driving force only the density difference between the two basins, shows close agreement between the model and the pattern of observed salinity fields (Fig.4.1a,b). Note that the heavy fluid flows in opposite directions in figures 4.1a and 4.1b. The density gradient and topographic effect are important in the establishment of this rotating dense water. On the basis of synoptic surveys LUNDBERG (1983) suggested that the flow of deep–water into the Bornholm Basin is hydraulically controlled.

The number of eddies and their salinity depend on the preconditioning of the flow. If we use the same salinities but a different initial distribution, it turns out that the salinity values will be different above the topography and in the eddies. A spin-down experiment was done, where after 4 days the barotropic forcing was switched off. The resulting density field is shown in figure 4.1c. Two small eddies are generated near the main eddy. One of them is anticyclonic. All the eddies have propagated away from the sill.
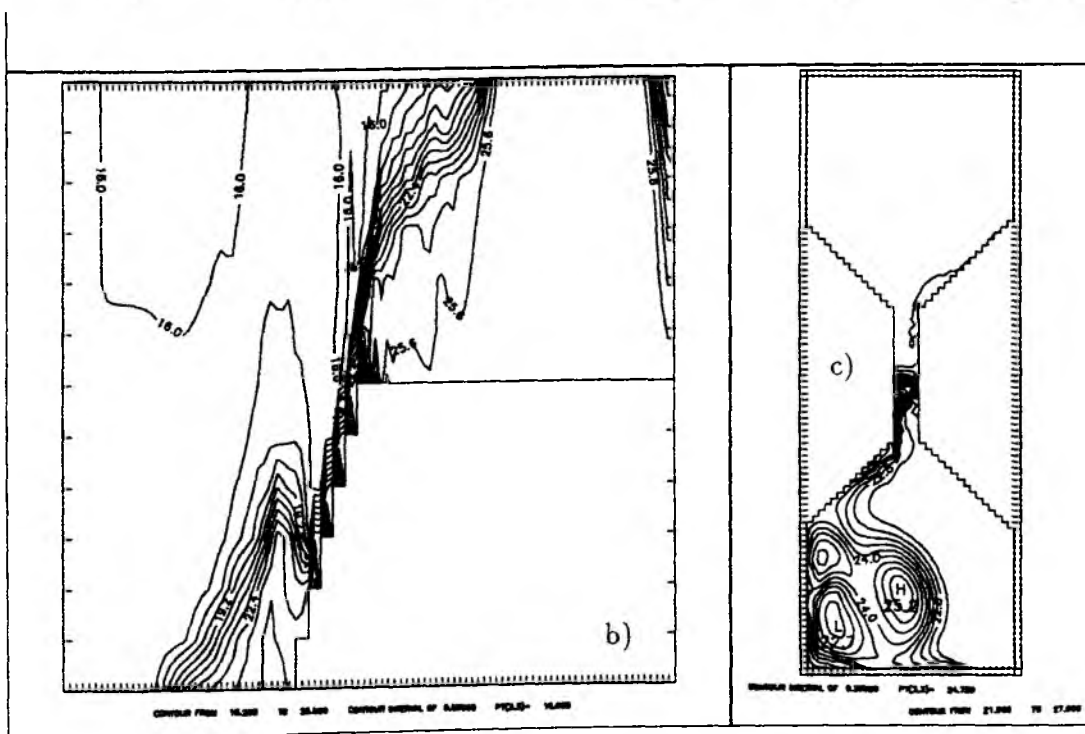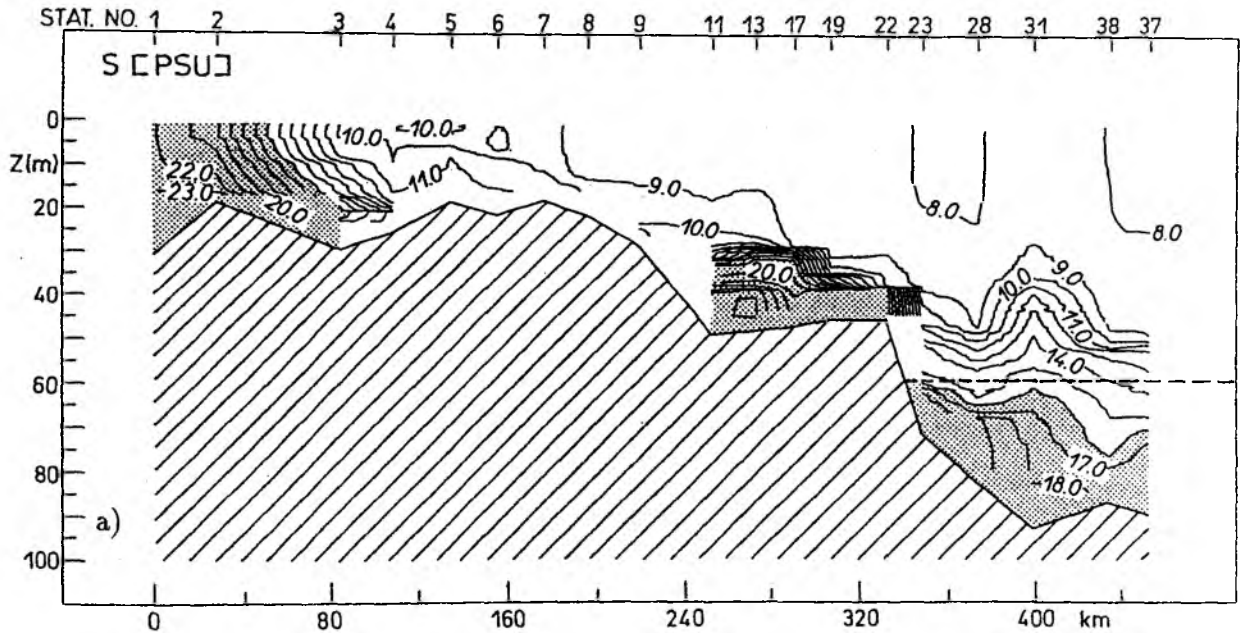
Figure 4.1: *a) Observed salinity values. Vertical section from the south of the Belt Sea, Arkona to Borholm Basin (Alkor, February 1993) b) Salinity values, vertical section ($x = 19$) for density driven case c) Horizontal density field for spin-down experiment (layer 7).*
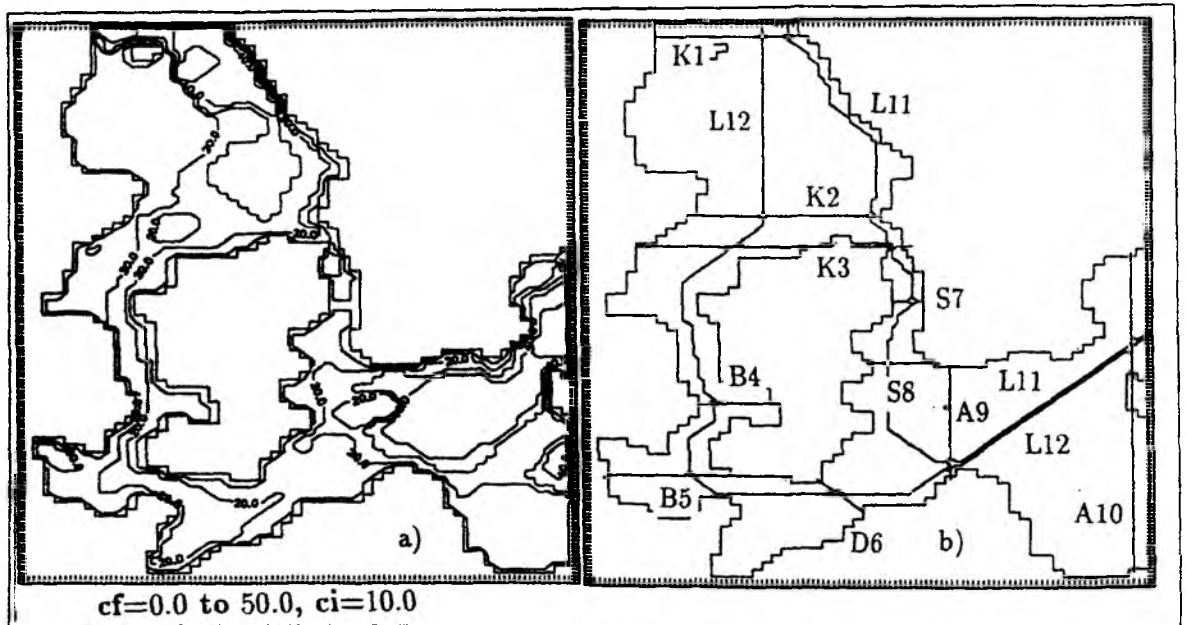
cf=0.0 to 50.0, ci=10.0

Figure 4.2: *a) Model topography b) Vertical sections.*

In the literature a great number of numerical models of the Baltic can be found for example box models by WALIN (1977), SVANSSON (1980), RAHM (1985) and OMSTEDT (1990), models based on hydraulic control by WELANDER (1974) and STIGEBRANDT (1983), and on geostrophic control by TOUI ANY and GARRETT (1984), a model for the vertical circulation by STIGEBRAN⁻JT (1987b) and a quasi-geostrophic model by AITSAM and ELKEN (1982). Some of the numerical models emphasize the importance of the meteorological forcing, such as the wind driven circulations by SIMONS (1978), KIELMANN (1981), KRAUSS and BRÜGGE (1991) and LEHMANN (1992).

The model presented here, has a horizontal grid distance of 2.5 km, and 12 layers in the vertical with reduced thickness at the surface and the bottom. The model area extends from the Kattegat, over the Danish straits to the Arkona basin. The vertical sections analyzed and the model-topography are shown in Figure 4.2. Salinity and temperature values are from BOCK (1971) and LENZ (1971) respectively.

4.1 Thermohaline Circulation

Thermohaline circulation produces bi-directional flow in the Danish Straits. This bi-directional flow is described in many studies, such as KÄNDLER (1951), WYRTKI (1953, 1954a, 1954b), MAGAARD and RHEINHEIMER (1974) and MÄLKKI and TAMSALU (1985). The less dense Baltic water flows to the North Sea in the upper and denser water returns in the lower layer into the Baltic. Bi-directional flow is often observed in the summer months or during calm wind situations. During most of the year bi-directional flow occurs in the Fehmarnbelt. This is observed in 50 % of all cases in summer and 29 % in winter (WYRTKI, 1954b). In the Great Belt the corresponding numbers are 95 % in summer and 65 % in winter (FARMER and MØLLER, 1990).

Model results for the density–driven flow are depicted in figure 4.3. Strong density gradients (Fig.4.3a) are obtained between the in– and outflowing water. Also shown are the barotropic (Fig.4.3d) and first layer total velocities (Fig.4.3b). The currents near the coast at the north have more baroclinic character; on the other hand currents flowing to the NE direction in the Arkona Basin are more or less barotropic. The surface elevation in the Baltic is higher than the surface elevation in the Kattegat (Fig.4.3c)

For detailed discussion we begin with the Arkona basin to show how the salinity field effects the neighbouring basin (Bornholm). The cross–section A9 in figure 4.4 shows the dense water entering the Arkona basin. The salinity values depend on the initial salinity distribution (preconditioning). If we prescribe the initial salinities that are typical for the Kattegat and Arkona basin also close to the Danish Straits, then a flow of more saline water into the Arkona basin should be expected. Two experiments were conducted to see the effect on the density distribution in the Arkona Basin (Fig.4.4 and 4.5). In the first experiment a small density gradient (small density–gradient case) is prescribed along the Danish Straits. In the other experiment a larger density gradient (large density–gradient case) is used. The latter can be typical for the density driven circulation after wind occurence. Barotropic
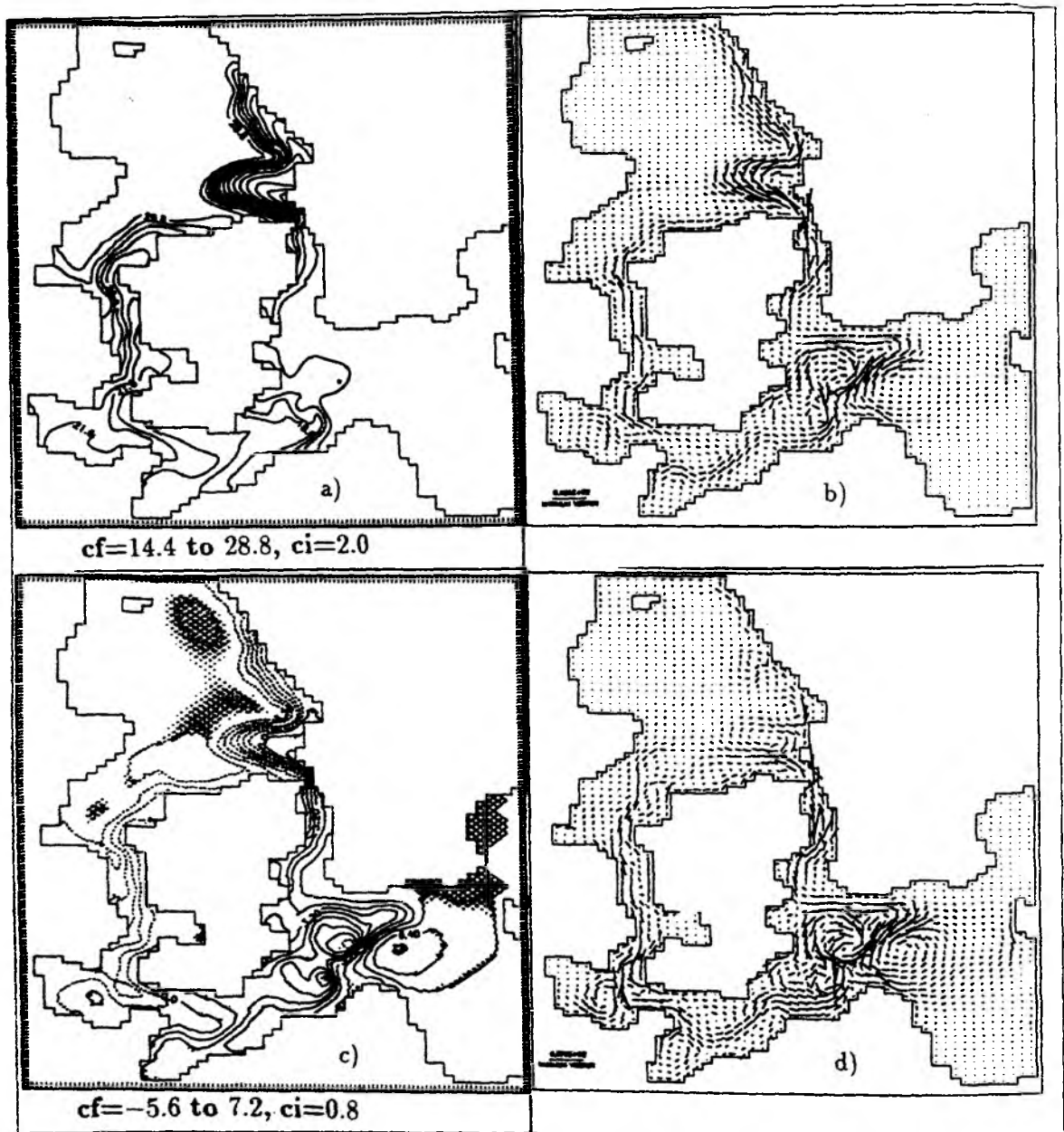
Figure 4.3: *Thermohaline circulation field for the Danish Straits at the end of day 12. a) Surface density field b) Horizontal velocities (k=1) c) Surface elevations and d) Barotropic velocities. Maximum velocity vector is 0.5 cm (60.5 cm/s for horizontal and 27.6 cm/s for barotropic velocities.*
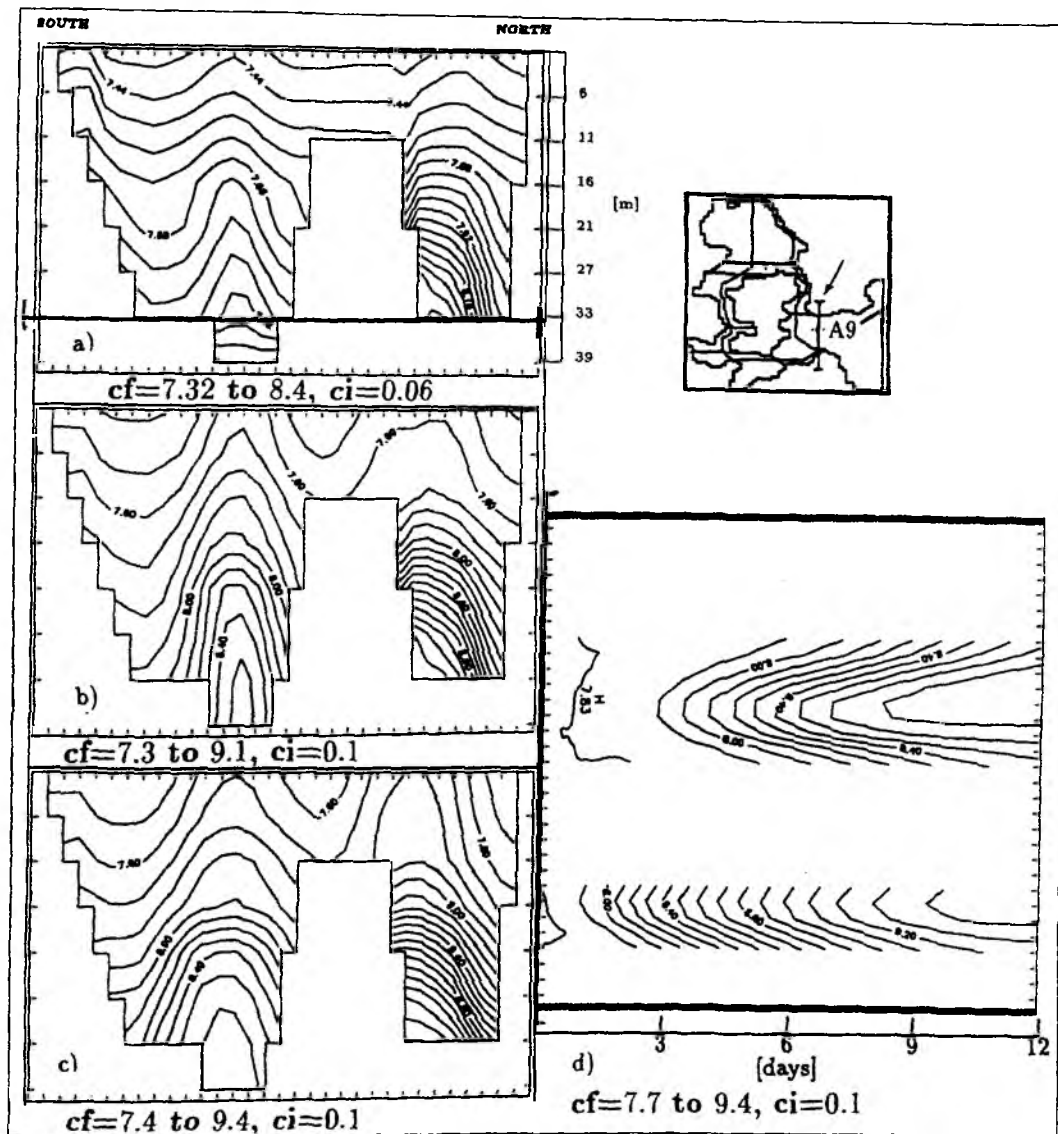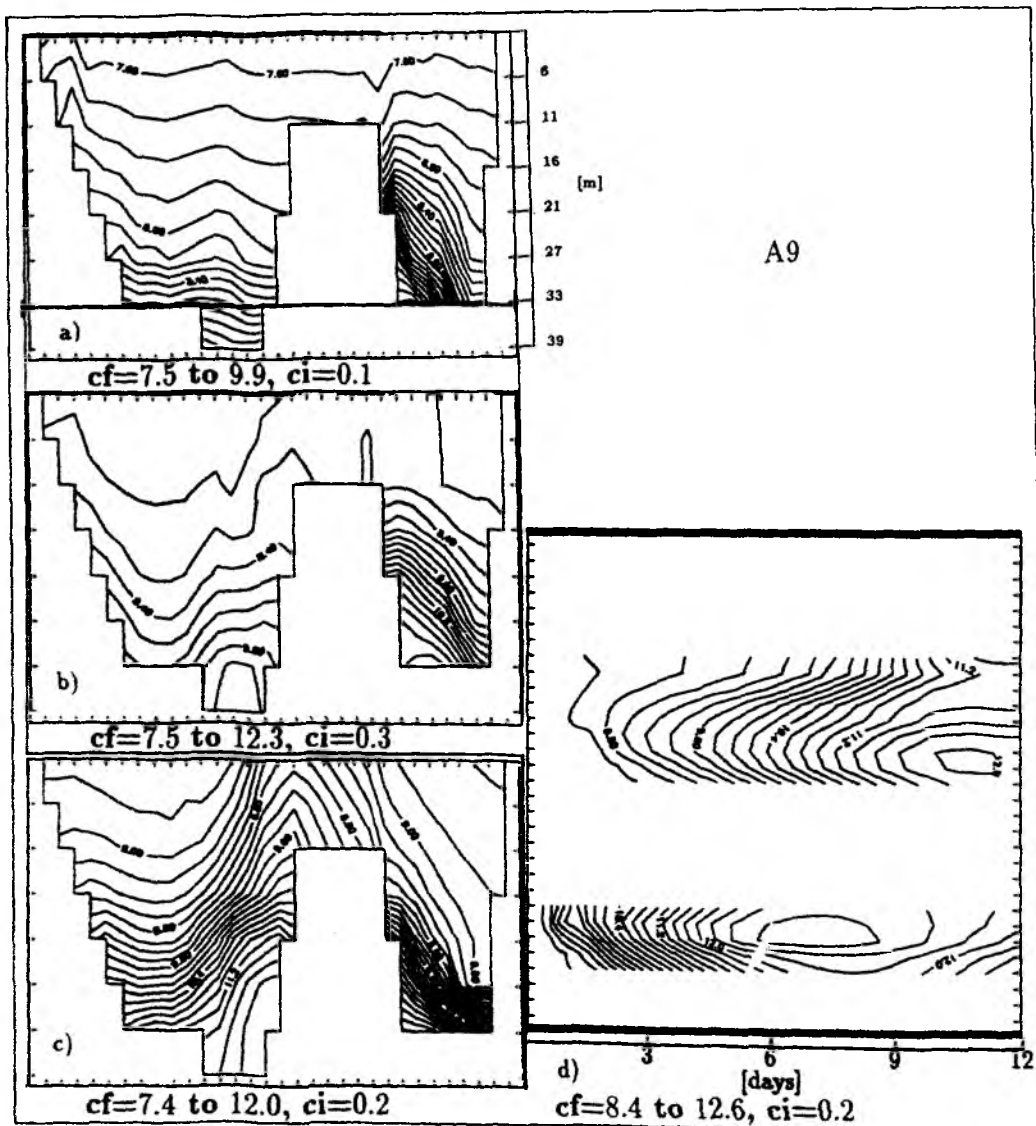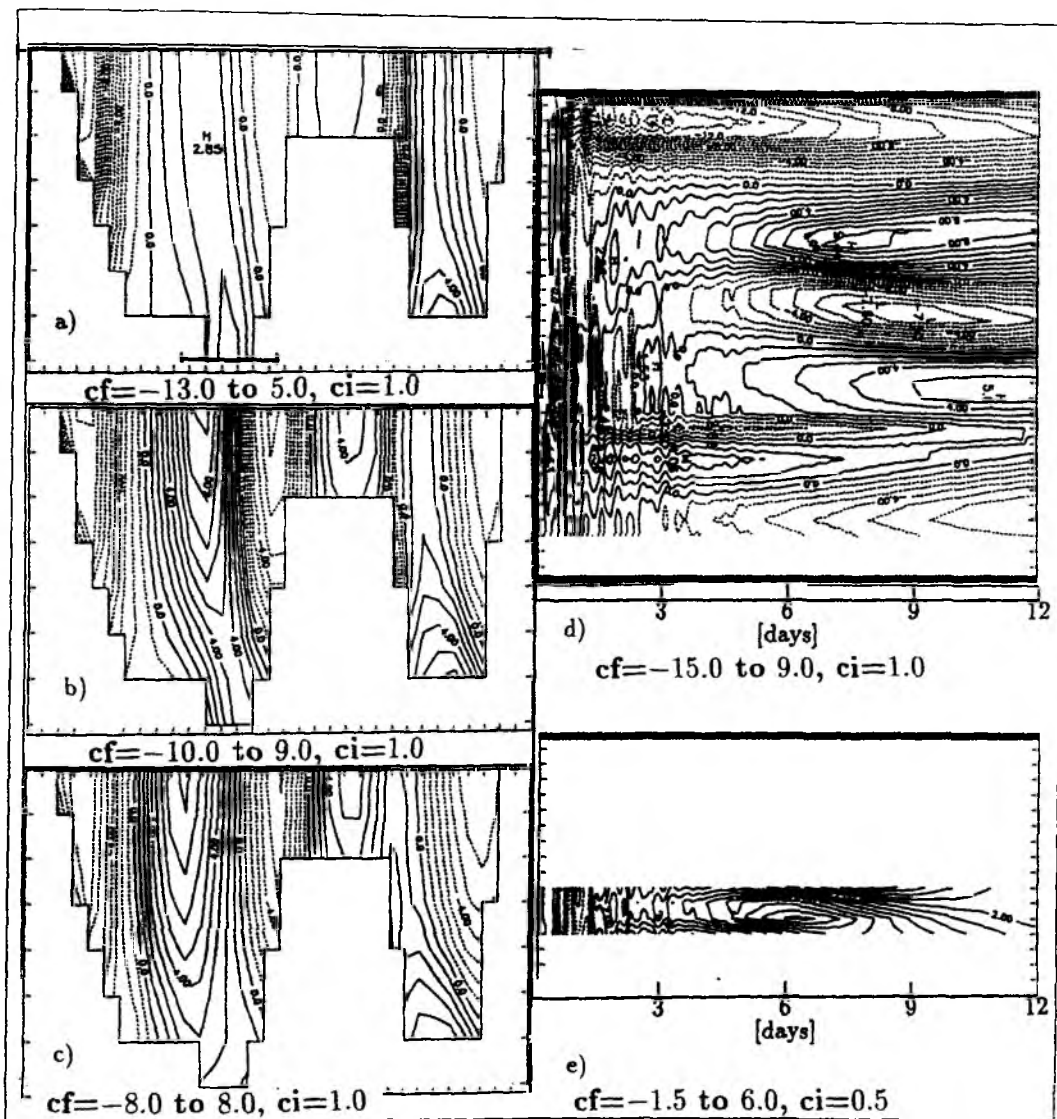
Figure 4.4: *Salinity values, Arkona vertical section A9 for the case of small density gradients between the two ends of the Danish Straits a) after 4 days b) after 8 days c) after 12 days d) space-time contour plot for the salinity of layer 7, as indicated in plot a.*

forcing displaces the density front over great distances and intensifies the horizontal density gradient. The large density gradient between the ends of the straits causes more salt and water exchange through the channel. Space–time contour plots from figure 4.4d and 4.5d show the salinity values of layer 7 (33m) during 12 days. Saltier water which comes from the Kattegat, prefers to flow through the northern part of
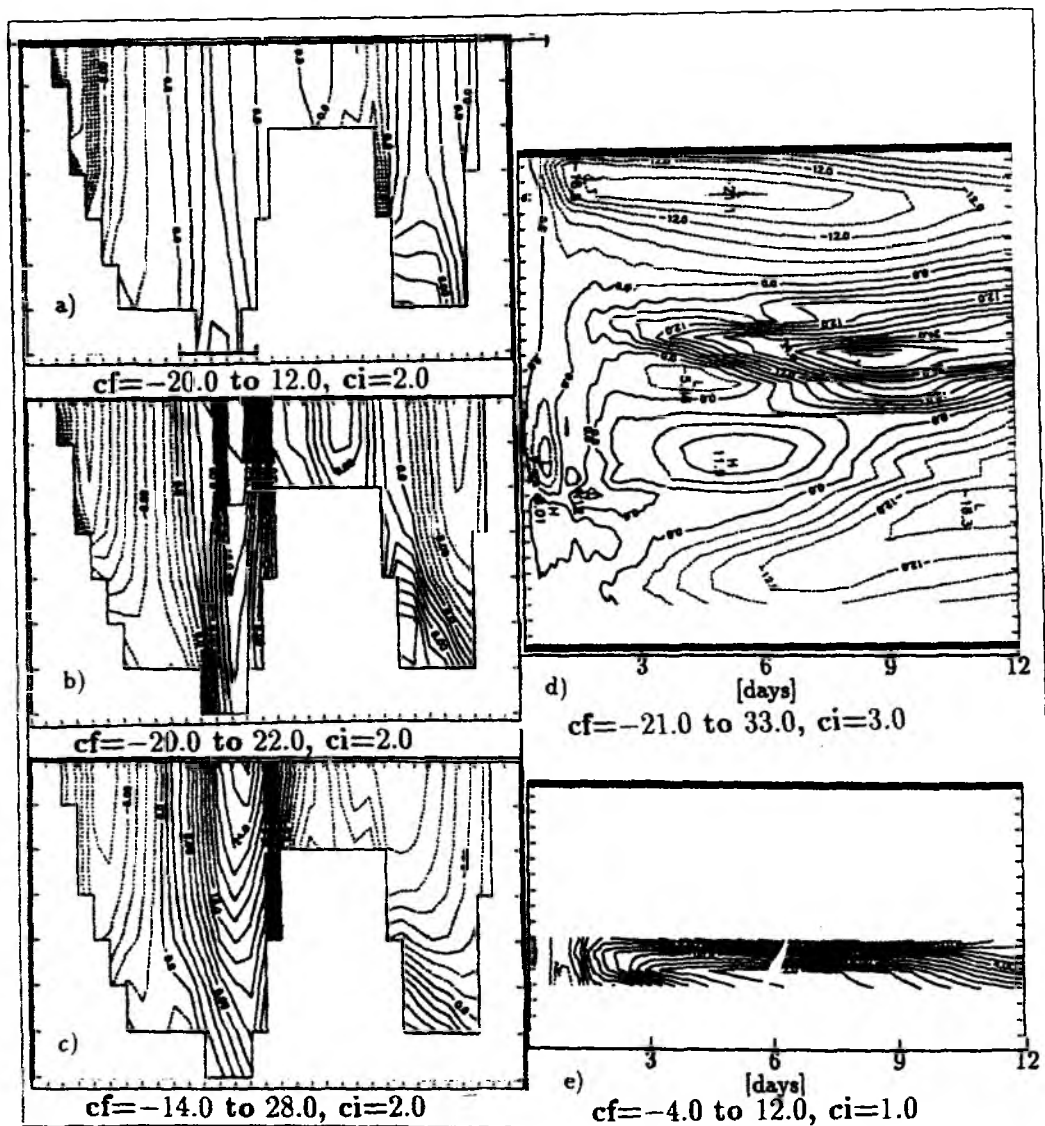
Figure 4.5: *Salinity values, Arkona vertical section A9 for the case of large density gradients between the two ends of the Danish Straits a) after 2 days b) after 6 days c) after 12 days d) space-time contour plot for the salinity of layer 7, as indicated in plot a.*

the Arkona Basin. Fast geostrophic adjustment and as a result quasi-steady flow are obvious from both plots. The dense bottom current entering the Arkona basin pushes the lighter fluid upwards (Fig.4.4a,b,c and Fig.4.5a,b,c). Therefore vertical advection is induced in the basin by the intruding dense current. This result is in agreement with STIGEBRANDT (1987b) and with the two-basin experiment described

Figure 4.6: *Velocity values (u–component), Arkona vertical section A9 for the case of a small density gradients between the two ends of the Danish Straits a) after 4 days b) after 8 days c) after 12 days d) space–time contour plot for the first layer velocity, e) space–time contour plot for the layer 8 velocity. The layers are indicated in plot a.*

in chapter 3. In Stigebrandt's study water entering the Arkona basin becomes diluted by upward displacing the original waters and associated vertical mixing.

In another work of STIGEBRANDT (1987a) he calculated the flow of dense water into the Baltic that leaks from the deepest part of the Arkona basin. He assumed that this leakage is contolled by the vertical stratification in the Arkona Basin and

Figure 4.7: *Velocity values (u-component), Arkona vertical section A9 for the case of a large density gradients between the two ends of the Danish Straits a) after 2 days b) after 6 days c) after 12 days d) space-time contour plot for the first layer velocity, e) space-time contour plot for the layer 8 velocity. The layers are indicated in plot a.*

the rotation (rotational baroclinic control). He found that there is a positive correlation between the flow rate and the salinity of the dense water.

The currents for both density distribution are stronger in the southern part of the section A9 (Arkona Basin) than the currents in the northern part. They decrease from the surface to the bottom in the south. On the other hand the currents are
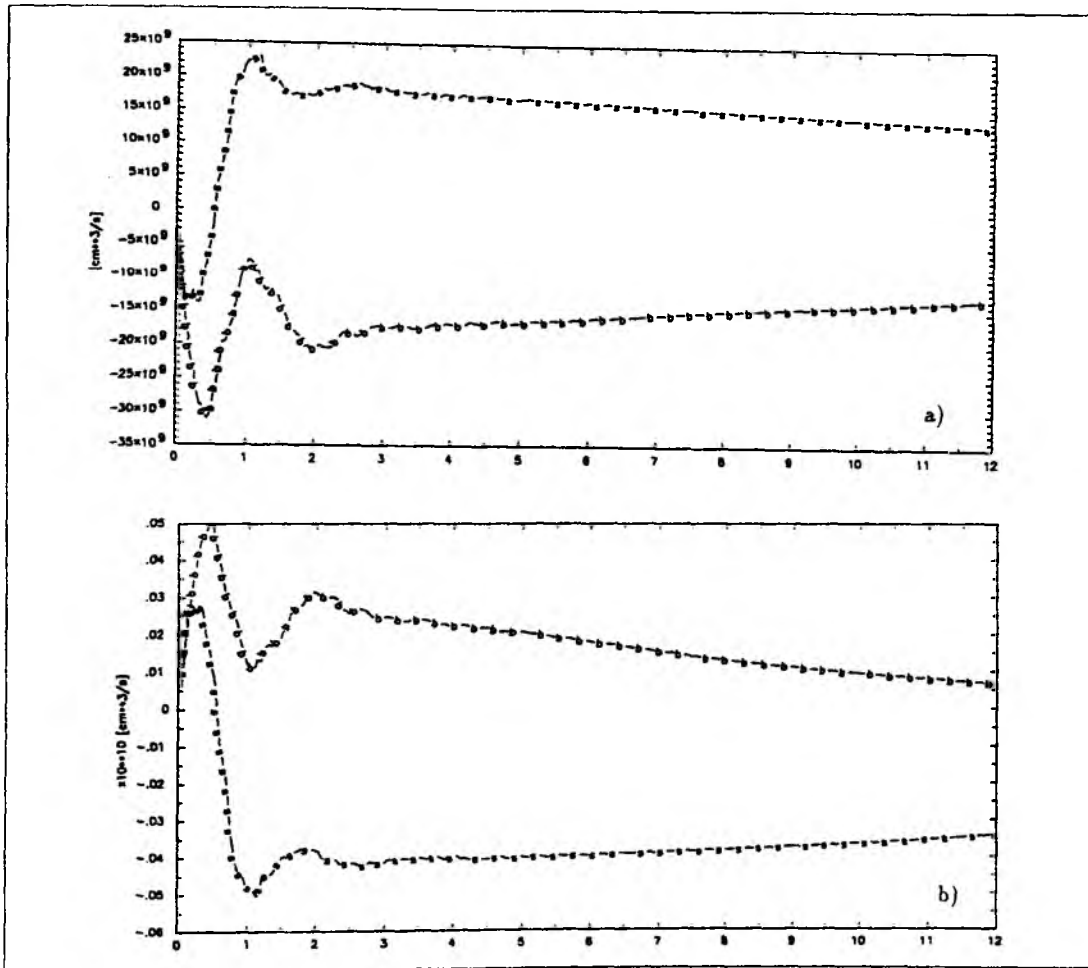
Figure 4.8: *Transport through Belt and Sound a) Volume transport, the negative values show inflow and positive values outflow b) Salt transport, positive values denote a salt gain for the Baltic. "b" represents Belt and "s" Sound.*

intensified at the bottom in the north of A9 (Fig.4.6a,b,c and 4.7a,b,c).

Space–time contour plots 4.6d,e show that in section A9 the superinertial oscillations effect the surface and bottom velocity fields during several inertial period for the small density–gradient case. The adjustment is faster for the large density–gradient case (Fig.4.7d,e). The system reaches a quasi–steady state in the Arkona Basin at the end of this adjustment process. The term "quasi-steady" is used, because the space-time contour plots show slow time variations with a period of the order of approximately 10 days after the adjustment process. The 10-day variability of the
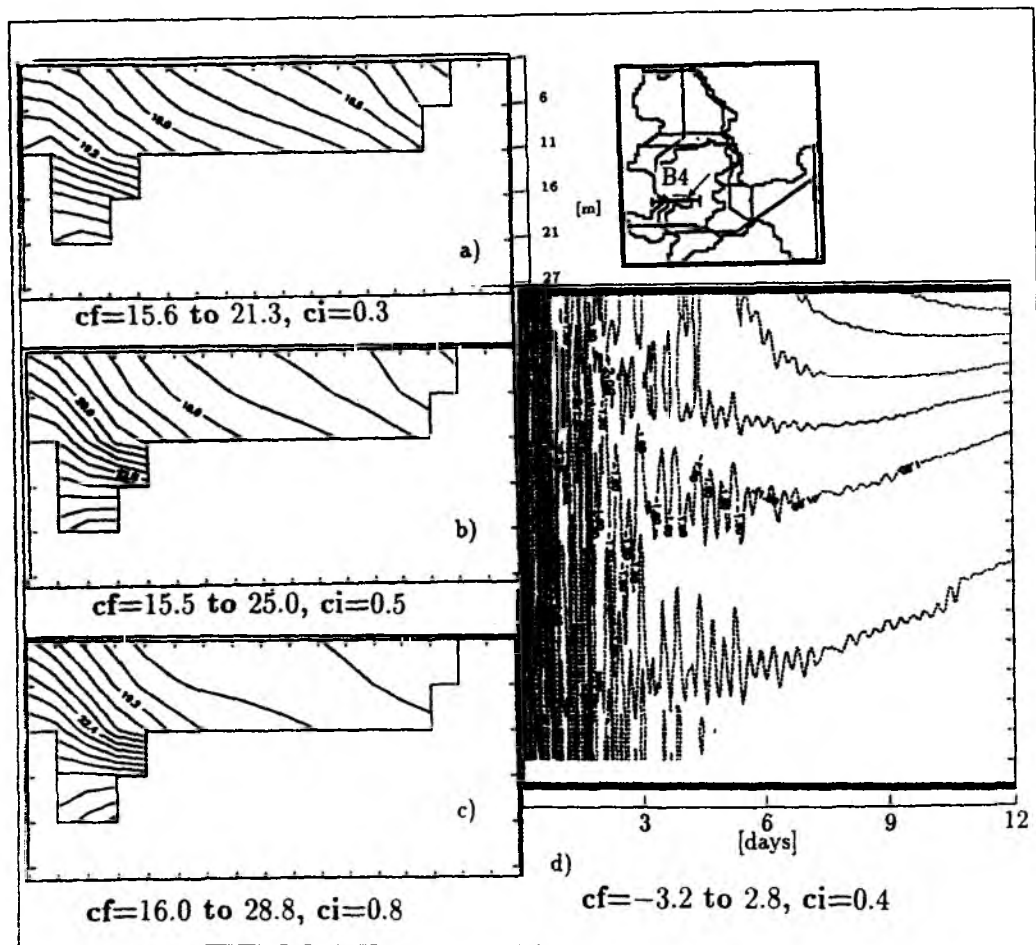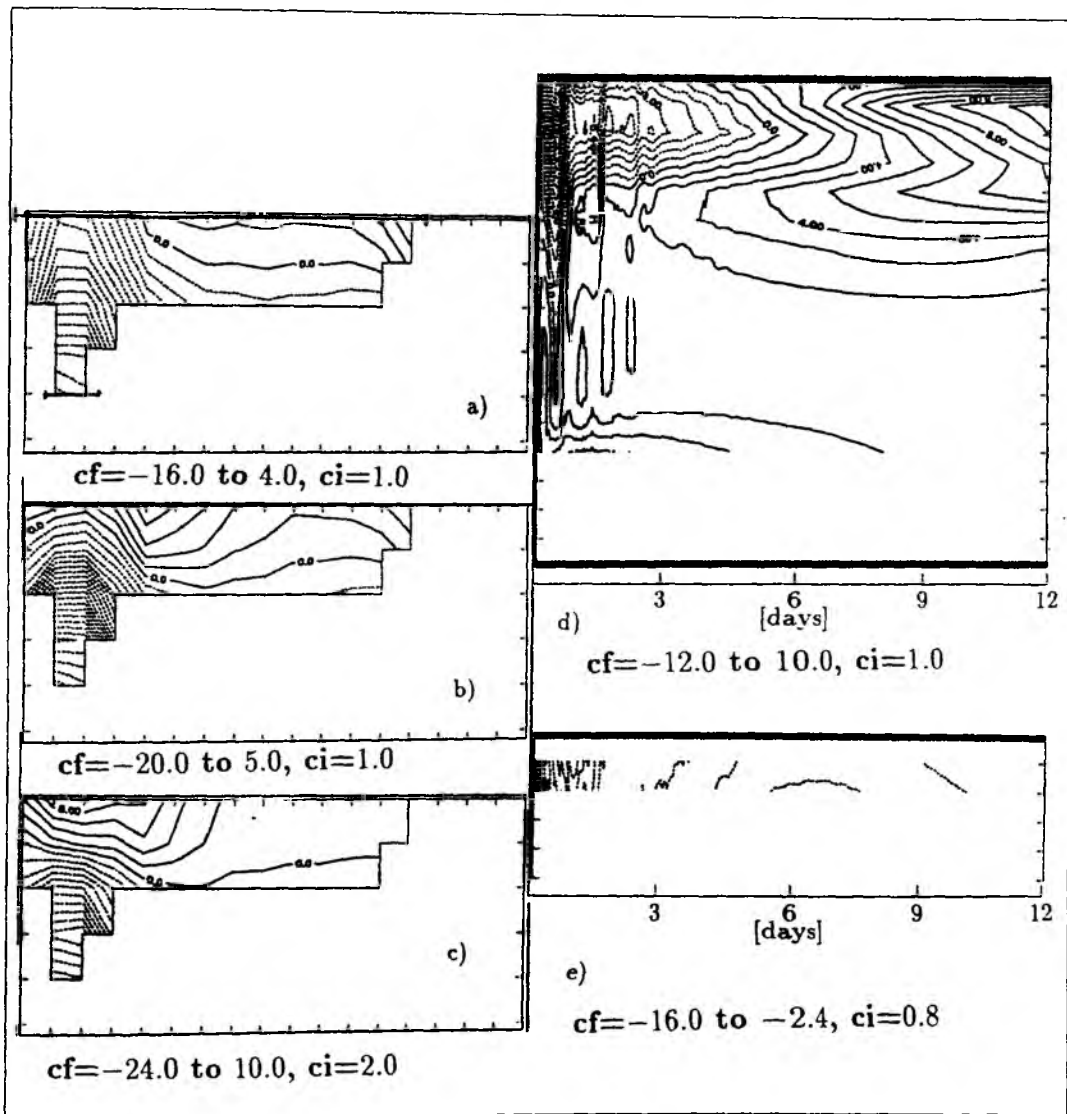
Figure 4.9: *Salinity values, Belt section B4 a) after 2 days b) after 6 days c) after 12 days d) space-time contour plot for surface elevation.*

surface current is only observed in the south of the Arkona section (Fig.4.7d). The topographic waves have a wavelength of approximately 30 km in both cases, in agreement with studies by SIMONS (1976), KIELMANN (1981) and LEHMANN (1992) and with observations by AITSAM and ELKEN (1982) and KRAUSS and BRÜGGE (1991).

The dense flow into the Arkona Basin as a result of the thermohaline circulation is not sufficient for the renewal of deep water in the Baltic. For the mean density distribution of November the volume transport through the Belt into the Arkona Basin is about 1.3×10^{10} cm^3 s^{-1} and same volume is transported through the Sound into the Kattegat. The salt transport is about 0.7×10^8 cm^3 s^{-1} through the Belt into the Arkona Basin and 3.4×10^8 cm^3 s^{-1} through the Sound into the Kattegat

Figure 4.10: *Velocity values (v–component), Belt section B4 a) after 2 days b) after 6 days c) after 12 days d) space-time contour plot for first layer velocity, e) space-time contour plot for the velocity of layer 5. The layers are shown in figure a.*

(Fig.4.8). It seems that the transports through the Sound is higher than through the Belt. The reason for this is that the current in the Sound is almost completely to the north, whereas in the Belt the current is bi-directional (Fig. 4.9,10,13 and 14). We now turn to the Danish Straits. The two vertical sections in the Belt which are depicted in Figure 4.9-11 show the bi-directional flow mentioned above. Common characteristics of both sections are:

65
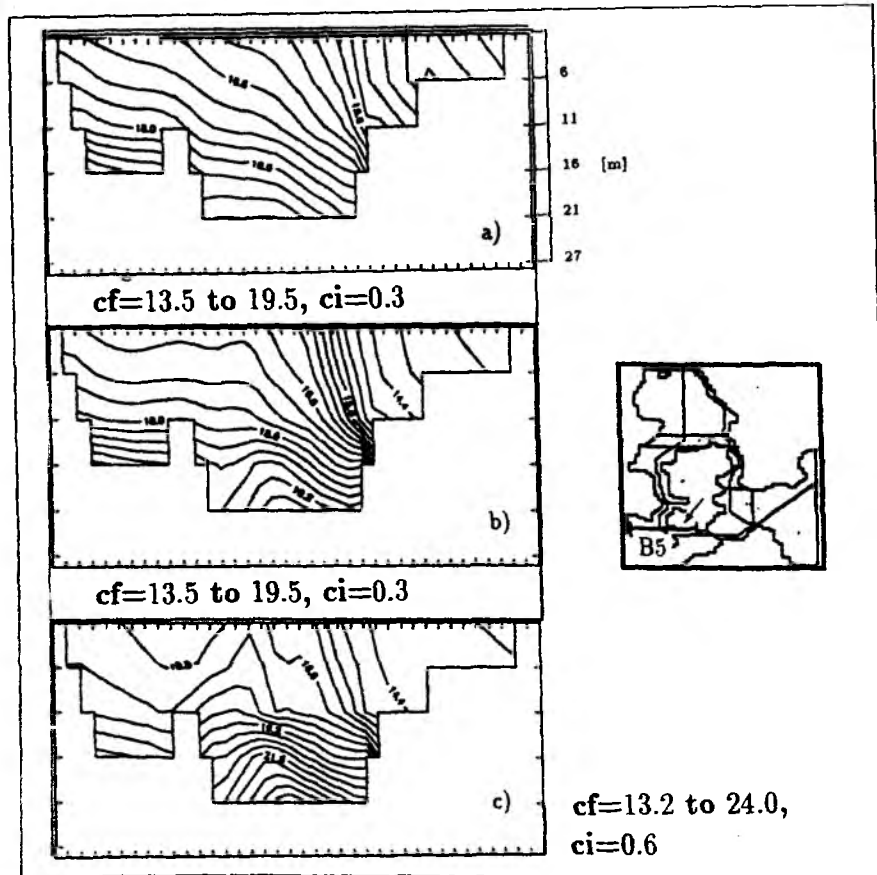
Figure 4.11: *Salinity values, Belt section B5 a) after 2 days b) after 6 days c) after 12 days.*

(a) The surface displacements are always higher at the right hand side of the straits in the direction of the current.

(b) The water in the lower layer becomes gradually saltier in time.

(c) The lower layer maximum velocity in the direction to the Baltic are greater (about 20 cm s^{-1}) than the upper layer velocity in the direction to the Kattegat (about 10 cm s^{-1}).
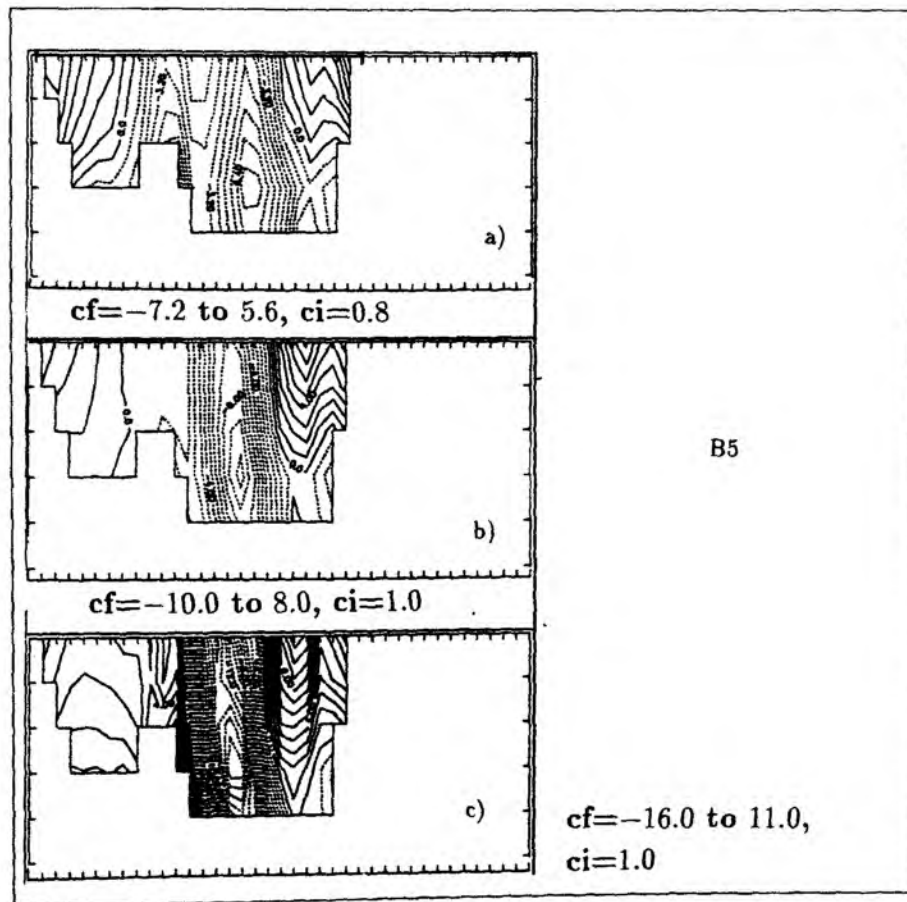
Figure 4.12: *Velocity values (v-component), Belt section B5 a) after 2 days b) after 6 days c) after 12 days.*

A *bore* formation in the Belt can be seen in the velocity section B5 (Fig.4.12). In the next section of this study we come back to this bore intrusion when we discuss the salinity section along the Belt (Section L12). It may be a result of the time-dependent circulation, also nonlinearities may be important. STERN (1980) and CHAO and BOICOURT (1986) examined the bore intrusion and Stern commented that after arresting the bore a large eddy is expected to form. LM (1978) meant that the bore formation is commonly found in restricted channels of a width much less than the barotropic Rossby radius. The velocity component transverse to the channel axis is suppressed and the effects of rotation are minimized. PRATT (1984) stated that a bore-like reflected wave is a sufficient (but not necessary) evidence that the flow is hydraulically controlled. HELFRICH and MELVILLE (1990) found analytic bore
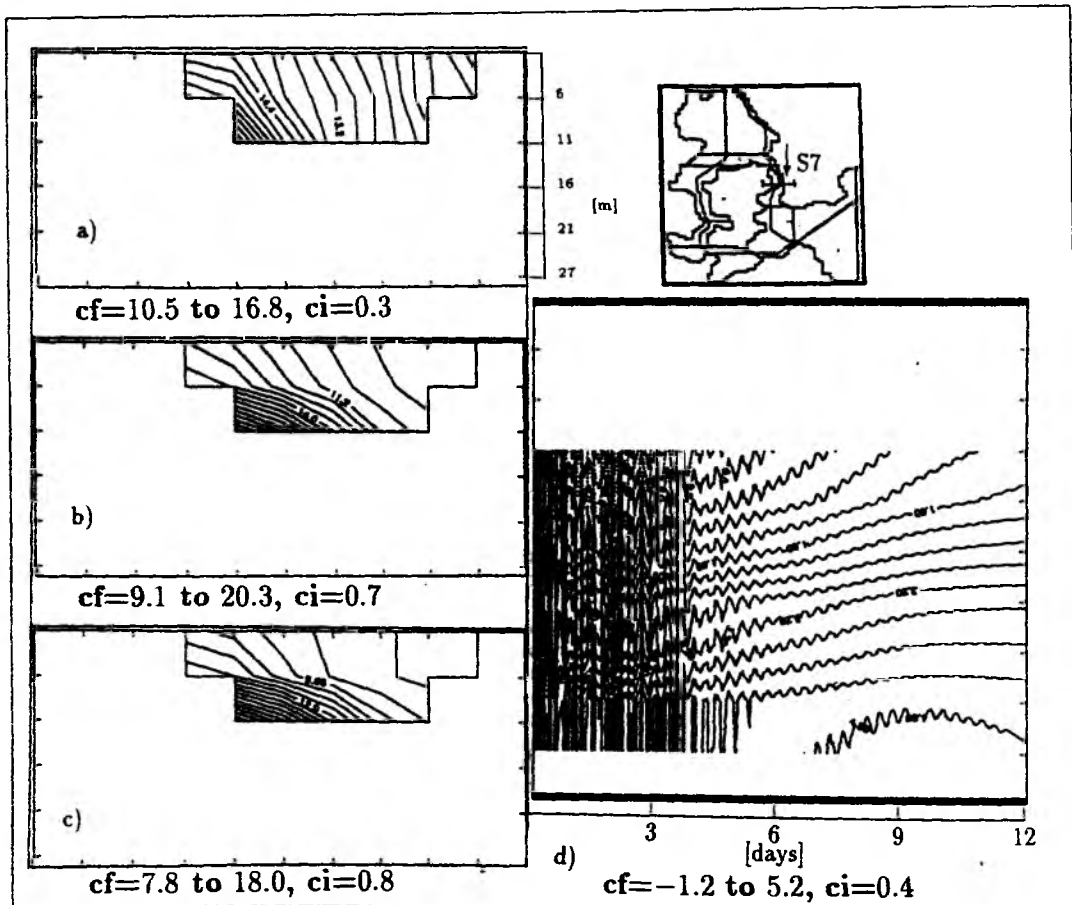
Figure 4.13: *Salinity values, Sound section S7 a) after 2 day b) after 6 days c) after 12 days d) space-time contour plot for the surface elevation.*

solutions. They explained that bores are generated by unsteady transcritical forcing and they are complementary pairs of solitary waves. NOF (1984, 1986) explained the bore formation with the help of shock waves. He meant that the bores are associated with a sudden change in depth accompanied by local energy loss.

In the Sound the current flows more or less only in the direction to the Kattegat (vertical section S7), but the surface layer maximum velocity (about 20 cm s^{-1}) is greater than the velocity in the lower layer (about 5 cm s^{-1}). Less dense water flows along the east coast in the Sound to the Kattegat (Fig.4.13a,b,c and Fig.4.14d,e) and the surface elevation is higher at the right hand side of the channel (Fig.4.13d). It is avoided to give salinity values for each section, because these values depend on the initial density distribution.
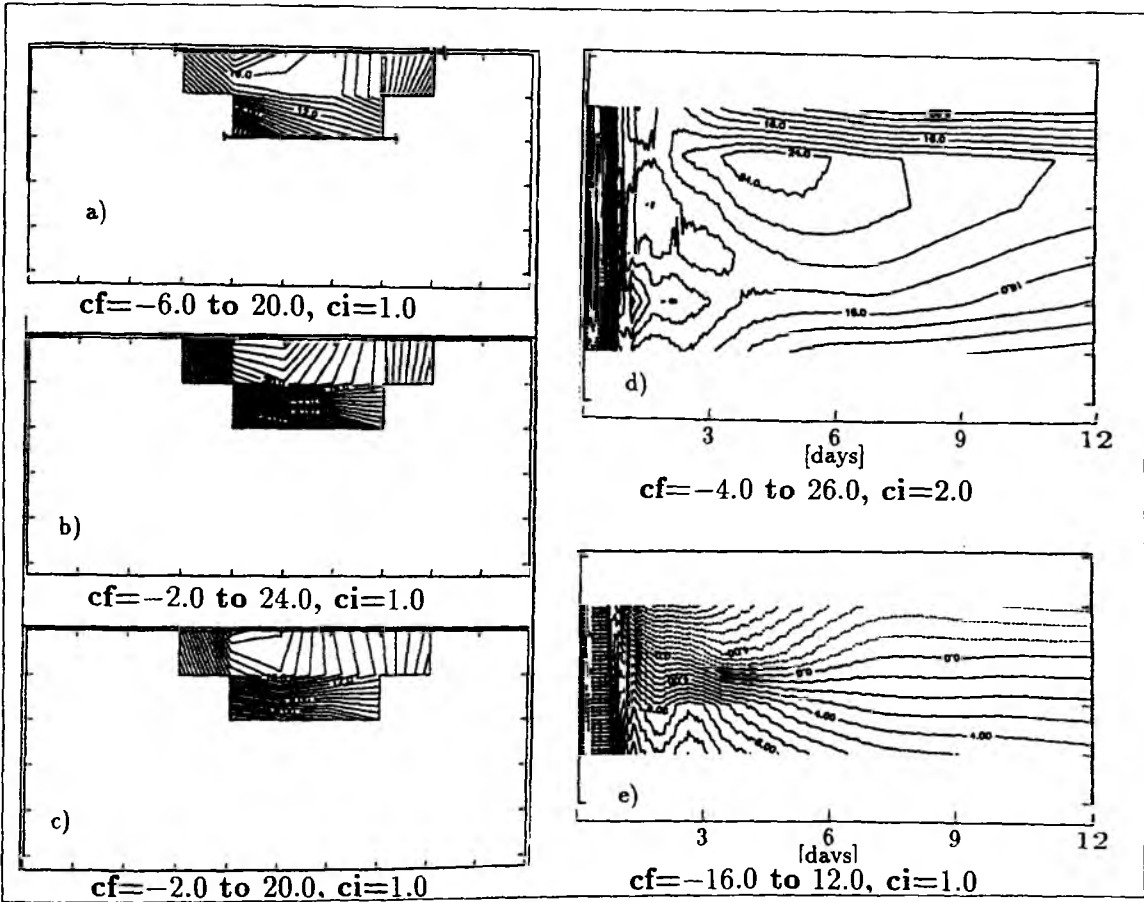
cf=−6.0 to 20.0, ci=1.0

cf=−2.0 to 24.0, ci=1.0

cf=−2.0 to 20.0, ci=1.0

cf=−4.0 to 26.0, ci=2.0

cf=−16.0 to 12.0, ci=1.0

Figure 4.14: *Velocity values (v–component), Sound section S7 a) after 2 days b) after 6 days c) after 12 days d) space-time contour plot for first layer velocity, e) space-time contour plot for the layer 3 velocity. The layers are shown in figure a.*

The importance of near inertial oscillations has been demonstrated by the two-basin experiments and also by the Baltic experiments. A quasi-steady state is established after the amplitude and the oscillations weaken. Inertial waves were analysed by KRAUSS (1979c) for the wind driven case. In his study also vertical motions occur in inertial waves. Inertial waves are mainly produced by a sudden change of the wind field. They also occur during any adaptation process to a new steady state (because f is a resonance frequency in the linear set of hydrodynamic equations). Free baroclinic modes are strongly dependent on f. TATRO and MOLLO–CHRISTENSEN (1967)

suggested that an instability in the Ekman boundary layer, which always has a frequency higher than the inertial frequency, can excite a first subharmonic with less than the inertial frequency, and resulting inertial waves are found to propagate throughout the region above the Ekman layer. In this case it is difficult distinguish between such waves and true turbulence associated with the inertial frequencies.

4.2 Barotropic Forcing

One of the most important driving forces is the along channel sea level inclination. The model shows that the thermohaline circulation alone can not supply the transport required for a renewal of the deep Baltic bottom water. LASS and SCHWABE (1988) found that the correlation between the sea level and the east component of the wind stress is positive and significant with 99.9 % probabilty. No time delay is observed. On the other hand the correlation between the sea level and the north component of the windstress reveals that the Ekman transport has only a minor influence on the sea level of the Kattegat. Volume and salt transport depend strongly on the sea level difference between the Kattegat and the Arkona Basin. Salinity anomalies of the bottom water in the Kattegat do not play an important dynamic role for a major salt water inflow (MATTHÄUS and FRANC, 1988; LASS and SCHWABE, 1988). The sea level difference can be established also by wind surge and barotropic circulation. The sea level at a certain position is influenced by seiches (WÜBBER and KRAUSS, 1979). The barotropic forces set up unidirectional currents in the Danish Straits. The system needs more energy for inflow than for outflow, because the flow from the Kattegat in the upper layer must dominate over the barotropic and baroclinic thermohaline circulation in the Belt and Sound. In case of outflow the current is only opposed to the baroclinic component of the thermohaline circulation in the lower layer. Inflow and outflow show different salt and volume transport relations. In the next section the volume and salt transport relations will be given for inflow and outflow through the Belt and the Sound. Flow through the straits takes place at the right–hand coast for both inflow and outflow. This means that the surface elevation is higher on the right side of the channel with respect to the direction of wave propagation (geostrophic flow, Fig.4.15c and 4.16c). The results change when we apply wind forcing. Comparison between the wind-driven case (constant west wind) and the inflow case will be given at the end of this section.
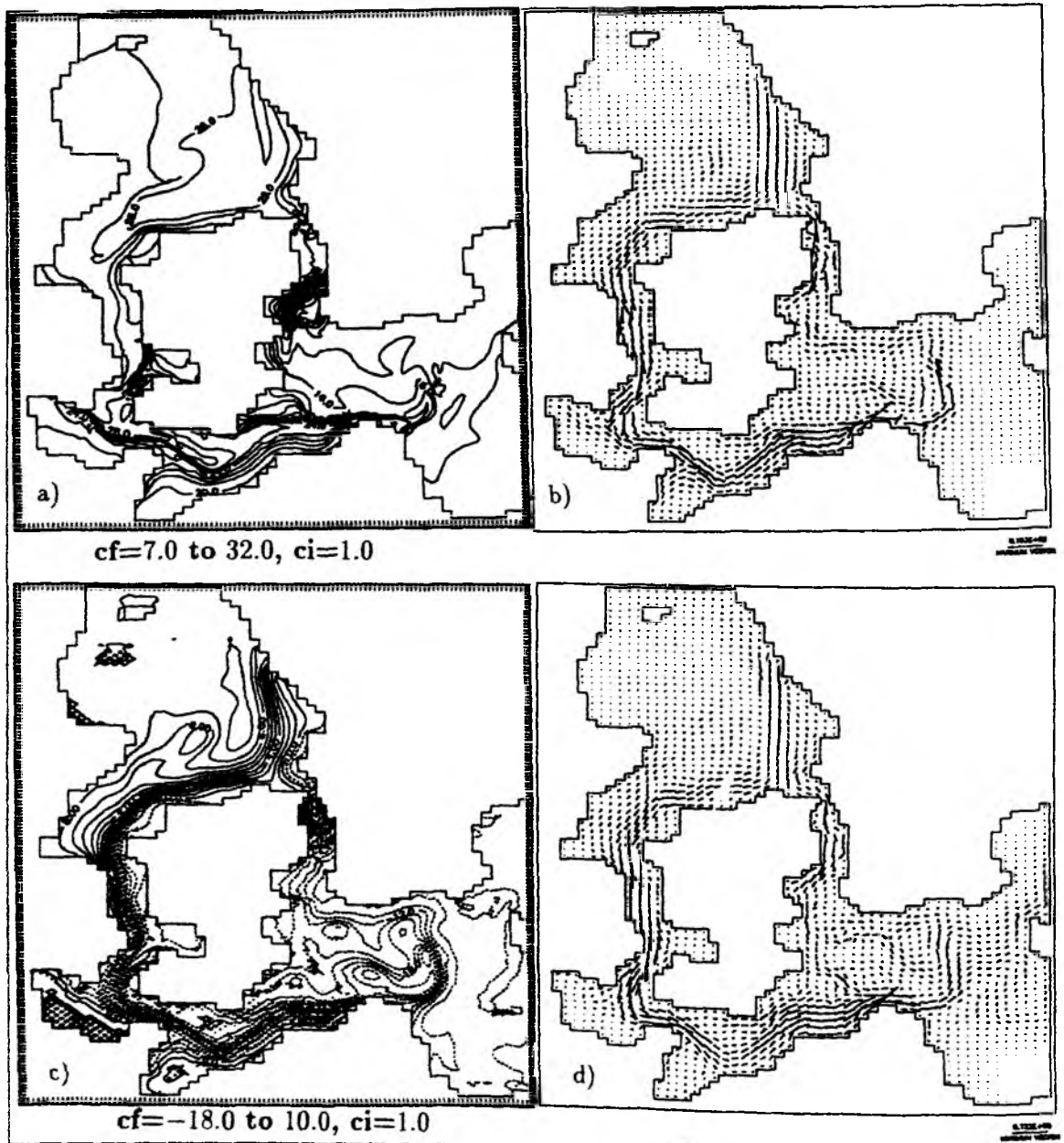
cf=7.0 to 32.0, ci=1.0

cf=−18.0 to 10.0, ci=1.0

Figure 4.15: *INFLOW circulation pattern at the end of Day 12 a) Surface density field b) Horizontal velocities (first layer) c) Surface elevations and d) Barotropic velocities. Maximum velocity vector is 0.5 cm (183.0 cm/s for horizontal and 122.0 cm/s for barotropic velocities.*
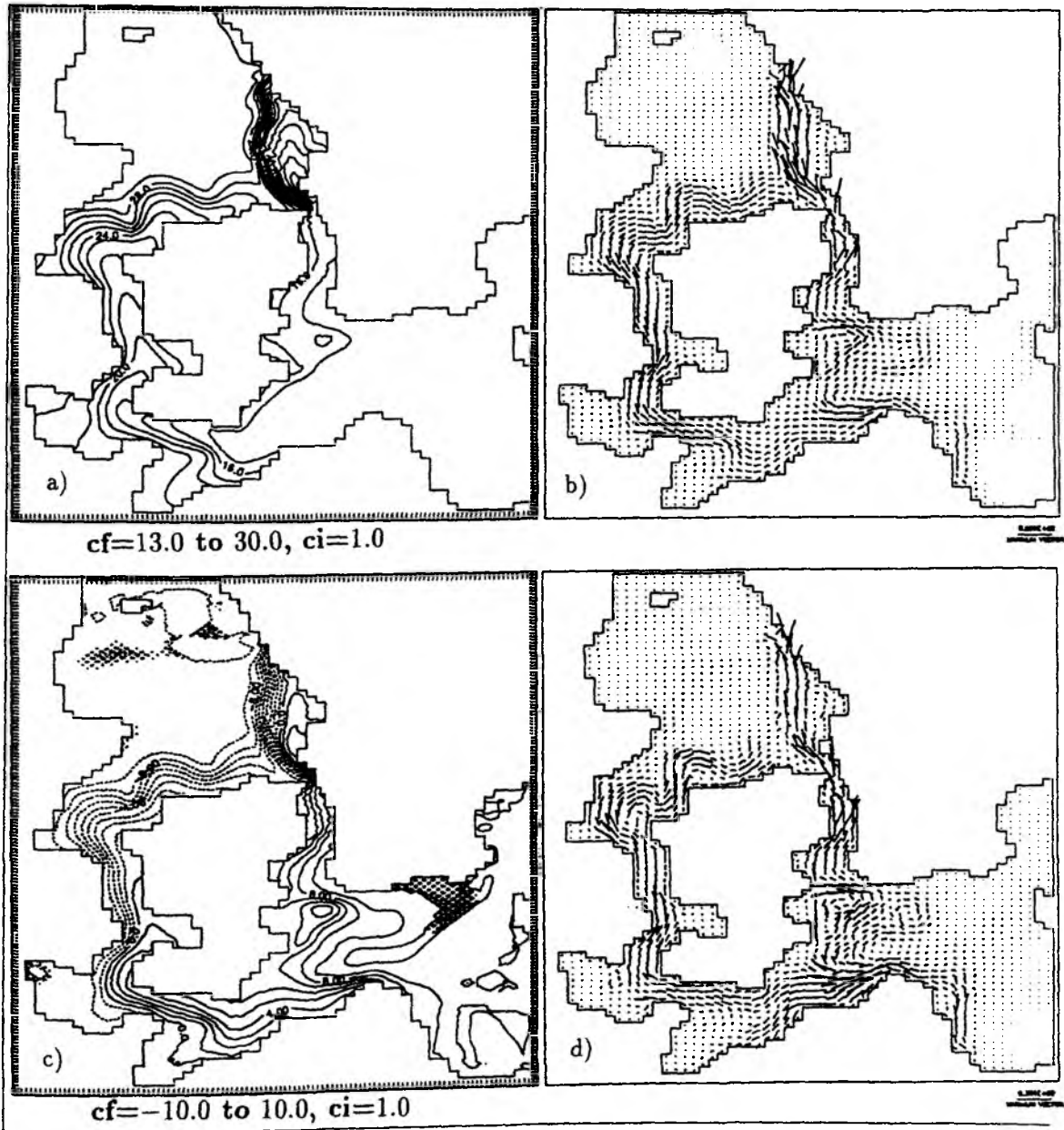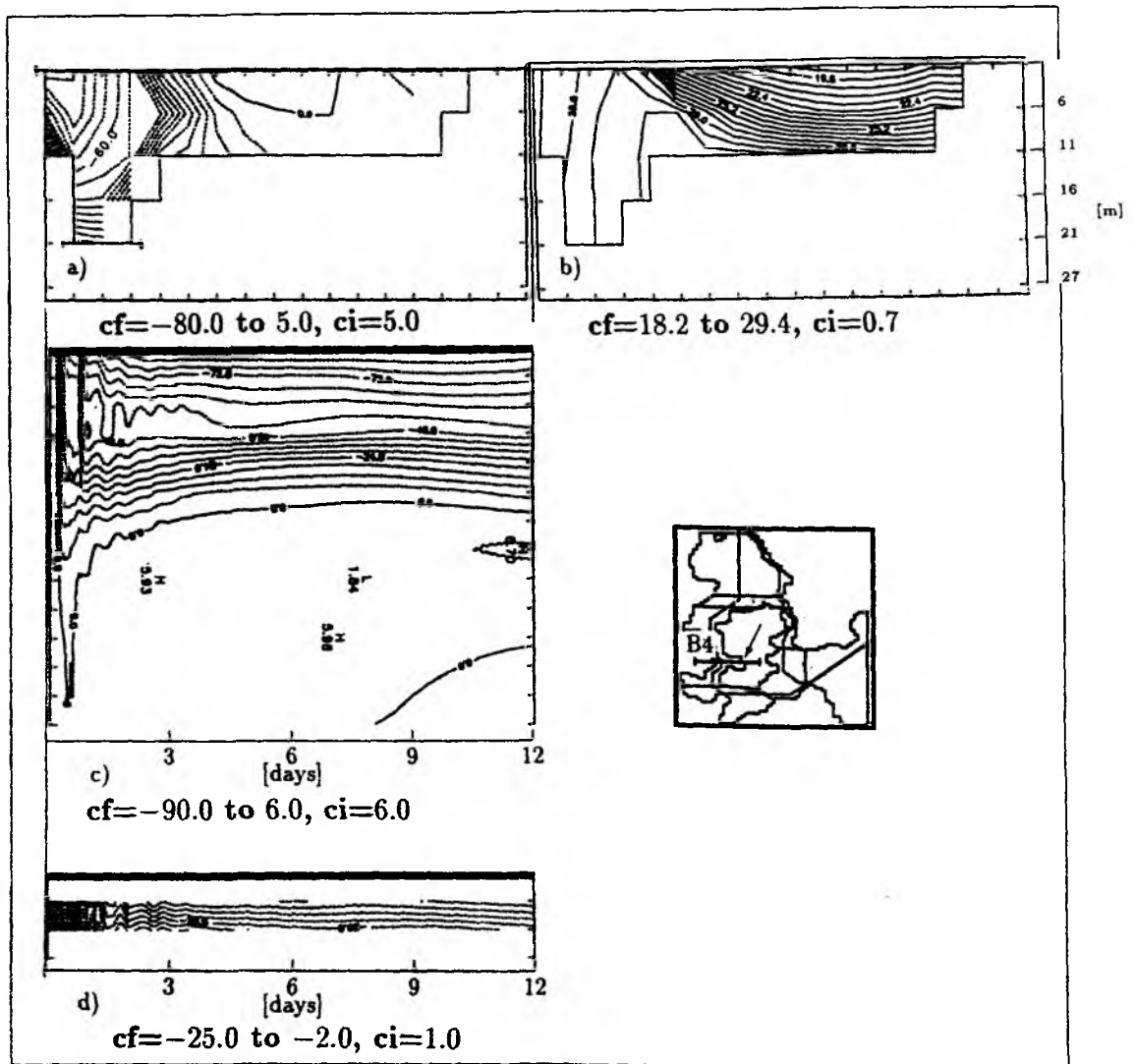
Figure 4.16: *OUTFLOW circulation pattern at the end of Day 12 a) Surface density field b) Horizontal velocities (first layer) c) Surface elevations and d) Barotropic velocities. Maximum velocity vector is 0.5 cm (80.9 cm/s for horizontal and 38.4 cm/s for barotropic velocities.*
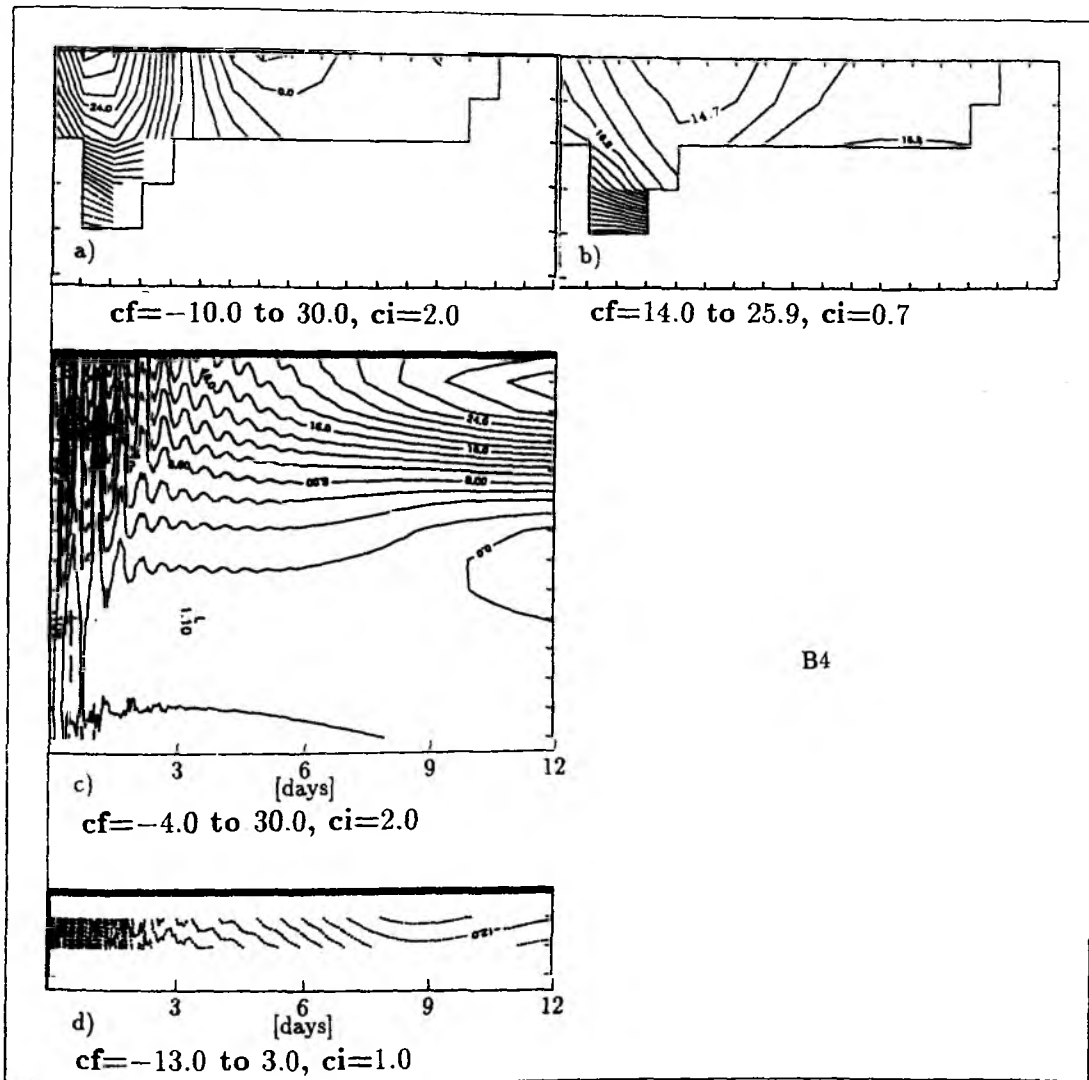
73

Figure 4.17: *Section B4 at the end of Day 12 (INFLOW) a) v-component of velocity b) Salinity. Space-time contour plot c) for the surface layer velocity and d) for the bottom layer.*

The barotropic force was applied similar to the barotropic force in chapter 3 by using surface displacements. This suface displacements are prescribed as a narrow band (10–15 grid points) at the northern and eastern boundaries. The prescribed surface displacements change linearly with increasing distance from the north of the Kattegat and the east of the Arkona basin.

a) cf=−10.0 to 30.0, ci=2.0

b) cf=14.0 to 25.9, ci=0.7

B4

c) cf=−4.0 to 30.0, ci=2.0

d) cf=−13.0 to 3.0, ci=1.0

Figure 4.18: *Section B4 at the end of Day 12 (OUTFLOW) a) v-component of velocity b) Salinity. Space-time contour plot c) for the surface layer velocity d) for the bottom layer.*

The upper layer density front extends along the Swedish coast to the north during outflow (Fig.4.16) and through the Belt along the southern Arkona Basin, where it forms a small tongue towards NE during inflow. In the Sound the separation of the density front from the left coast is observed (looking towards inflow direction) (Fig.4.15). The upper layer density fields, velocities, surface elevation patterns and the barotropic velocities are shown in figure 4.15 and 4.16 for inflow and outflow,
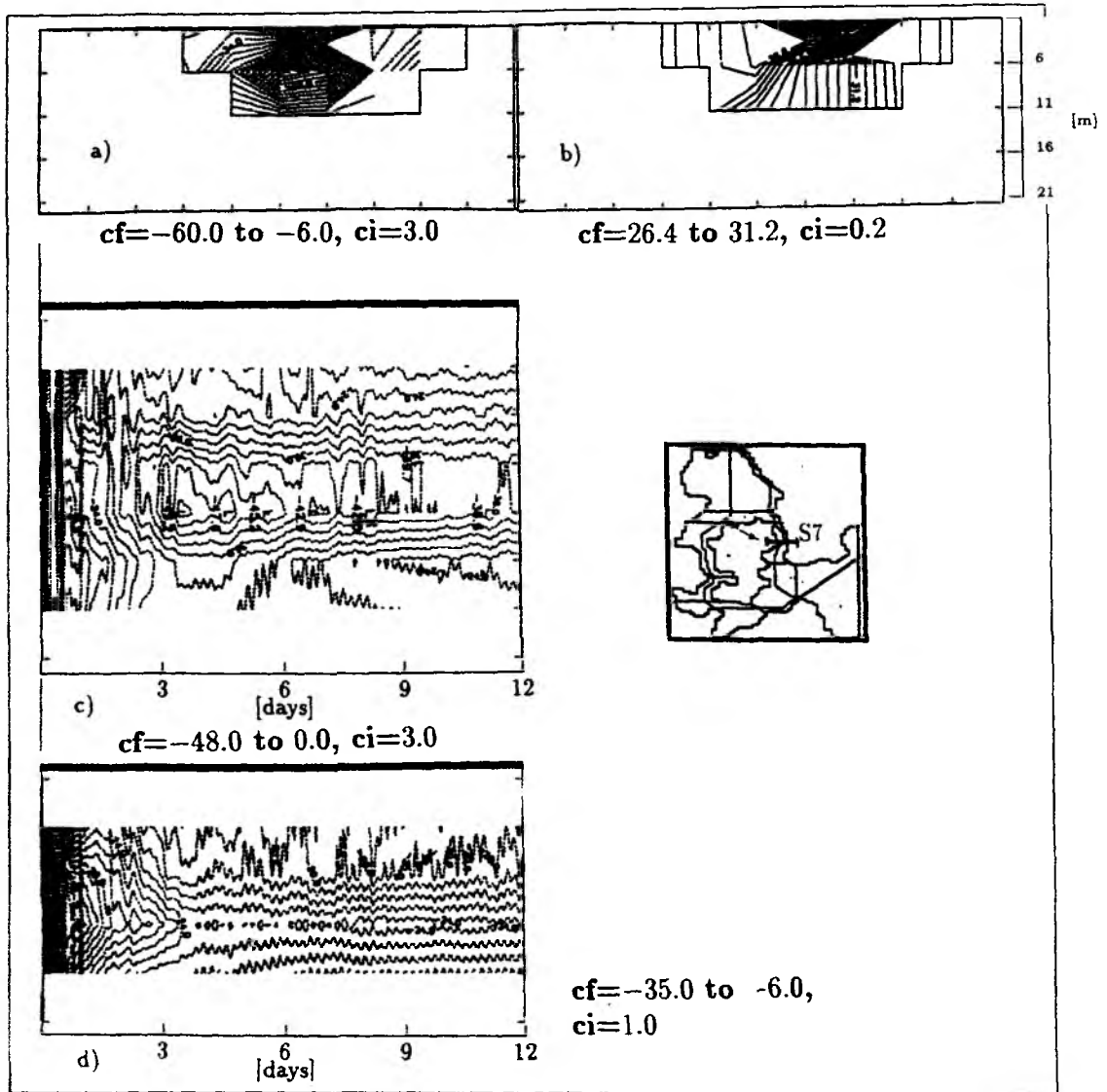
cf=−60.0 to −6.0, ci=3.0   cf=26.4 to 31.2, ci=0.2

cf=−48.0 to 0.0, ci=3.0

cf=−35.0 to -6.0,
ci=1.0

Figure 4.19: *Section S7 at the end of Day 12 (INFLOW) a) v-component of velocity b) Salinity. Space-time contour plot c) for the surface layer velocity d) for the bottom layer.*

respectively. These figures give a qualitative picture of the outflow and inflow situations. It can be concluded from the comparison of the barotropic velocities with the total velocities (Fig.4.15b,d and Fig.4.16b,d) that both inflow and outflow velocities are mostly barotropic.

In the following, details of the salinity distributions and the velocity values will be given for selected sections. Steady state inflow and outflow patterns and salinity
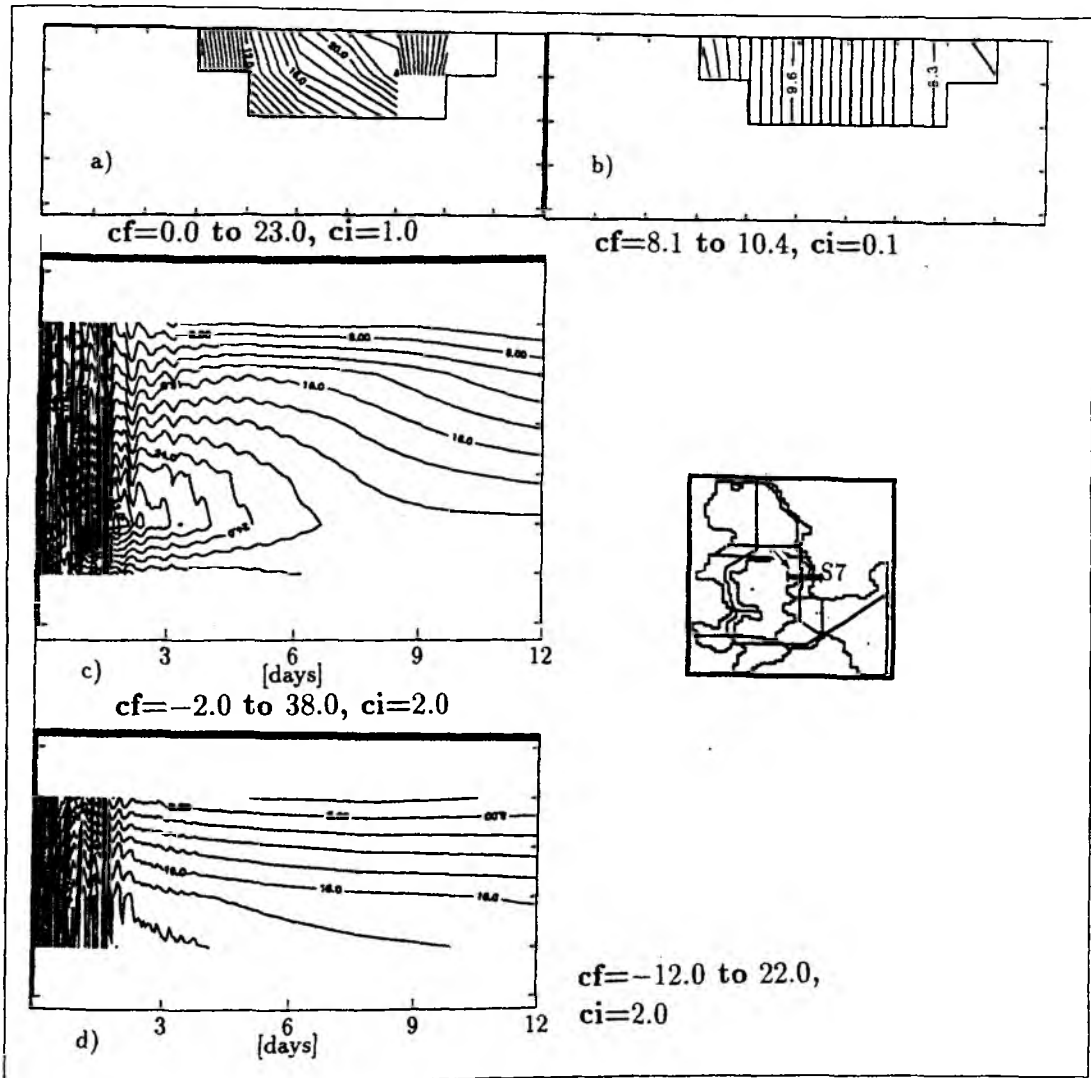
Figure 4.20: *Section S7 at the end of Day 12 (OUTFLOW) a) v-component of velocity b) Salinity. Space-time contour plot c) for the surface layer velocity d) for the bottom layer.*

distributions are shown for the Belt (section B4) and the Sound (section S7, Fig.4.17-20). The direction of the currents is different from the thermohaline case. In general, from the surface to the bottom the velocities are to the south in the case of inflow and to the north in the outflow case. Only in the Belt the barotropic forcing used is not strong enough to overcome the thermohaline component in the bottom layer completely in the outflow case. This situation is also seen in section B5 (Fig.4.21).
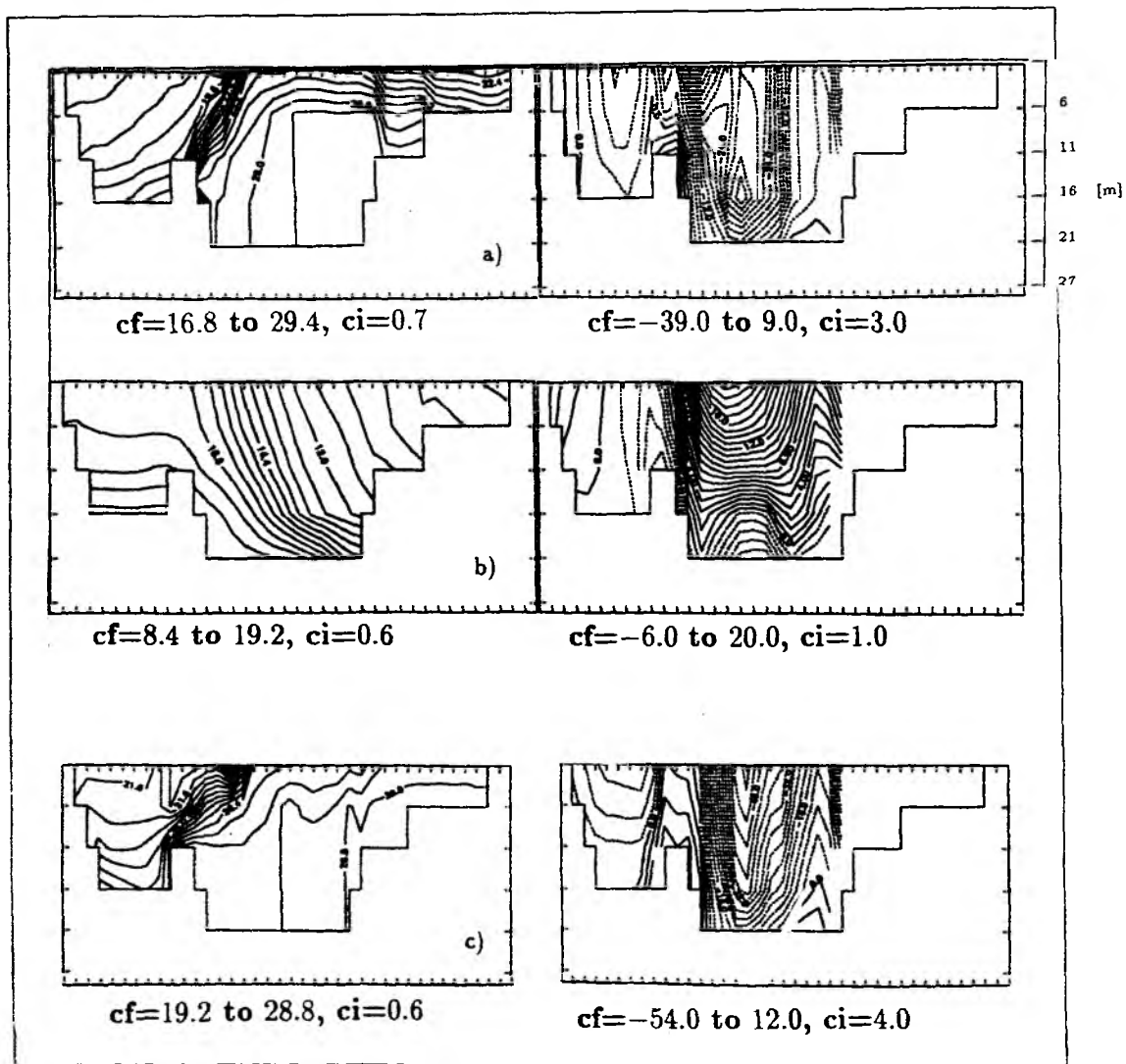
cf=16.8 to 29.4, ci=0.7 **cf=−39.0 to 9.0, ci=3.0**

cf=8.4 to 19.2, ci=0.6 **cf=−6.0 to 20.0, ci=1.0**

cf=19.2 to 28.8, ci=0.6 **cf=−54.0 to 12.0, ci=4.0**

Figure 4.21: *Salinity and velocity distributions (v-component) for section B5 at the end of Day 12, for a) INFLOW b) OUTFLOW and c) INFLOW with constant west wind. Location of the section is shown in figure 4.2*

The maximum velocity values for the inflow are approximately three times as large as the values for the outflow case, although the strength of the barotropic forcing is the same for both cases. Perhaps the areas in which the surface displacements are prescribed, are not chosen exactly same. But in chapter 3 barotropic forcing was applied symmetrically and of exactly the same strength with the same results, that the velocities have larger values in the inflow case. The question arises, why the ve-

locities for the inflow case are greater than those for the outflow. The answer is, that during outflow continuous stratification is maintained (no topographic breaktrough, KILLWORTH, 1989b), and coastal trapped waves can be seen in the outer part of the channels. On the other hand during inflow the dense fluid near the topography at the Kattegat has a fundamental effect on the transmission of wave energy. In this case topography intersects the density–layers. After the quasi–steady state is reached not only coastal trapped waves but also topographically trapped waves exist in the system, and a finite amount of mass can be transported (oscillatory) along the topography.

After the quasi–steady state is reached in the Belt (section B4), the maximum velocities are 90 cm/s for inflow and 30 cm/s for outflow in the upper layer (Fig.4.17c and 4.18c) and 24 cm/s for inflow and 12 cm/s for outflow in the lower layer (Fig.4.17d and 4.18d). In the Sound (section S7) maximum velocities are 36 cm/s and 27 cm/s for inflow in the upper and lower layers, respectively (Fig.4.19c and 4.19d) and 20 cm/s and 16 cm/s for outflow (Fig.4.20c and 4.20d). Maximum velocities during outflow occur in the upper layer (section B4, B5 and S7, Fig.4.18a, 4.21b and 4.20a). During inflow the maximum appears close to the bottom in shape of a bore (sections B5 and S7, Fig.4.17a and 4.19a). As mentioned before, in case of inflow barotropic and baroclinic components are in balance with the external forcing in the upper layer. Consequently maximum velocities must occur in the lower layer due to the addition of the thermohaline component and barotropic external forcing there. This can also be explained by the hydraulic theory (STIGEBRANDT, 1976, 1980 and BAINES and GRANEK, 1990). According to this theory a significant amount of water flows in the lower layer, if the Froude number $F > 1$. In the present study it is found that the Froude number is always greater than 1 for the inflow case (this result is not presented). During almost all of the time in the upper layer the maximum velocity values in the Sound are smaller than the values in the Belt for both inflow (compare figure 4.17c and 4.19c) and outflow (compare figure 4.18c and 4.20c). On the other hand, in the lower layer the maximum velocity values in the Sound are larger than the values in the Belt for both inflow (Fig.4.17d and 4.19d) and outflow
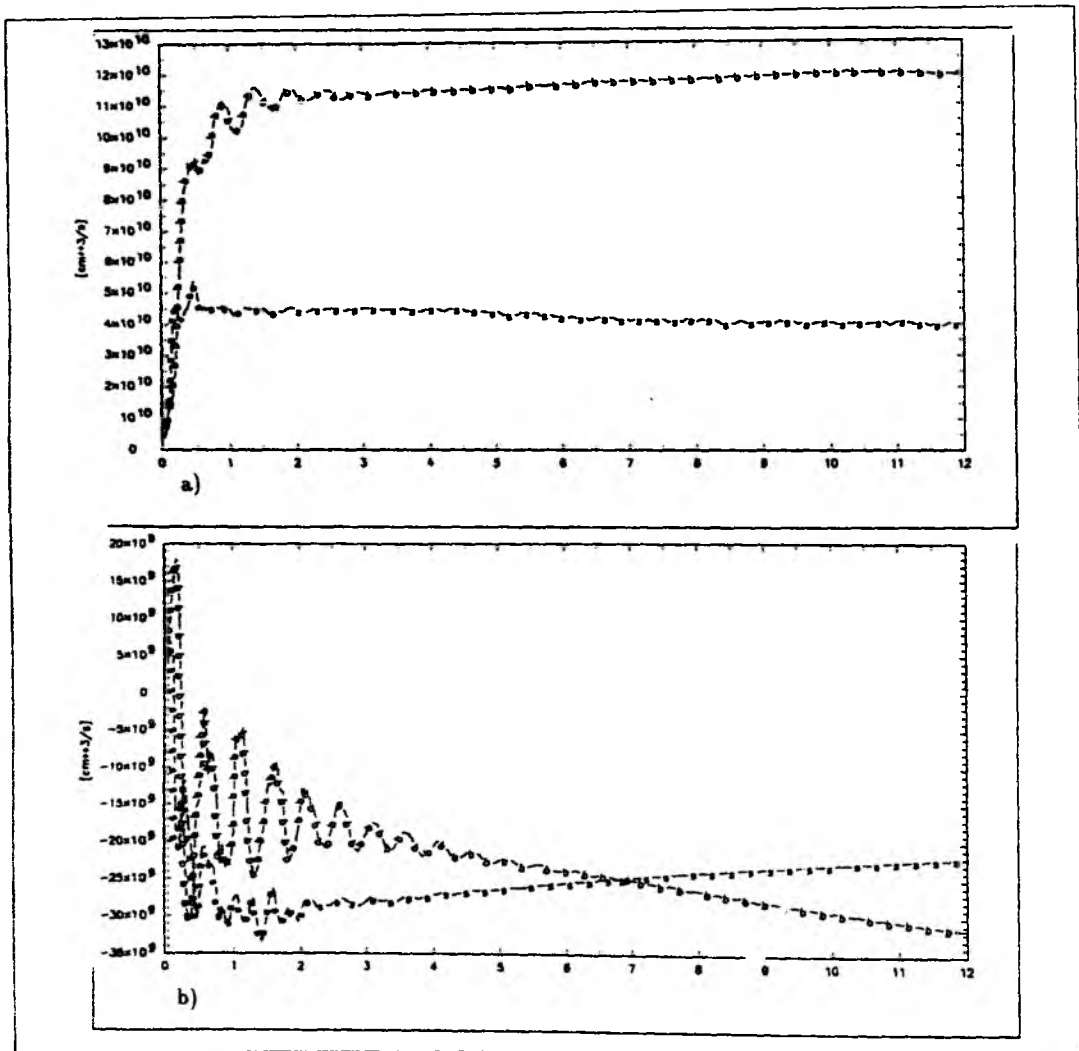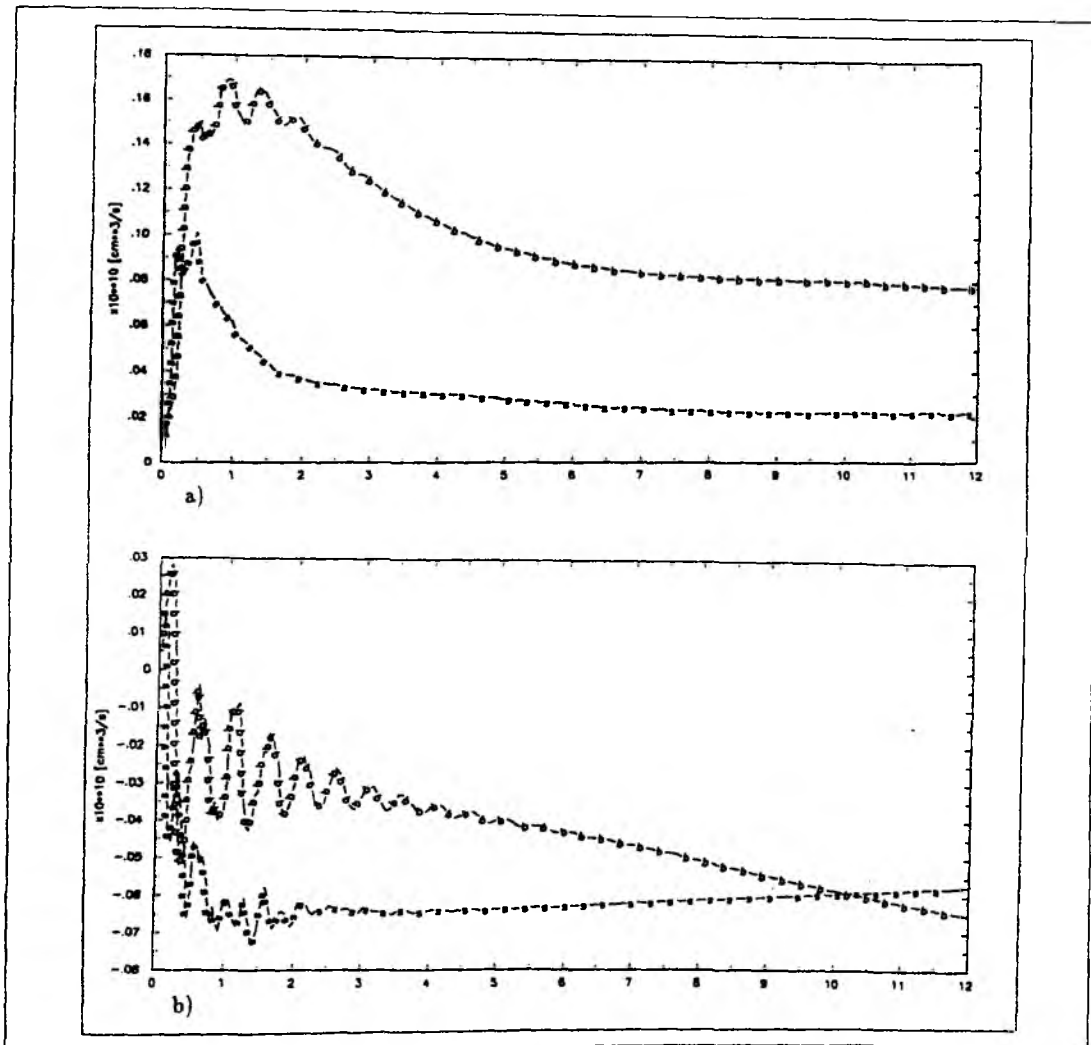
Figure 4.22: Volume transport versus time (days) for the strongly stratified case and for constant $\Delta\eta(= 20\ cm)$ a) INFLOW and b) OUTFLOW experiments, b–Belt and s–Sound.

(Fig.4.18d and 4.20d).

Figure 4.21c shows the result of the inflow experiment with constant west wind. This case will be explained in more detail after the transport relation in the Belt and the Sound is given.

Values of the volume transport in the Belt are greater than the values in the Sound.

Examples of the volume and salt transports in the Belt (B4) and in the Sound (S7)

Figure 4.23: Salt transport versus time (days) for the strongly stratified case and for constant $\Delta\eta(= 20\ cm)$ a) INFLOW and b) OUTFLOW experiments, b-Belt and s-Sound.

for the outflow and for the inflow situations are shown in figures 4.22,23. The transport values depend strongly on the difference in surface elevation prescribed between the far ends of the straits. A constant difference in surface elevations causes almost constant volume and salt transports in both straits. The propagation of salt for the outflow case is very slow and the phase speed of the front is approximately 2.8 km/day. Given an inclination of the sea surface of 20 cm between the Kattegat

and the Arkona basin, the volume transport in the Sound amounts to $4. \times 10^{10} \ cm^3/s$ in the inflow case. In the Belt the volume transport is $11.9 \times 10^{10} \ cm^3/s$. Thus, 25% of the volume transport occur in the Sound and 75% in the Belt (Table 4.1).

Table 4.1: Volume transport ($\times \ 10^{10} \ cm^3 \ s^{-1}$) for the strongly stratified case and for a given constant $\Delta\eta$ along the straits ($\Delta\eta = 20 \ cm$ between the far ends of the straits) (inflow, outflow and wind driven experiments). The second values are the percentage of the total transport.

	Inflow	Outflow	Inflow(W)
Belt	11.9 75.0 %	3.15 59.0 %	14.4 72.0 %
Sound	4.0 25.0 %	2.2 41.0 %	5.6 28.0 %

For the inflow case the same relation holds for the salt transport, 22% ($0.022 \times 10^{10} \ cm^3/s$) in the Sound and 78% ($0.078 \times 10^{10} \ cm^3/s$) in the Belt (Table 4.2). The outflow case gives a different relation, one reason being the prescribed density gradient that is concentrated in the straits region. This density field drives internal dynamics and affects the transport relations in the outflow case. In the stratified case an outflow in the upper layer and also in the lower layer occurs very rarely in the Belt (WYRTKI, 1954b). If the stratification is weak in the straits, the volume and the salt transport relation agree with the observed relations in the Belt and the Sound.

Table 4.2: Salt transport ($\times \ 10^{10} \ cm^3 \ s^{-1}$) , same as Table 4.1.

	Inflow	Outflow	Inflow(W)
Belt	0.078 78.0 %	0.065 59.0 %	0.089 64.0 %
Sound	0.022 22.0 %	0.057 41.0 %	0.050 36.0 %

The volume and salt transport relations are summarized in table 4.3 for the strongly stratified case. They are given as a function of $\Delta\eta$ (difference in surface elevations between the Kattegat and the Arkona basin). In the next section the transport relations for the weakly stratified case will be given. Some relations will be presented as a function of the difference in surface elevations not along but across the straits.
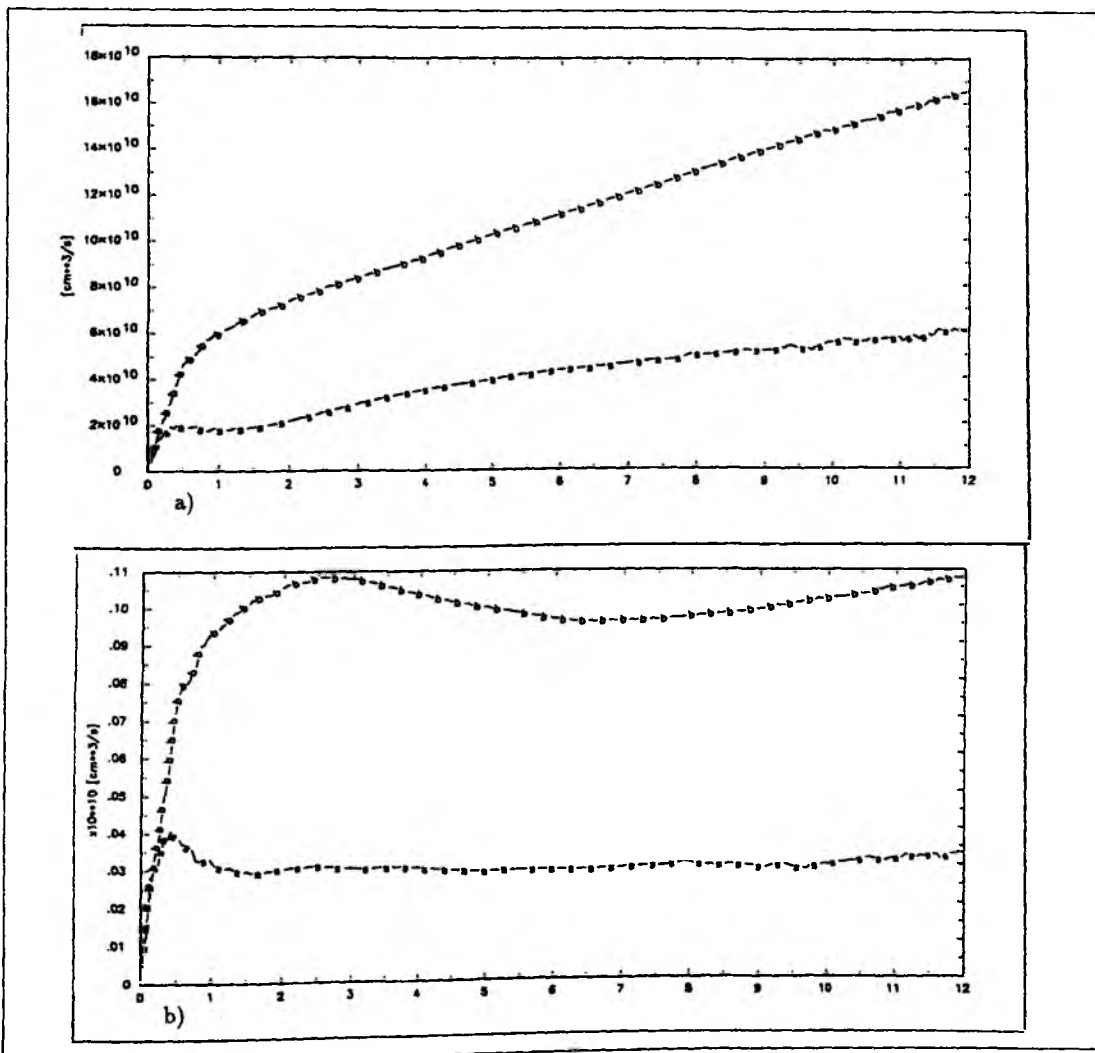

Figure 4.24: a) Volume and b) salt transport versus time (days) for the strongly stratified case and for linearly increasing $\Delta\eta$, $\Delta\eta$ increases from zero to 20 cm during 12 days. INFLOW case, b–Belt and s–Sound.

For the inflow case a boundary layer forms at the bottom in all sections and in both straits: In section S7 the water is mixed vertically from the surface to the bottom for the outflow case. In the other sections boundary layer formation can not be determined for the outflow case due to the absence of topographic waves.
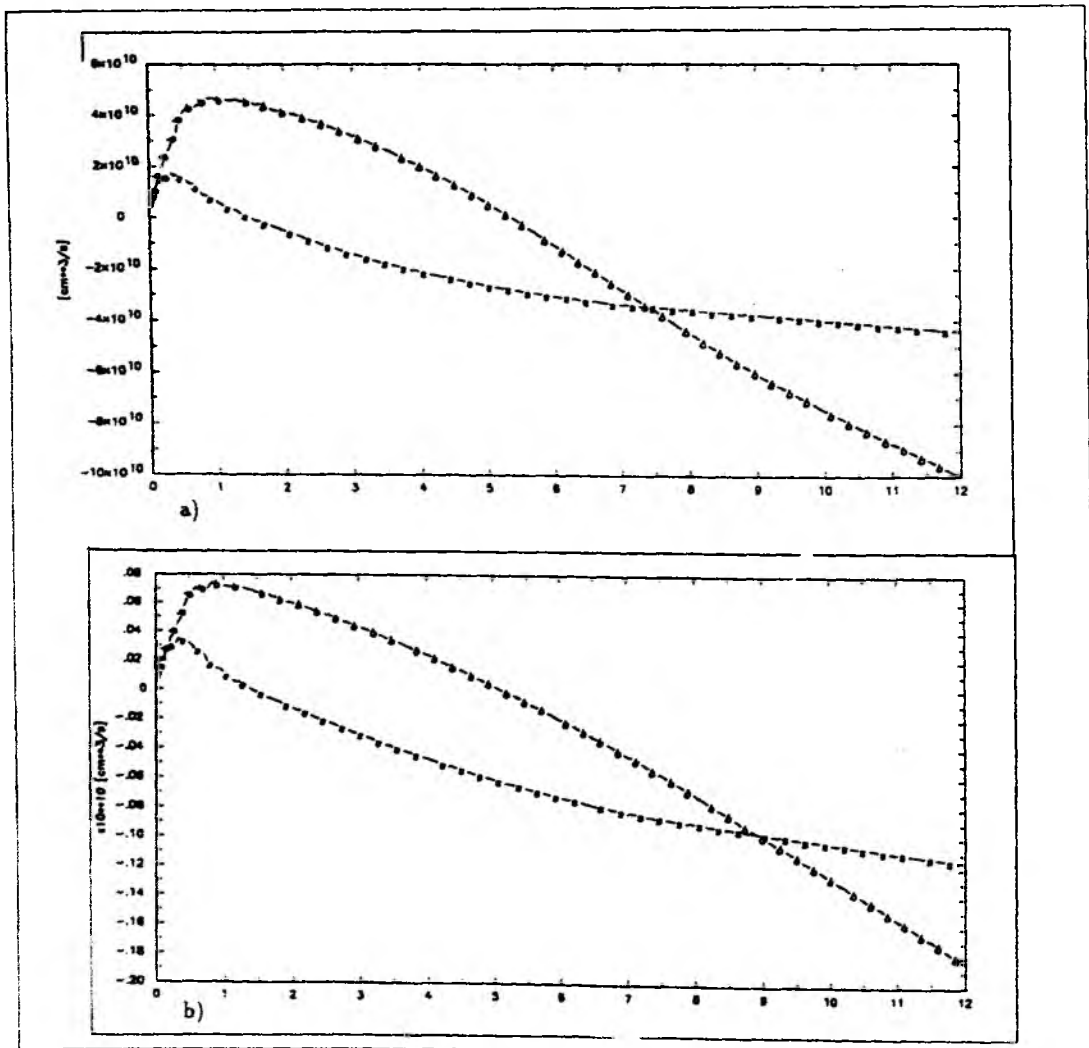

Figure 4.25: a) Volume and b) salt transport versus time (days) for the strongly stratified case and for linearly increasing $\Delta \eta$, $\Delta \eta$ increases from zero to 20 cm during 12 days. OUTFLOW case, b–Belt and s–Sound.

Table 4.3: Volume transport ($\times$ 10^{10} cm^3 s^{-1}) for the strongly stratified case and for a given constant $\Delta\eta$ along the straits ($\Delta\eta = 40$ cm between the two far ends of the straits) (inflow and outflow experiments). The second values are the percentage of the total transport, and third line gives the transport relation as a function of $\Delta\eta$ (from figures 4.24a and 4.25a).

	Inflow	Outflow
Belt	16.7 73.6 % $0.27\Delta\eta + 5.9$	10.0 69.5 % $0.39\Delta\eta - 5.6$
Sound	6.0 26.4 % $0.1\Delta\eta + 2.$	4.4 30.5 % $0.06\Delta\eta + 2.$

An additional experiment was performed to determine the effect of wind forcing. The wind stress is chosen constant in x-direction ($\tau = 2g$ cm^{-1} s^{-2}) and the same sea level difference between the northern and eastern boundary is used as in the previous experiments. The differences to the inflow case with barotropic forcing only are the following:

- Small-scale structures in the velocity fields have disappeared in all sections. The reason is the existence of an Ekman layers. Velocities decrease gradually from the surface to the Ekman depth. No strong currents are formed over topography; the topographic effect is not so strong as in the inflow case. Short wave oscillations dissapear. Maximum velocities can be found in the upper layer in the middle of the channel and not in the lower layer, as is the case without wind forcing (Fig.4.21a,c). Flow shear does not occur near topography.

- Vertical homogenization can be seen in the salinity field. Also the horizontal salinity differences are smaller across the straits (Fig.4.21a,c and 4.26a,c). At the end of day 12 (Fig.4.26) water above the Drodgen sill is more saline for the wind driven case than for the other inflow case. An additional sea level difference due to the west wind is responsible for the appearance of more saline water.
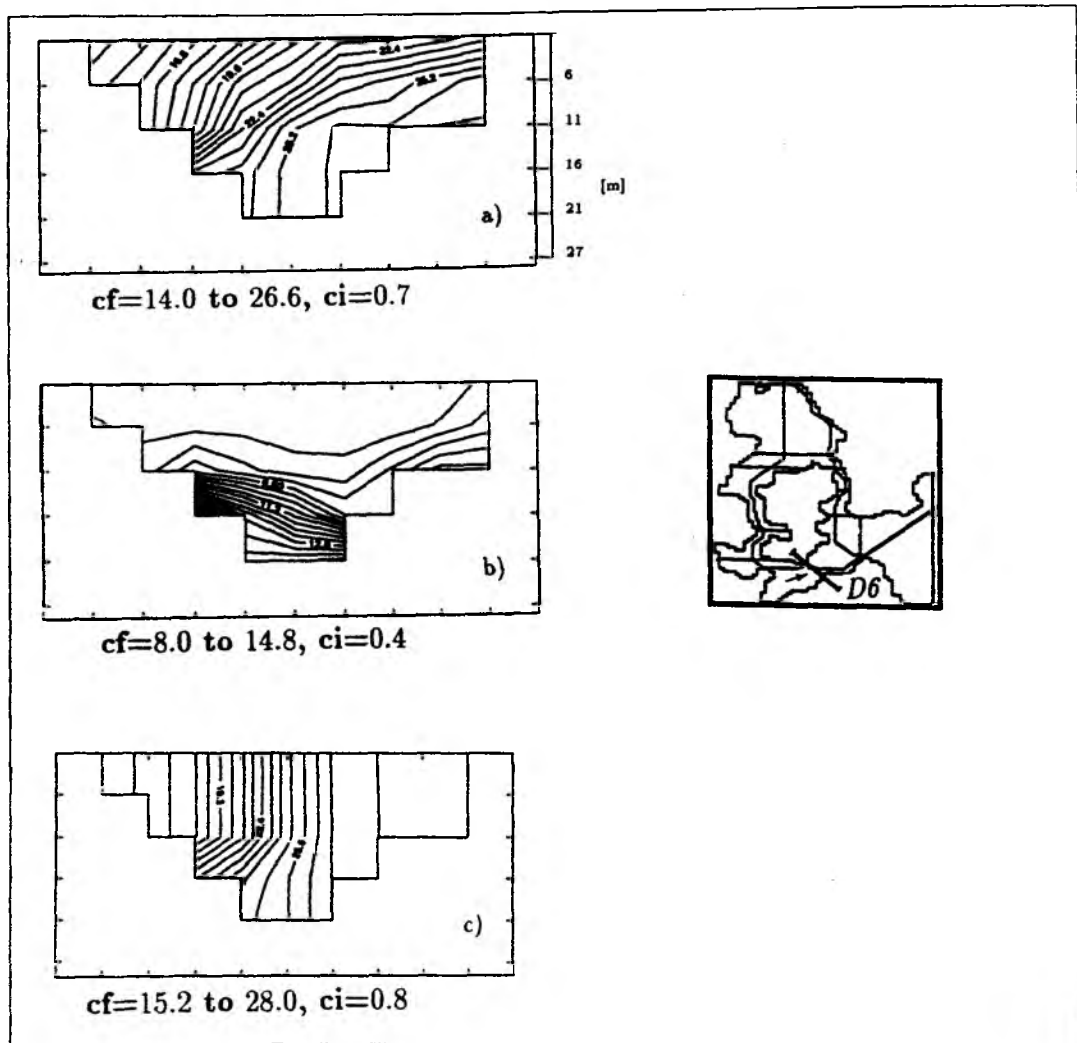
cf=14.0 to 26.6, ci=0.7

cf=8.0 to 14.8, ci=0.4

cf=15.2 to 28.0, ci=0.8

Figure 4.26: *Salinity values for section D6 (Drodgen) at ᵤₜe end of Day 12, for a) INFLOW b) OUTFLOW and c) INFLOW at constant west wind.*

- In the Arkona basin (section A9, Fig.4.27) homogenization occurs in the salinity field in the lower layer and also in the upper layer. Consequently, a strong vertical salinity gradient is established at mid-depth. In the space-time contour plot the salinity values of layer 7 (Fig.4.28) show that the more saline water reaches the Arkona basin in a shorter time for the case with constant westerly wind than for the case without wind forcing. For example, water with a salinity of 24 psu reaches section A9 in 6 days for the wind driven case. The same salinity value is found in the Arkona basin after 9 days for the case without wind forcing (Fig.4.28a). The section along the Belt (L12, Fig.4.29) shows more intensive vertical mixing as a result of wind forcing and the flow of more saline water into the Arkona basin in comparison to the case without wind.
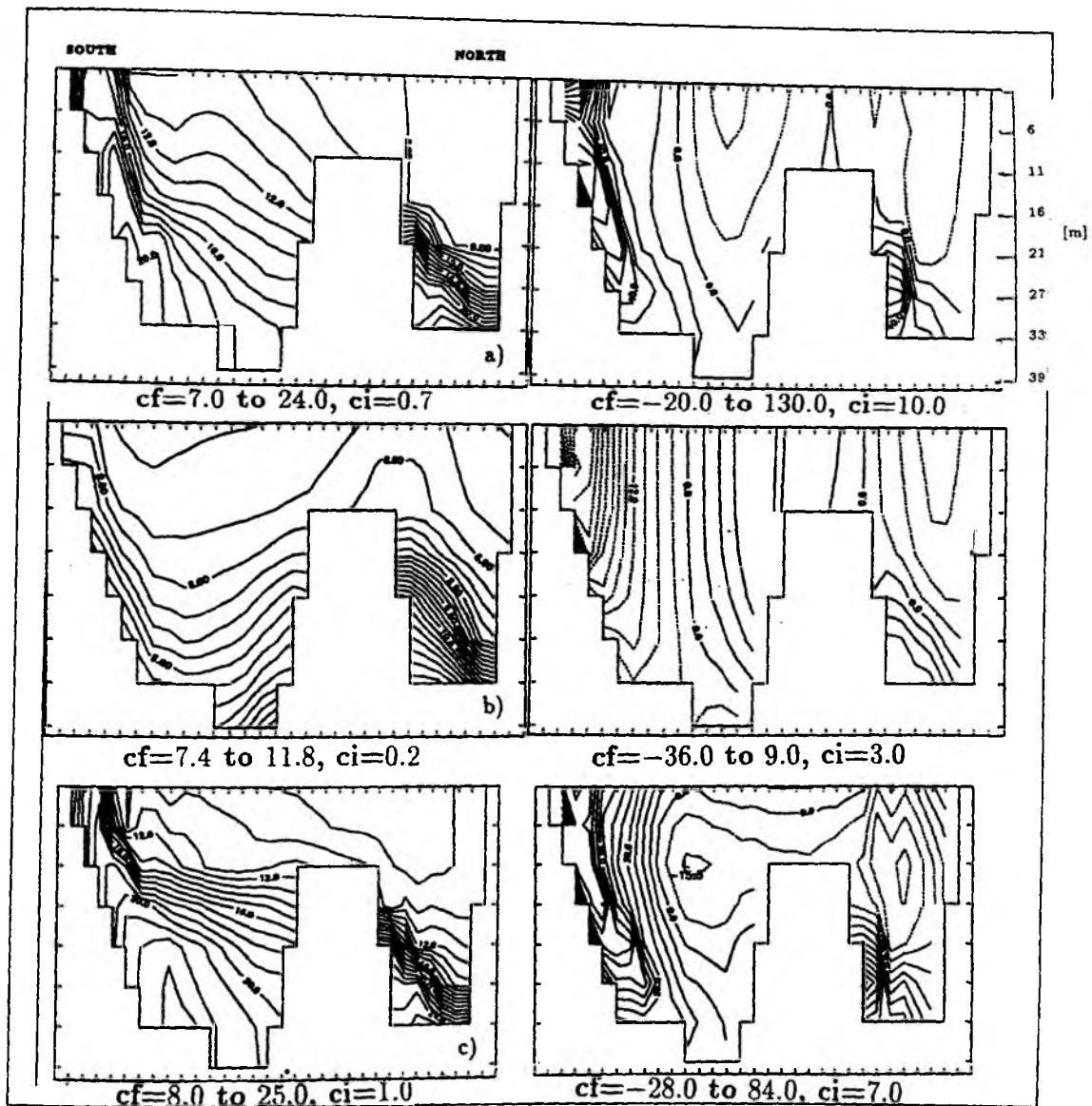
86

Figure 4.27: *Salinity and velocity values (u-component) for section A9 (Arkona) at the end of Day 12, for a) INFLOW b) OUTFLOW and c) INFLOW at constant west wind.*

- An important result is the salt transport in the Belt. At the beginning of the adjustment process the salt front has an intrusion speed of 26.8 *km/day* and at the end of day 12 with 16.0 *km/day*. In the wind driven case during the first adjustment phase salt is intruded faster with an speed of 28.5 *km/day* and at day 12 with 15.9 *km/day*. The calculated intrusion speeds for both cases at the beginning of the adjustment do agree with the values observed for mid-November 1976 by LASS and SCHWABE (1988). They found the speed of the salinity front to be 30 *cm/s* (25.9 *km/day*). Altough the first adjustment process is more rapid for the wind–driven case than for the case without wind

87

forcing, after 12 days the salt front speed is approximately equal in both cases (Fig.4.30a,c). Figure 4.28b and 4.28b show that the salt intrusion is weak in the outflow case compared to the two inflow cases. Figures 4.21b,4.26b,4.27b
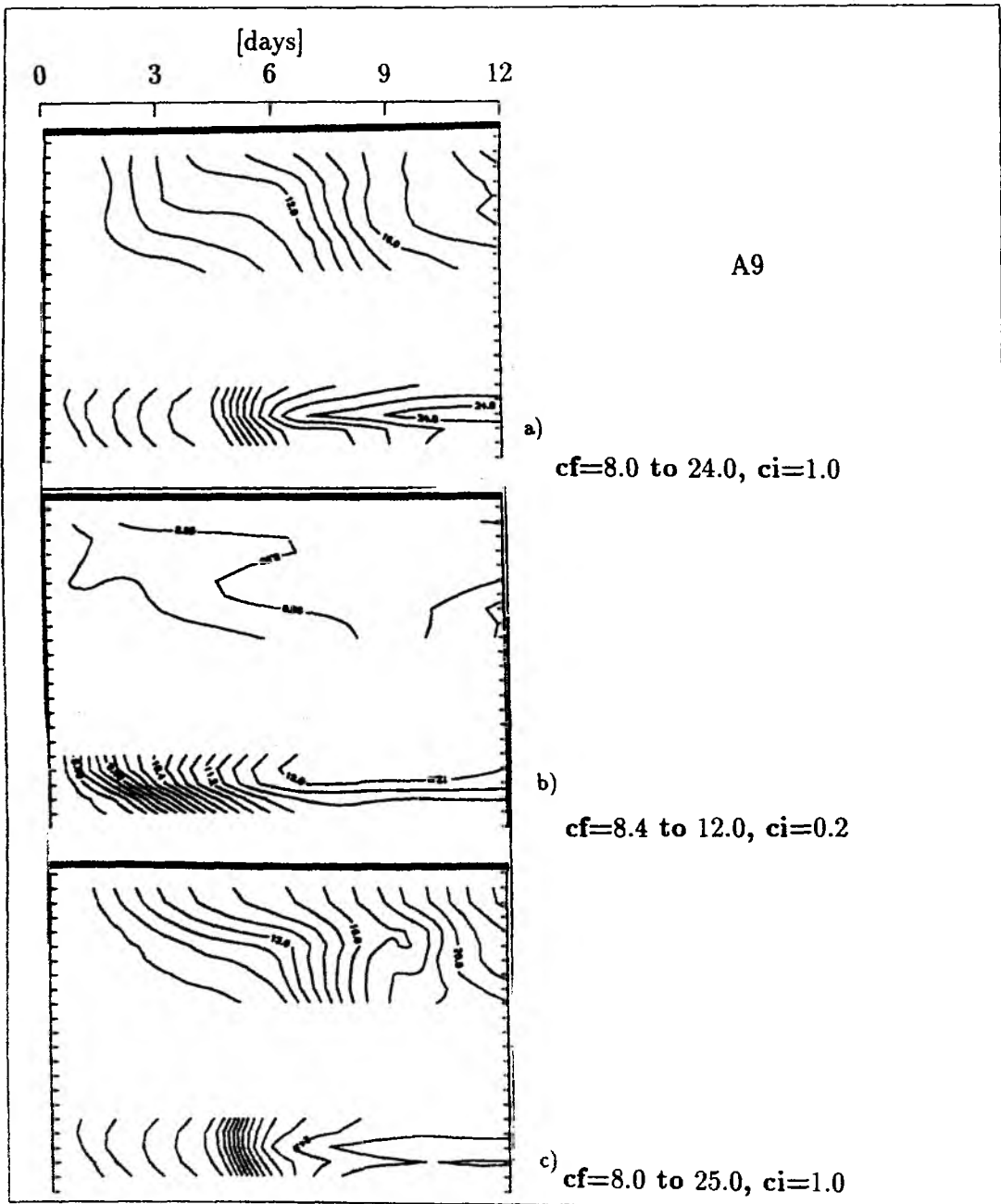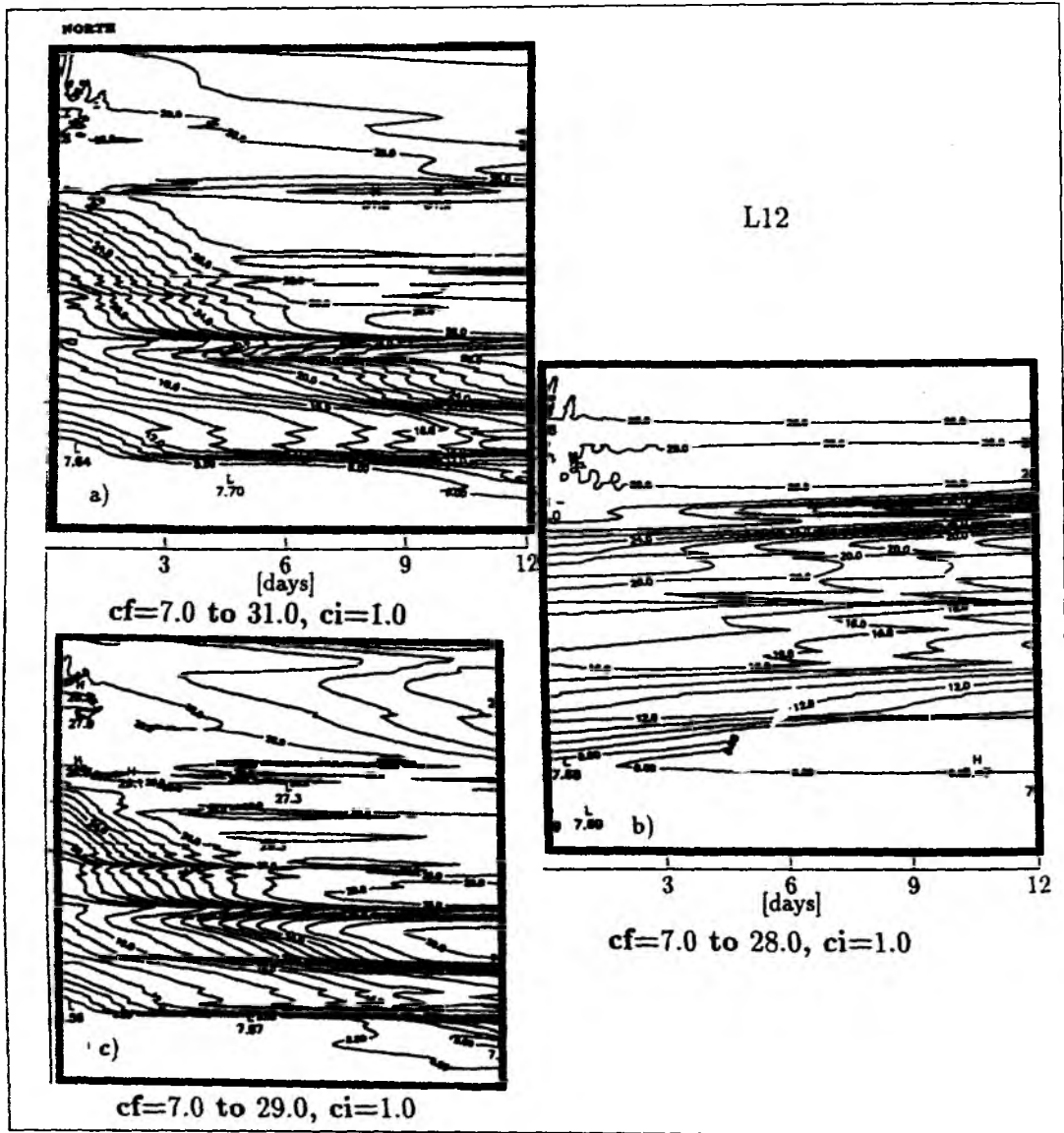

Figure 4.28: *Salinity at section A9 (layer 7). Space-time contour plot for three cases a) INFLOW b) OUTFLOW and c) INFLOW at constant west wind.*

and 4.29b show that the salt stratification occur in the lower layer for the outflow case. Salt intrusion during outflow is very slow and the intrusion speed is approximately 2.8 km/day.
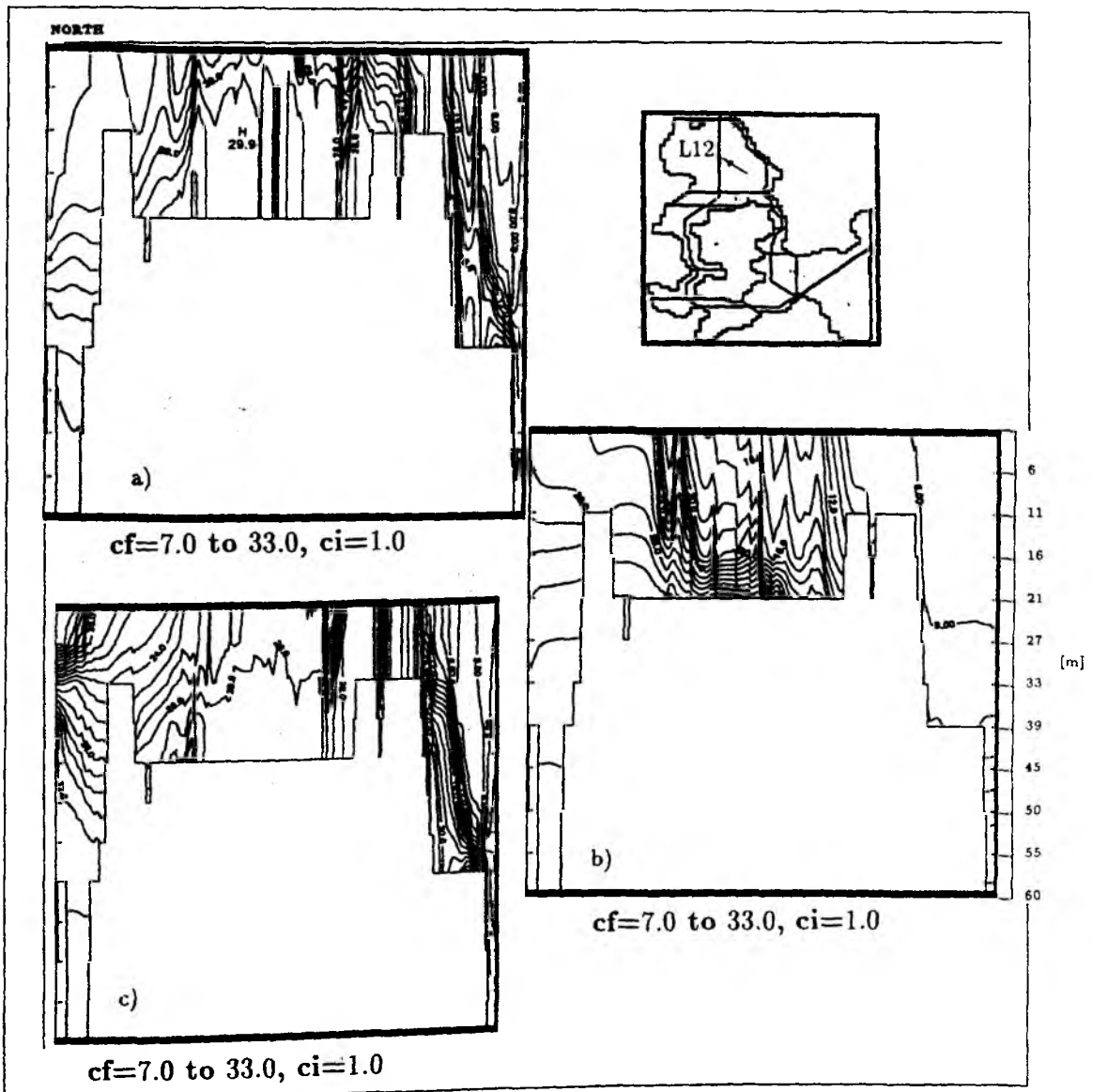
Figure 4.29: *Salinity at section L12 (along the Belt) a) INFLOW b) OUTFLOW and c) INFLOW at constant west wind.*

Figure 4.30: *Salinity at section L12 (layer 3). Space-time contour plot for a) IN-FLOW b) OUTFLOW and c) INFLOW using constant west wind.*

- Volume and salt transport are increased in the wind-driven case (Fig.4.31). The total volume transport in both straits is 15.9×10^{10} cm^3/s without wind and 20.0×10^{10} cm^3/s for the wind-driven case. The relative transport in the Sound and the Belt change with wind forcing. The volume and salt transports increase in the Sound and decrease in the Belt (Table 4.3).
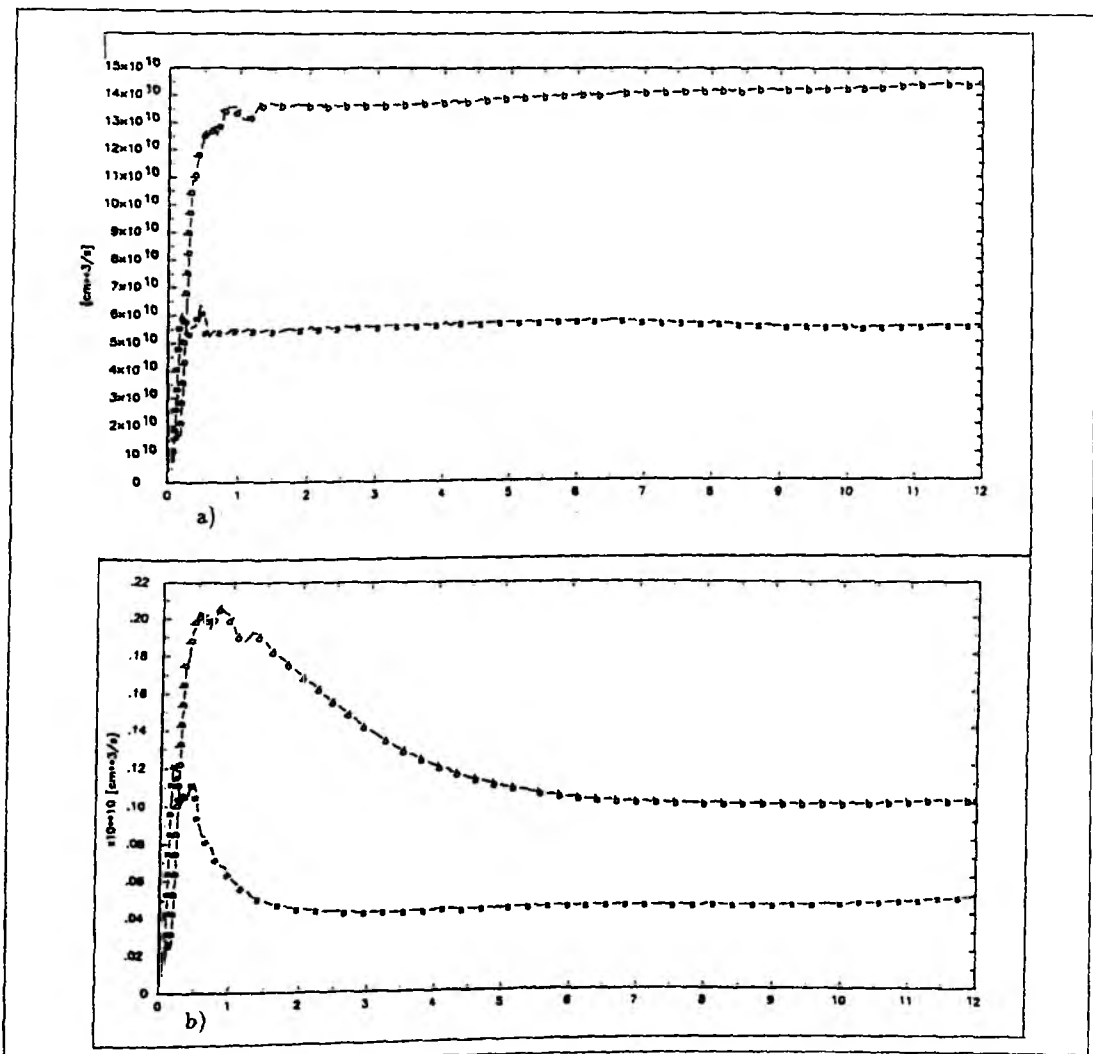
Figure 4.31: a) Volume and b) salt transport versus time (days) for the strongly stratified case and for constant $\Delta\eta(= 20 \ cm)$, wind driven experiments, b-Belt and s Sound.

4.3 The Relation Between Surface Elevation and Volume Transport

The volume transport through the Belt has been discussed by a number of authors. The water exchange was described with the *Helmholtz resonator* principle by SVANSSON (1980) and STIGEBRANDT (1980). WELANDER (1974), STIGEBRANDT (1983) and FARMER and MØLLER (1990) tried to describe the exchange of water in the Belt using the hydraulic relation. The geostrophic water exchange was studied by TOULANY and GARRETT (1984, here after TG), LASS and SCHWABE (1988) and LUNDBERG and WALIN (1990). Another approach not related to the Belt) is by WHITEHEAD (1986), who added a second term to the hydraulic relation for the transport through a channel which arises from lateral shear due to rotation Except for the Helmholtz resonator, these relations will be compared with the .model results described here. From the results of the two–basin and Baltic experiments we have found that the barotropic force supplies all the necessary transport. In this comparison the baroclinic effect on the transport relations is ignored. It is assumed that the transport is dominantly barotropic. Otherwise a correction term can be added to the transport relations. The expressions for the transport are as follows: The geostrophic relation

$$Q_g = gh\Delta\eta/f, \qquad (4.1)$$

the hydraulic relation

$$Q_h = Wh(2g\Delta\eta)^{1/2} \qquad (4.2)$$

and Whitehead's hydraulic equation

$$Q_w = Q_h - \frac{1}{2}fW^2h. \qquad (4.3)$$

Here g is the acceleration due to gravity, f is the Coriolis parameter, W is the width of the strait, h is the depth and $\Delta\eta$ is the difference in surface elevation across the channel. We used the surface elevations across the channel instead of surface elevations along the channel, also for the hydraulic relations, which needs
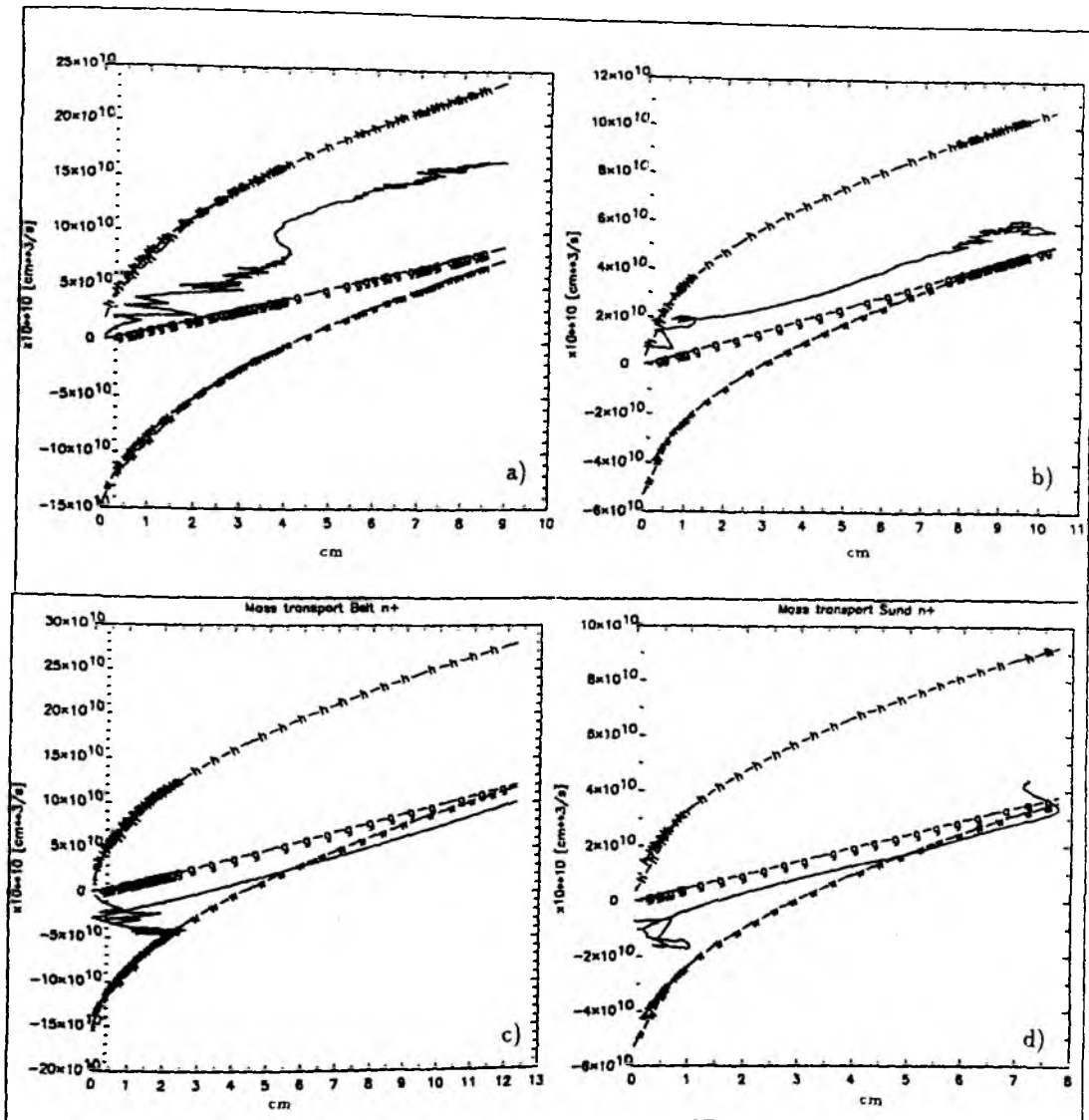
Figure 4.32: Comparison of three methods for calculating the volume transport with the model results (straight line) (h–hydraulic, g–geostrophic, w–Whitehead's hydraulic relations): Volume transport as function of the difference in surface inclination across the straits. a) INFLOW in the Belt b) INFLOW in the Sound c) OUTFLOW in the Belt and d) OUTFLOW in the Sound.

surface elevations along the channel. They can be used for the hydraulic relation if the assumption made by TG is correct. This assumption requires that the difference in surface level along the strait is equal to the difference in surface level across the strait. LASS and SCHWABE (1988) assumed that the longitudinal sea level difference between the Baltic and the Kattegat forces the transverse one. They obtained a correlation factor of 0.65 for this assumption. They also found that the

93
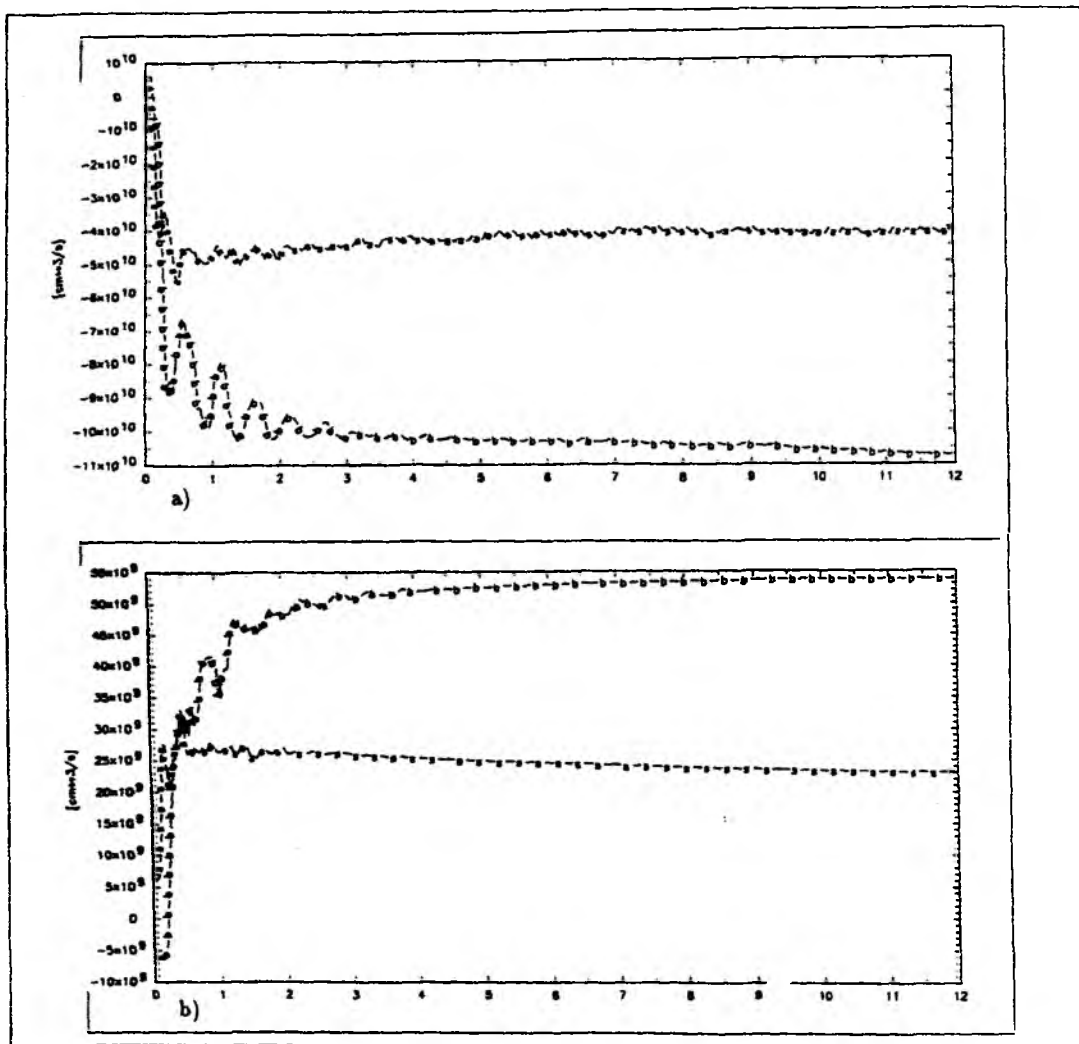
Figure 4.33: Volume transport versus time (days) for the weakly stratified case and for constant $\Delta \eta (= 20\ cm)$ a) INFLOW and b) OUTFLOW experiments, b-Belt and s-Sound.

time delay between both pressure gradients (along and across the channel) suggests that the transverse gradient adjusts after one inertial period and that the transverse sea level difference amounts to about half of the longitudinal sea level difference. In the present study we changed the surface levels linearly at the boundaries. Thus the surface elevations were maintained along the Belt. As a result of these along surface elevations a surface elevation across the channel were produced. A section 4.2 transport curves have been plotted versus along surface elevations. Figure 4.24a and 4.25a show the linear relation between the volume transport in the Belt and the along surface elevations in both cases, inflow and outflow. In Figure 4.32 the
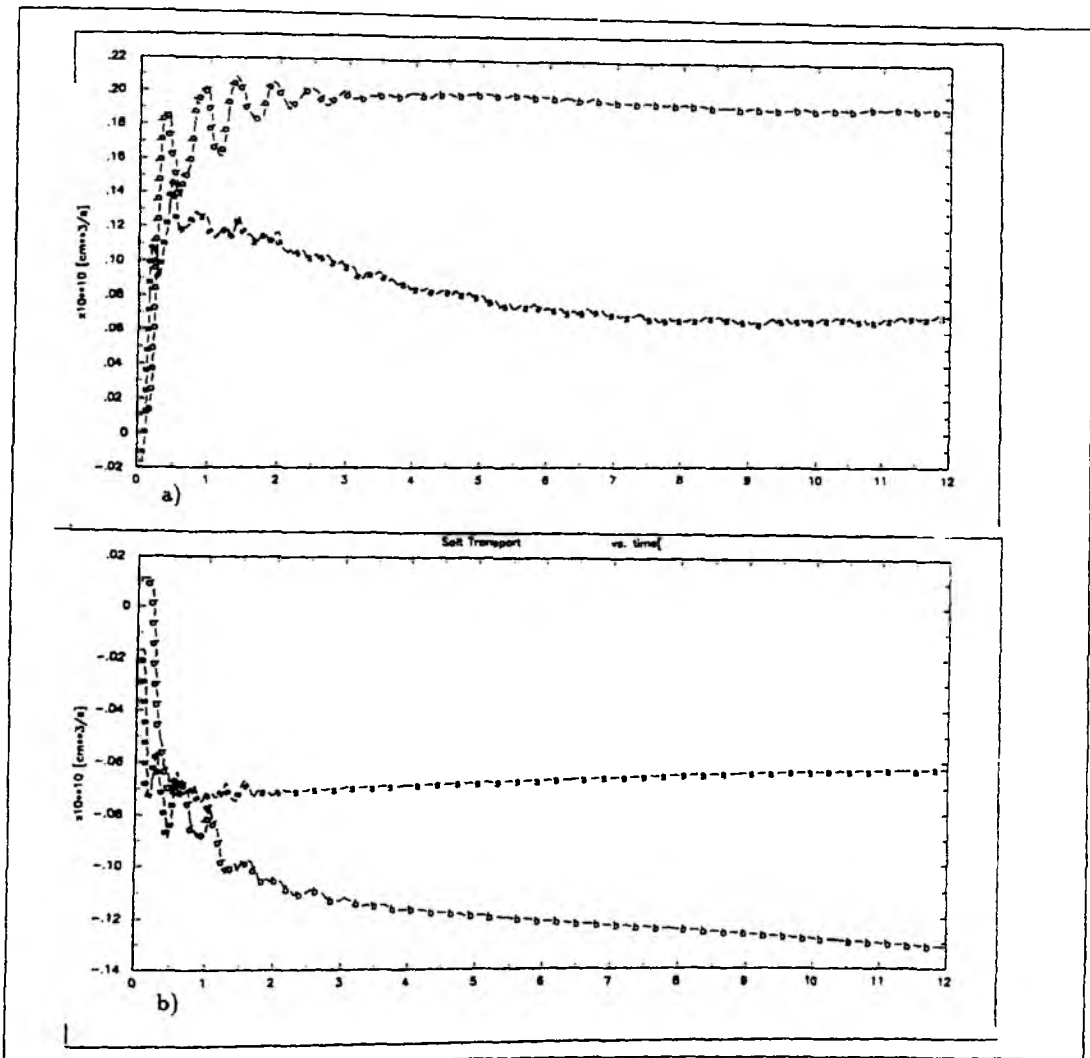
94

Figure 4.34: Salt transport versus time (days) for the weakly stratified case and for constant $\Delta\eta(= 20\ cm)$ a) INFLOW and b) OUTFLOW experiments, b–Belt and s–Sound.

volume transports are plotted versus the $\Delta\eta$ across the channel (not prescribed, result of the longitudinal surface elevations) using the assumption of TG and relations 4.1–4.3. From these figures 4.24a,4.25a and 4.32c,d (the curves drawn with straight line) we can conclude that in the Belt the transport can be described by the geostrophic relation during outflow situations. The small shift between the curves of the geostrophic relation and the model results is due to the baroclinic effect. This means that we must add a correction terms to the geostrophic relations due to the density currents. Figure 4.25b shows that the salt transport is linearly dependent on $\Delta\eta$. The transport values for the inflow situation in the Belt however deviate from
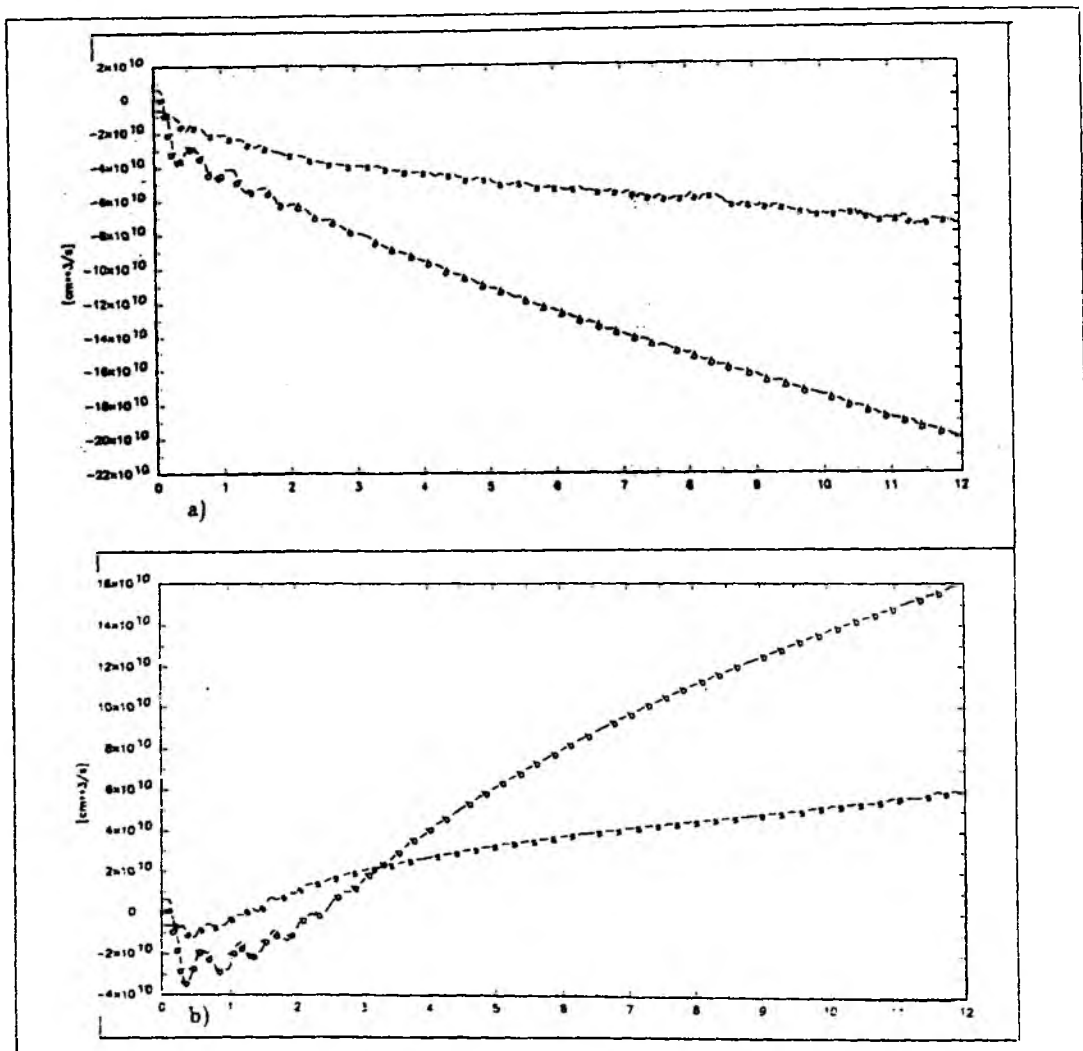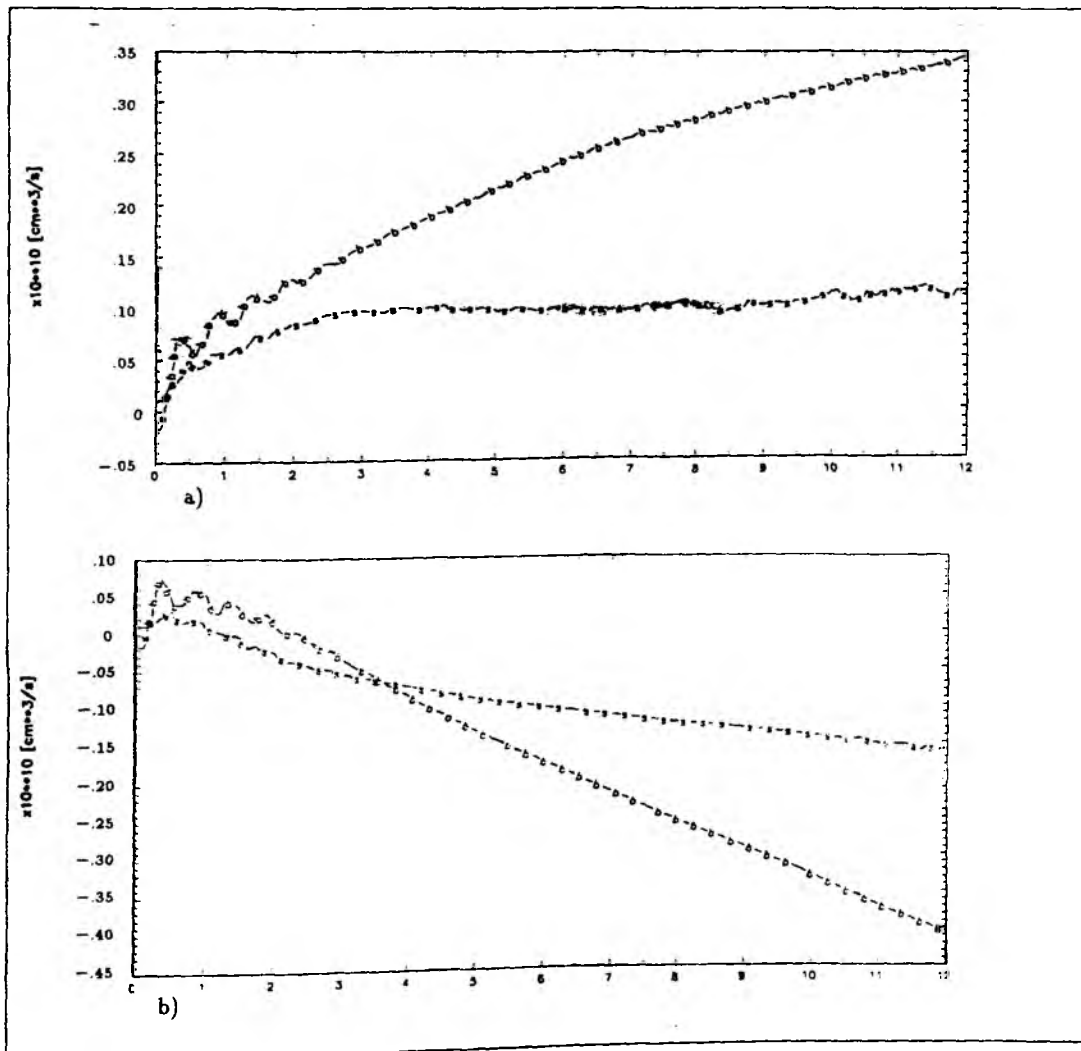
95

Figure 4.35: Volume transport versus time (days) for the weakly stratified case and for linearly increasing $\Delta\eta$ ($\Delta\eta$ increases from zero to 40 cm during 12 days), a) INFLOW and b) OUTFLOW experiments, b–Belt and s–Sound.

geostrophy. A small part of the curve for outflow in the Sound shows also deviations from geostrophy at higher surface displacements across the strait. This could be caused by internal wave generation. These waves may be reflected and a system of standing internal waves may be sustained. Another candidate is topographical scattering. As mentioned before topographic effects are favorable if the topography intersects the density–layers (KILLWORTH, 1989b). It must be remarked that for this experiment a stronger density gradient was applied between the two ends of the straits. Figure 4.24b shows that the salt transport is not linearly dependent on the

96

surface elevations in the Belt in inflow cases. From this salt transport curves we can assume that the 10 days-variability, which is mentioned before in section 4, affects the density current. It is obvious that nonlinearities play an important role for the deviation from geostrophy. In addition, Whitehead's hydraulic curves all show small transport values for small surface displacements especially at the beginning of the numerical integration (Fig.4.32). From Whitehead's study we can say that the flow in the channel is faster than Bernoulli's law allows. These curves approach to the geostrophic one with the increasing of surface dispacements with time.

Figure 4.36: Salt transport versus time (days) for the weakly stratified case and for linearly increasing $\Delta\eta$ ($\Delta\eta$ increases from zero to 40 cm during 12 days), a) INFLOW and b) OUTFLOW experiments, b–Belt and s–Sound.

In section 4.2 the transport relations were given as function of time and surface inclinations along the straits. Now, the same density values but a different distribution (weak stratification in the straits) are applied. Volume and salt transport versus time are given for the outflow and inflow cases (Fig.4.33-36). For the inflow case volume and salt transport in the Belt amount to 72% and 73%, respectively, 28% and 27% remain for the Sound (Table 4.4-5). This is in agreement with observed values for the inflow situation for almost all surface level differences across the Straits (Table 4.4-5). Large differences in surface level or weak stratification are responsible that this relation is also true for the outflow case. The slope of the curves in figure 4.35 gives the possibility to obtain a relation between the given difference in surface elevations and the transport in the Straits. Table 4.6 shows these relations for the inflow and outflow situations in the Belt and in the Sound.

Table 4.4: Volume transport ($\times 10^{10}$ cm^3 s^{-1}) for the weakly stratified case and for a given constant $\Delta\eta$ along the straits ($\Delta\eta = 20$ cm between the two far ends of the straits) (inflow and outflow experiments). The second values are the percentage of the total transport.

	Inflow	Outflow
Belt	10.7 72.3%	5.4 70.1%
Sound	4.1 27.7%	2.3 29.9%

Table 4.5: Salt transport ($\times 10^{10}$ cm^3 s^{-1}) , same as Table 4.4.

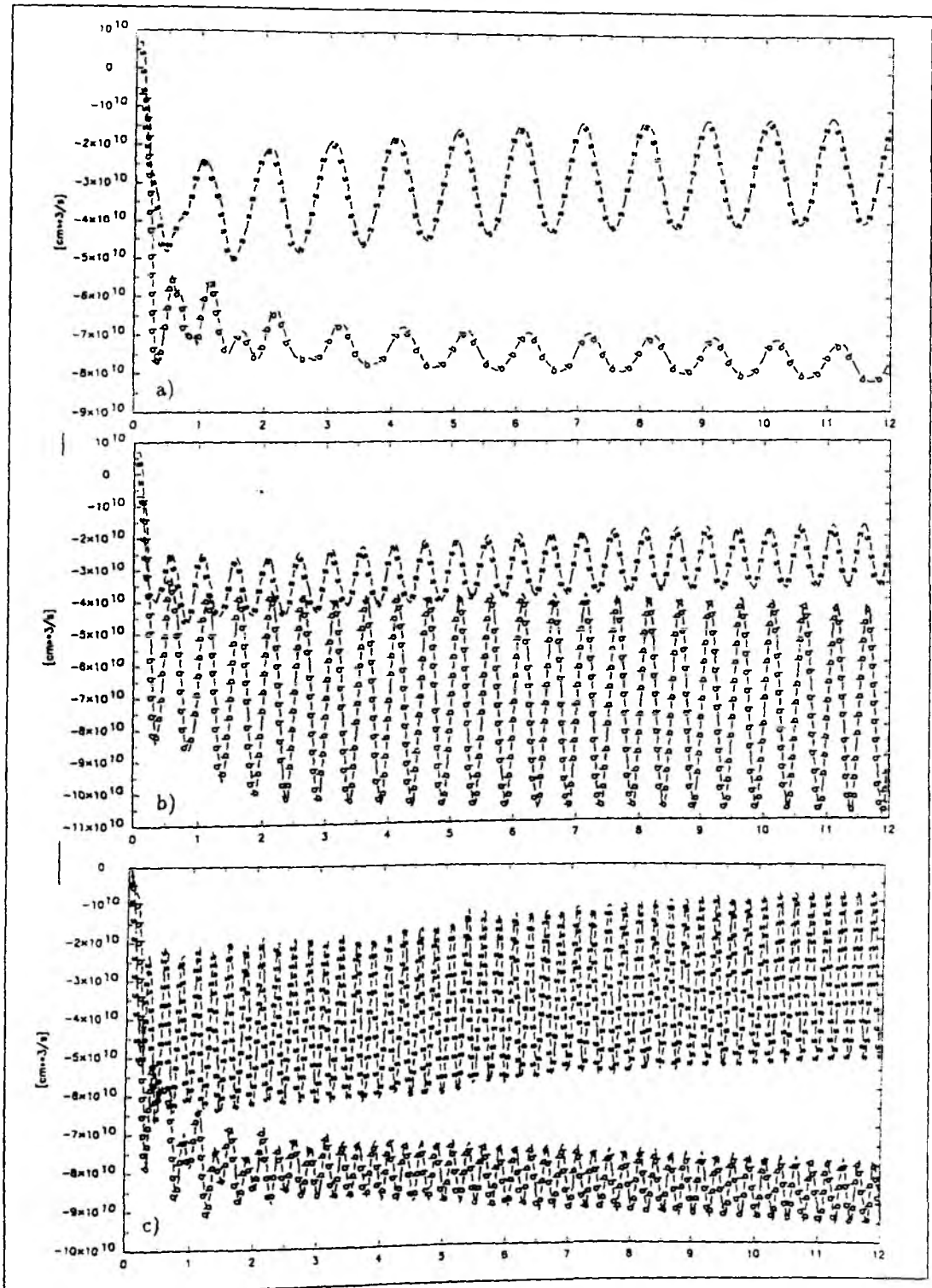|	Inflow	Outflow
Belt	0.192 73.3%	0.132 68.0%
Sound	0.070 26.7%	0.062 32.0%

Figure 4.37: Volume transport versus time (days) for oscillating $\Delta\eta$ with frequency a) $\omega = f/2$, b) $\omega = f$ and c) $\omega = 2f$, b–Belt and s–Sound.

99

In addition, the frequency response of the transport in the Belt and in the Sound is examined. Figure 4.37 shows three cases for fluctuating barotropic forcing. In the first case the oscillations prescribed as boundary condition have a frequency of twice the inertial frequency, in the second case the barotropic fluctuations have the same frequency as the inertial frequency, and in the last case the frequency of the forcing is half that of the inertial frequency. The result is that in the Belt the amplitude of the oscillating part of the transport increases, if the system is forced with a frequency near the inertial frequency. In the Sound the amplitude of the oscillating part of the transport decreases, if a frequency near the inertial frequency is chosen.

Table 4.6: Volume transport ($\times$ 10^{10} cm^3 s^{-1}) for the weak stratified case and for a given constant $\Delta\eta$ along the straits ($\Delta\eta = 40$ cm between the two far ends of the straits) (Inflow and Outflow experiments). The second values are the percentage of the total transport and the third line gives the transport relation as a function of $\Delta\eta$ (from figures 4.35a and 4.35b).

	Inflow	Outflow
Belt	15.1 71.6% $0.27\Delta\eta + 4.2$	11.2 70.9% $0.32\Delta\eta - 1.6$
Sound	6.0 28.4% $0.09\Delta\eta + 2.4$	4.6 29.1% $0.08\Delta\eta + 1.4$

Chapter 5

Comparison between Model and Data

In this chapter we compare the results of the thermohaline and the forced Baltic experiments with observed data. As outlined at the beginning the wind-driven circulation can not give realistic sea level rise and fall because of the smallness of the model region compared to the real Baltic. In order to see, whether sea level is realistically modeled in the straits, we prescribe observed surface elevations at both far ends of the channels. The stations used for the boundaries and for comparison in the interior are shown in figure 5.1. Kolobrzek and Smögen which are not shown
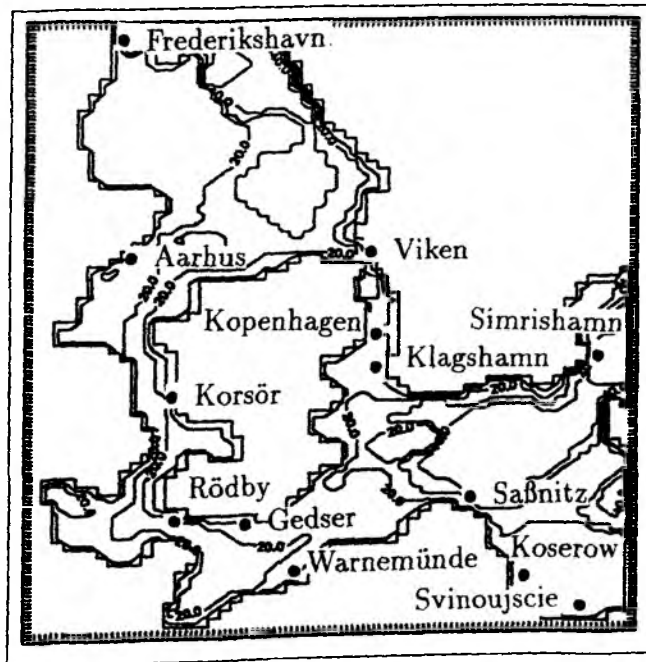
Figure 5.1: Location of the stations.
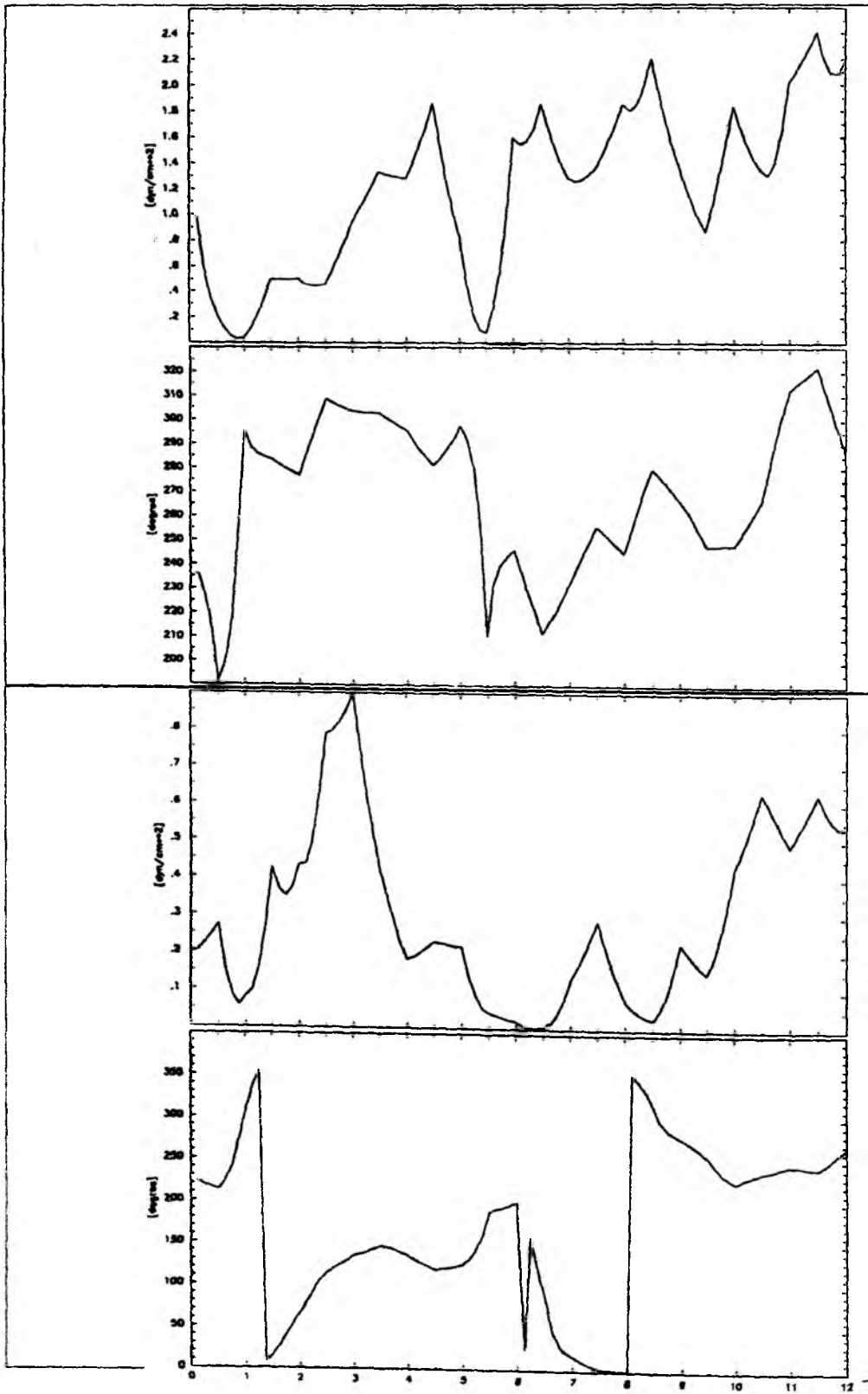
Figure 5.2: Applied wind stress (dyn/cm^2) and wind directions ($degree$) versus time ($days$) for the months a) January and b) July.
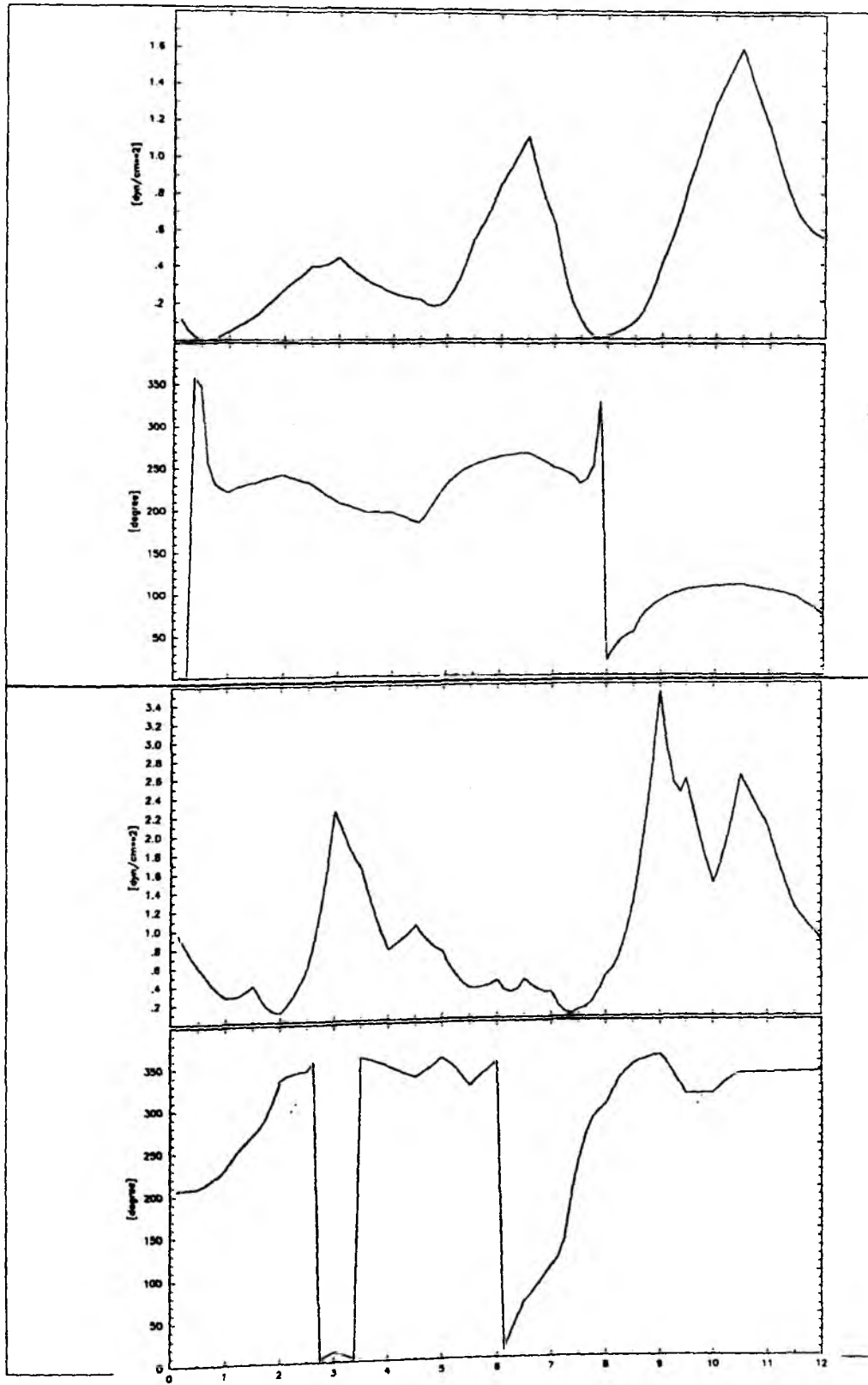
102

Figure 5.3: same as figure 5.2 for the months a) September and b) November.

103

in the figure are included. Surface elevations change linearly with increasing distance from the ends and take self adjusted values in the interior of the model region. The wind stress used in the model, is computed from air pressure data of the Europe model of the DWD (for more information, see LEHMANN, 1992). Case studies have been done for the months January, July, September and November 1990. Time series of the wind stress for these periods are presented in figure 5.2-3. Average surface elevation values along the northern boundary are drived from stations Aarhus, Frederikshavn, Kopenhagen, Korsör, Viken and Smögen and along the eastern boundary from stations Svinoujscie, Kolobrzek, Simrishamn, Warnemünde, Saßnitz and Koserow. They are prescribed within a narrow band of 25 km. However, it was not possible to find available data for every station and every month to calculate average value from 6 stations.
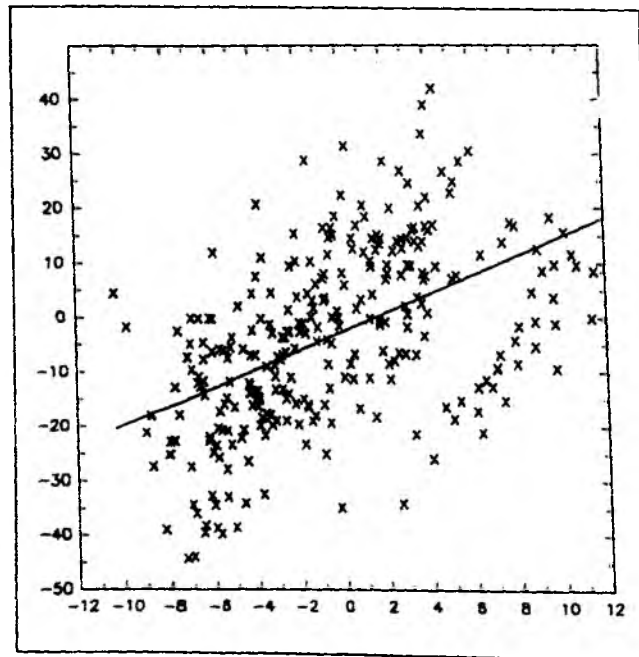

Figure 5.4: Linear regression, volume transport ($\times 10^{10}$ cm^3 s^{-1}) versus the difference in the surface elevations (cm) between Aarhus and Warnemünde.

5.1 Transport Relation

Regression analysis shows that the volume transport through the Belt is not linearly dependent on the difference in surface elevations between the stations Aarhus and Warnemünde (Fig.5.4). The linear regression correlation coefficient is only $r = 0.51$. The reason for this low value is that the transport relation during outflow situations is not identical with the relation in the inflow case. This was shown in chapter 4. Figures 5.5 and 5.6 depict transports through Belt and Sound for 12 day periods of the 4 selected months. Inflow occurs during the first 12 days in January. At the beginning calm winds cause only small amounts of volume transport. On day 5, with increasing wind stress, increases the volume transport and after day 10, although the wind stress increases, the inflowing volume decreases because of the changing wind direction from west to NNW (Fig.5.2a and Fig.5.5a). During July wind is weak. At the beginning the wind direction varies. The peak in wind stress at day 3 (SE wind) causes leight outflow and after day 9 westerly wind causes weak inflow (Fig.5.2b and Fig.5.5b). In September the wind stress shows two maxima. One of them is between days 6 and 7, and westerly wind dominates at that time, leading to inflow for both straits. The other maximum is between days 10 and 11; this time easterly wind is dominant which favours outflow (Fig.5.3a and Fig.5.5c). In November strong northerly wind occurs during days 3-5 and 8-12 without significant inflow (Fig.5.3b and Fig.5.5d). This corresponds to observations at light vessel Fehmarnbelt, where either out- or inflow is observed for wind from NNE (DIETRICH, 1951).

Volume transport values which are given in this study, are in agreement with transport values in several studies with respect to the order of magnitude. In general, west wind causes inflow in the straits and east wind outflow. The transport relation between the Belt and Sound is also in agreement with the observed values in both straits. Salt transport values for the four month are shown in figure 5.6, they depend
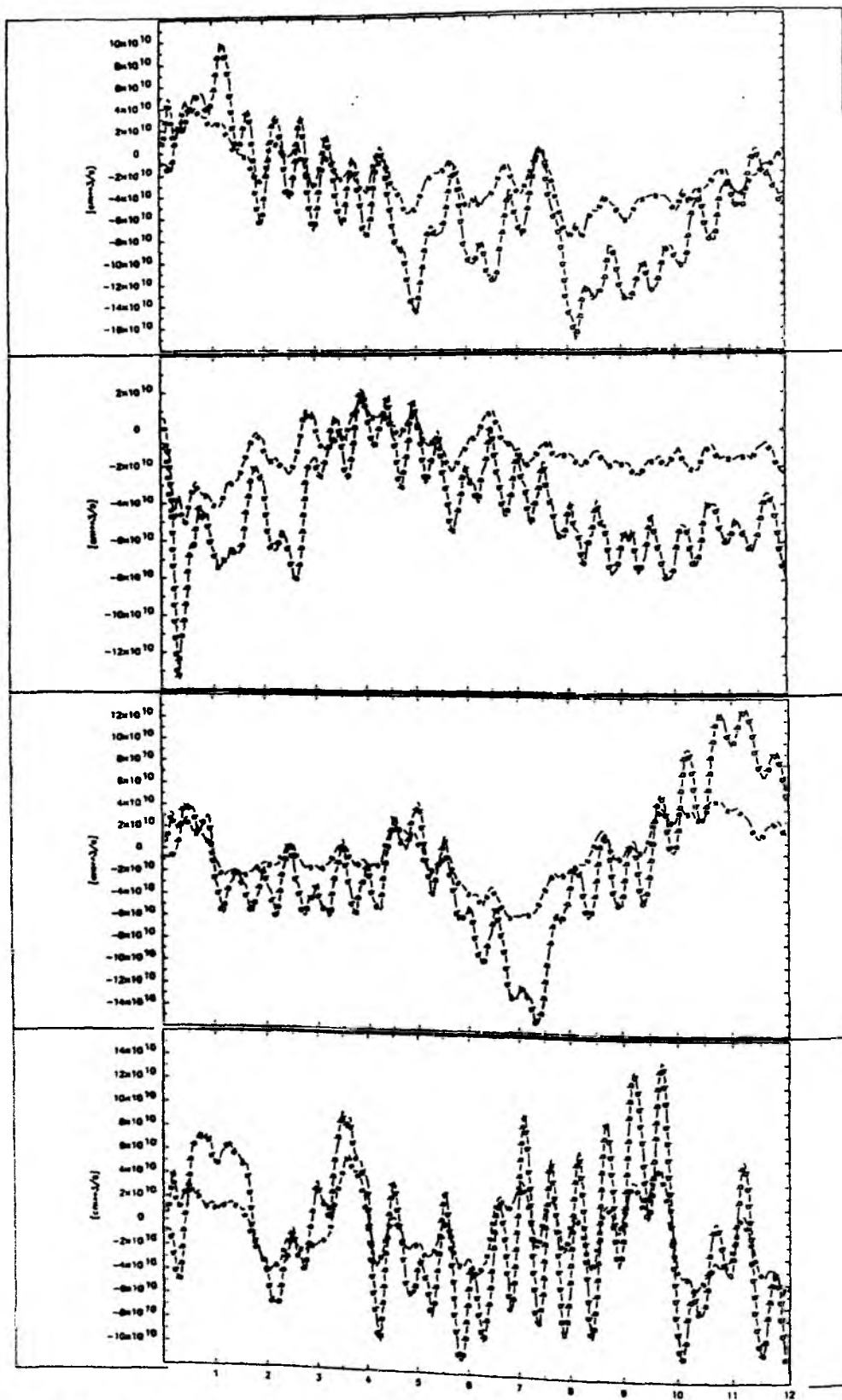
Figure 5.5: Volume transport versus time (*days*) for the months a) January b) July c) September and d)November, b–Belt and s–Sound, positive values are for outflow.
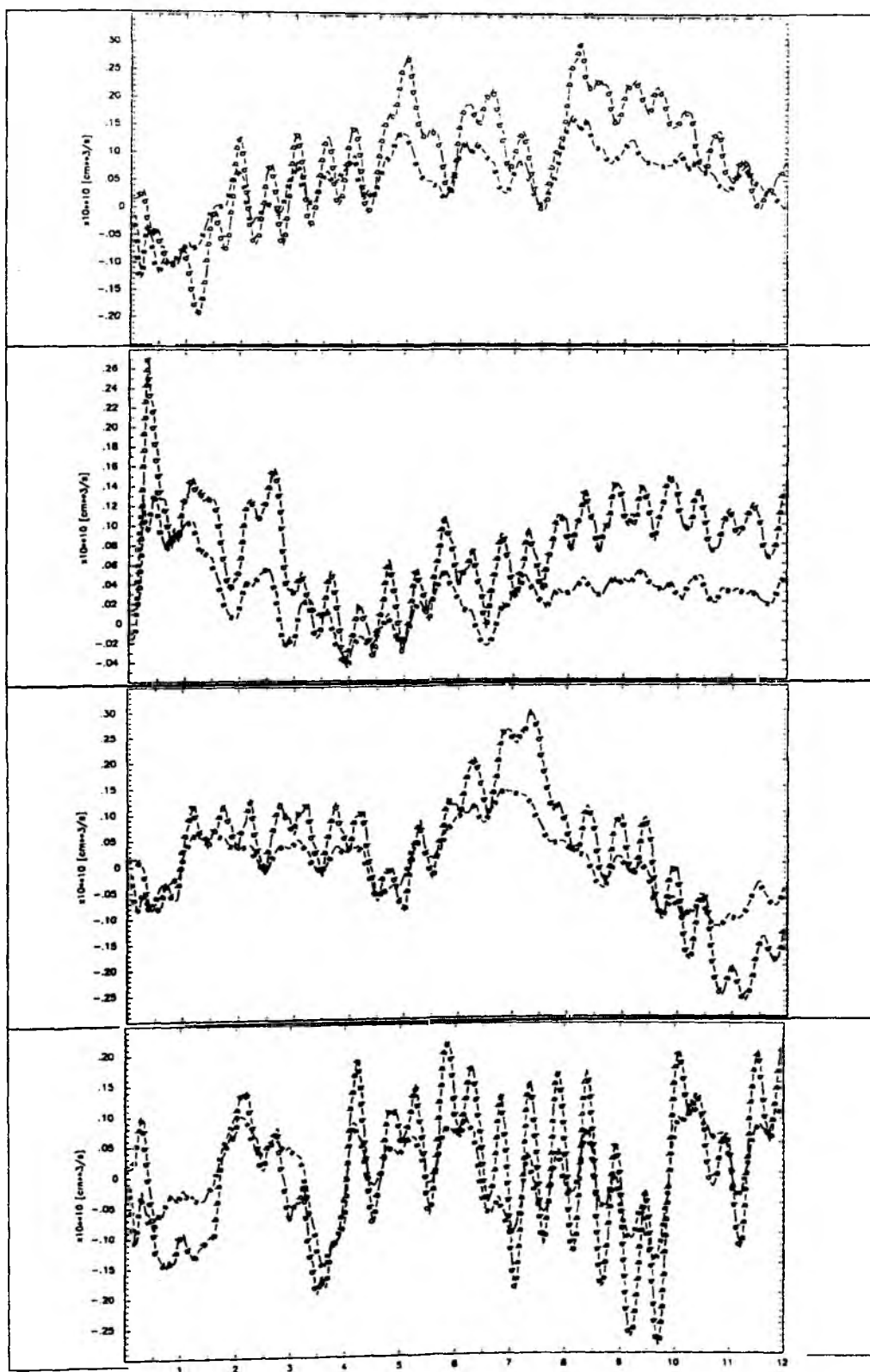
Figure 5.6: Salt transport versus time (*days*) for the months a) January b) July c) September and d)November, b–Belt and s–Sound, positive values represent salt gain of the Baltic.

on the volume transport. Increasing volume transport causes increasing salt transport.

5.2 Sea Surface Elevations of Selected Regions

If surface elevations of the model are compared with observed values at 9 stations during November, one recognizes good agreement especially for the stations in the east of the area (Fig.5.7-9). Although the surface elevations are prescribed at both the eastern and northern boundaries, the same high correlation could not be obtained for the stations in the north. The agreement for the stations in the central region and in the north in November and also for the other months (January, July and September) is not always satisfactory. The linear regression curves for 4 stations (one of them is in the north, Aarhus, two in the Belt, Gedser and Rödby, another one in the east, Saßnitz) and the month November are shown in figure 5.10. The fitted curve and the small deviation of the values from this curve for the surface elevations of Saßnitz denote the high correlation between the model values and the observed ones (correlation coefficient, $r = 0.94$). The correlation for the stations Gedser (r=0.80) and Rödby (0.80) is higher than for Aarhus (0.69). Table 5.1 gives the results of the linear regression analysis for all 9 stations for the months January, July, September and November. From the estimated intercepts and slopes of the fitted line a constant bias between model and observed surface elevations cannot be determined. In general, the correlation is higher for the stations in the eastern part of the area than in the other regions. Four explainations can be given for the discrepance between the model values and the observed ones:

(a) Errors due to the fact that the tide gauge are not located in the open sea.

(b) The model topography is not constructed well enough.

(c) The closed model region favours seiches oscillations different from the real basin oscillations.

(d) Model deficiencies.

Table 5.1: Results of the linear regression analysis for 9 stations for the months January, July, September and November 1989. Here a–estimated intercept of the fitted line, b–estimated slope of the fitted line and r–correlation coefficient. *– no data available.

|	JA	JU	S	N
Aarhus	a=-5.27 b=1.11 r=0.77	a=0.66 b=1.15 r=0.60	a=* b=* r=*	a=9.32 b=0.60 r=0.69
Kopenhagen	a=* b=* r=*	a=3.38 b=0.84 r=0.63	a=* b=* r=*	a=0.76 b=0.84 r=0.64
Korsör	a=* b=* r=*	a=3.12 b=1.01 r=0.61	a=9.66 b=0.83 r=0.54	a=11.33 b=0.82 r=0.85
Viken	a=-2.05 b=0.98 r=0.69	a=0.73 b=0.84 r=0.67	a=-2.98 b=0.92 r=0.52	a=-1.02 b=0.80 r=0.68
Warnemünde	a=1.10 b=0.81 r=0.75	a=1.78 b=0.91 r=0.70	a=0.23 b=1.14 r=0.73	a=3.0 b=0.72 r=0.86
Saßnitz	a=-10.17 b=1.18 r=0.89	a=-2.68 b=0.81 r=0.87	a=-4.58 b=1.26 r=0.94	a=3.77 b=0.81 r=0.91
Gedser	a=13.49 b=0.85 r=0.70	a=* b=* r=*	a=* b=* r=*	a=18.45 b=0.80 r=0.80
Rödby	a=12.17 b=0.89 r=0.66	a=* b=* r=*	a=6.15 b=1.59 r=0.85	a=13.69 b=0.64 r=0.80
Klagshamn	a=11.49 b=0.93 r=0.77	a=1.99 b=0.77 r=0.70	a=2.04 b=0.90 r=0.90	a=7.62 b=0.66 r= 0.75
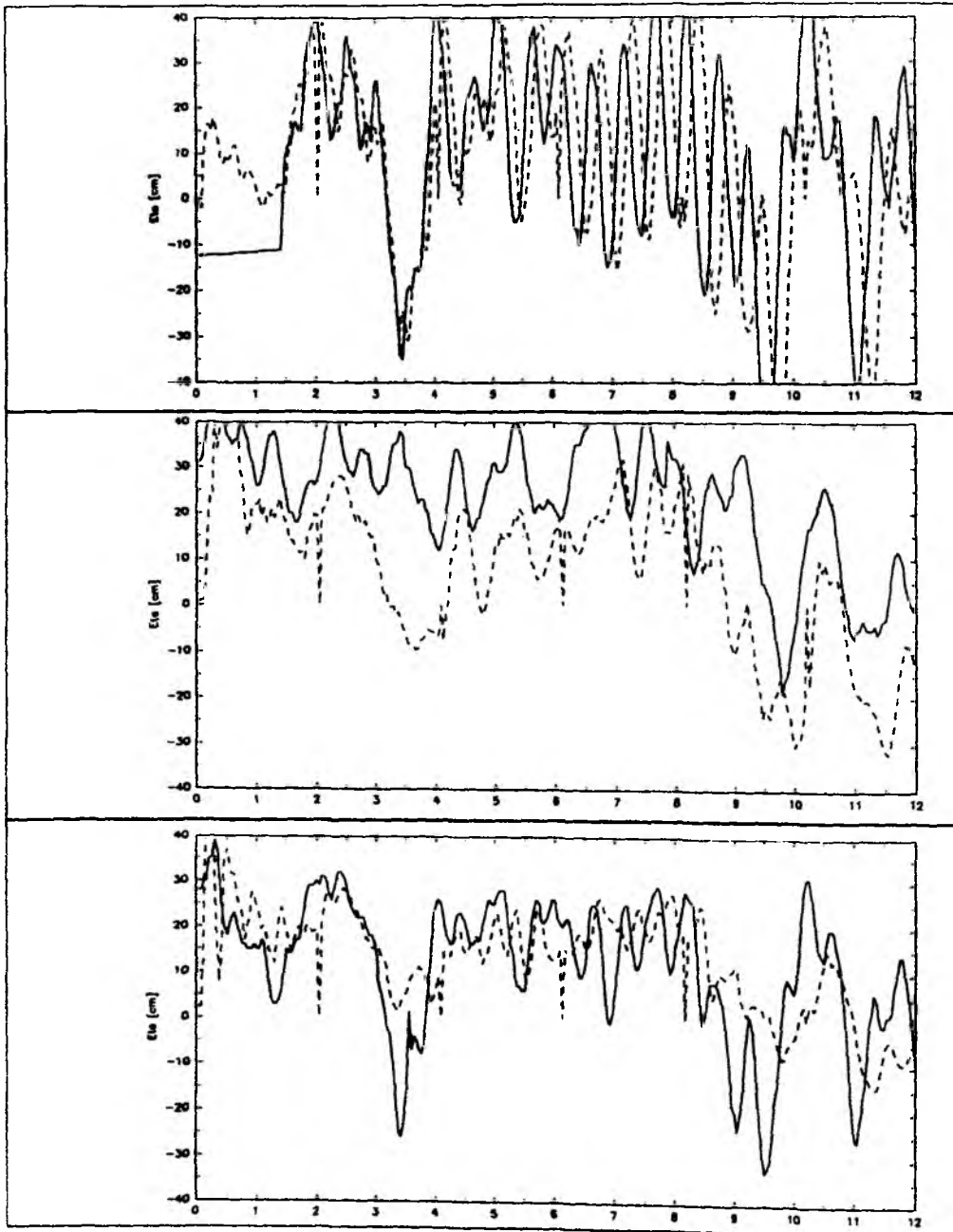
Figure 5.7: Comparison of surface elevations (cm) of the model (broken lines) with observed values (full line) for 12 days (November 1989) a) Aarhus b) Gedser c) Kopenhagen.
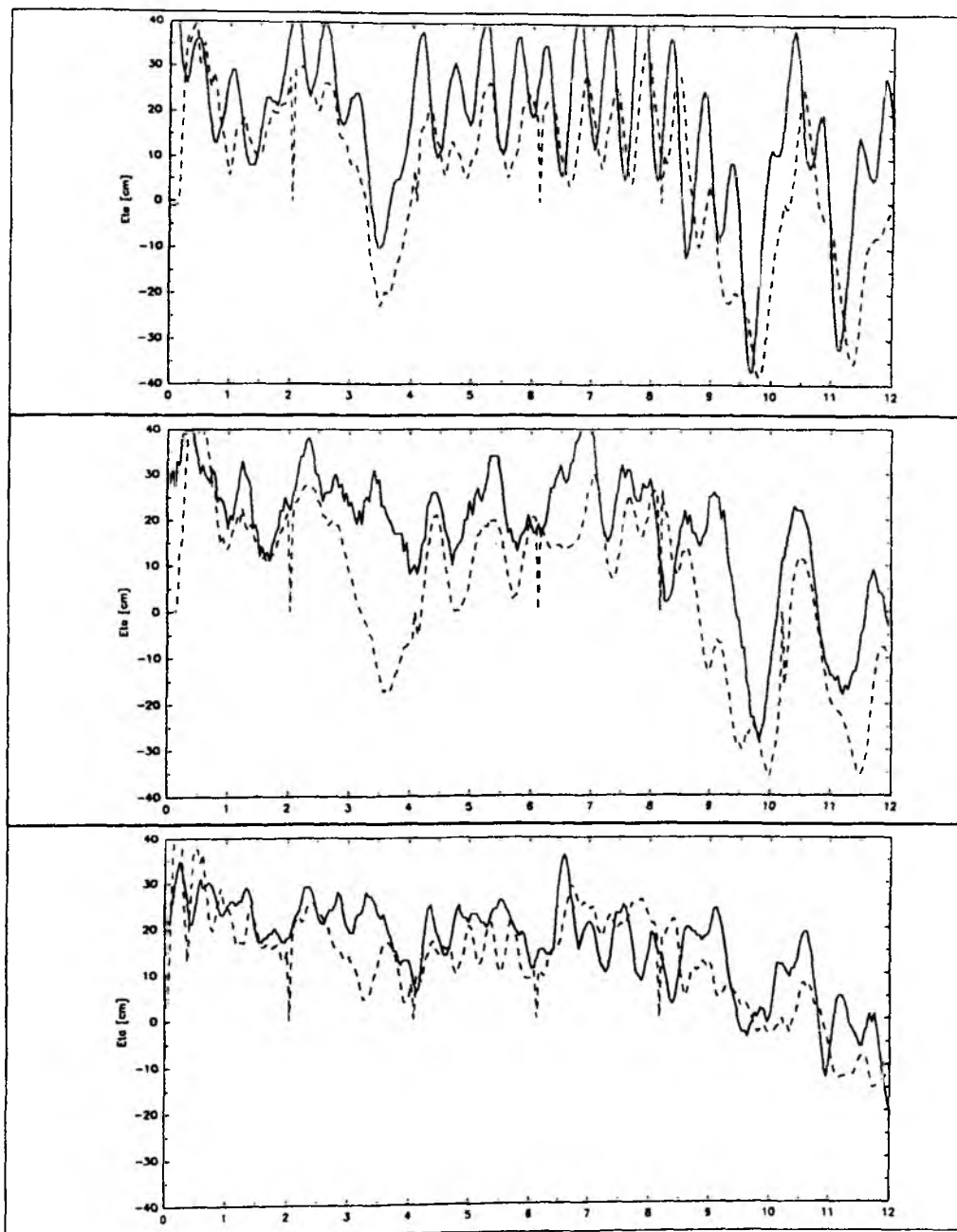
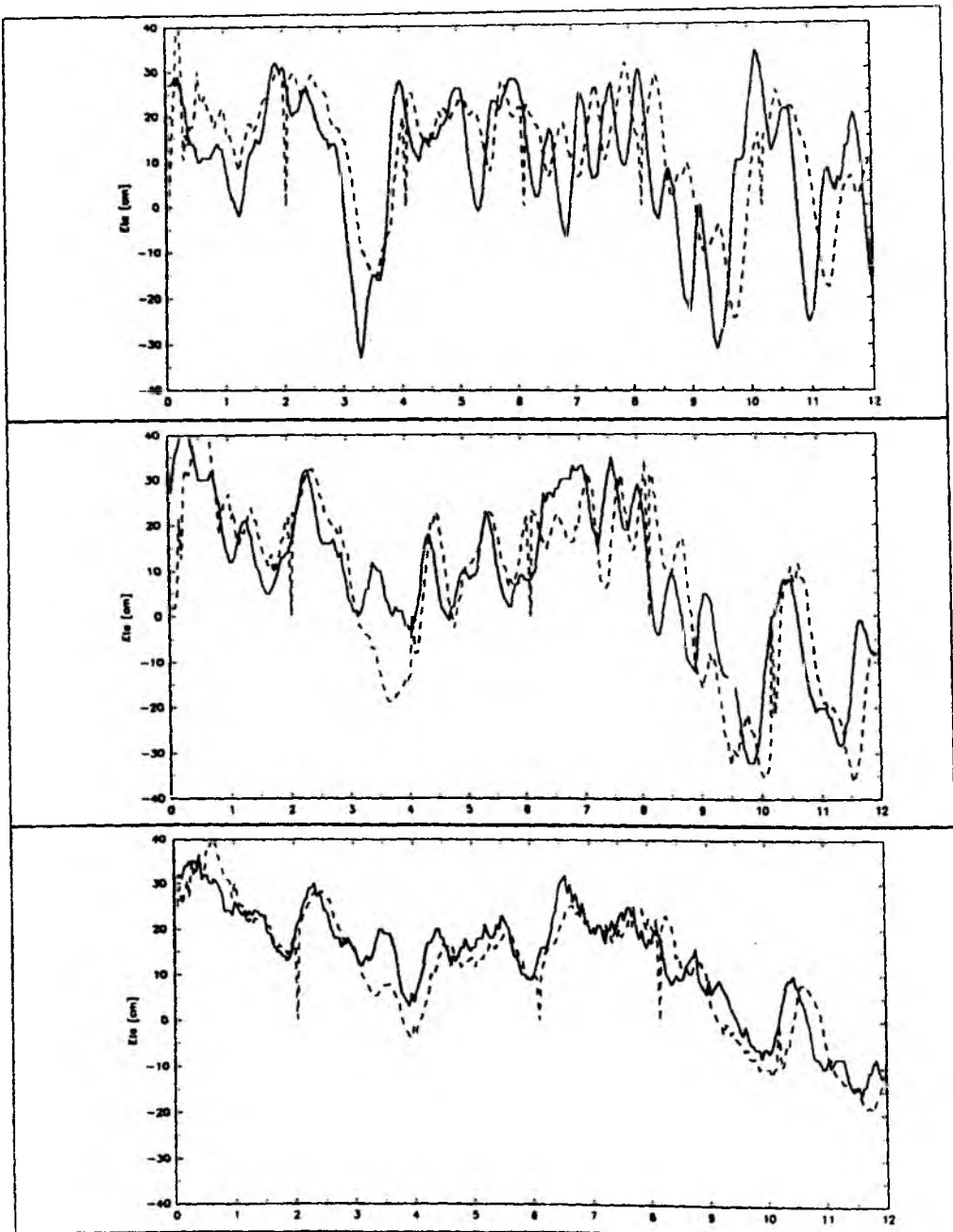Figure 5.8: Same as figure 5.7 a) Korsör b) Rödby c) Klagshamn.

Figure 5.9: Same as figure 5.7 a) Viken b) Warnemünde c) Saßnitz.

The spectral peaks show agreement between data and model results at frequency bands higher than the inertial frequency (Fig 5.11-14, full lines show data). The short periodic oscillations could not be analyzed very well, they show phase differences compared to the model results. The model is in good agreement with the data for less than the inertial frequency. The frequency peaks in the spectrum of the surface elavations are very similar to the frequency peaks which were found in the two–basin experiments. Especially the spectrum of Aarhus for the month of November shows excellent agreement with the data and the frequencies for the crossoscillations and also for the trapped and inertial waves.
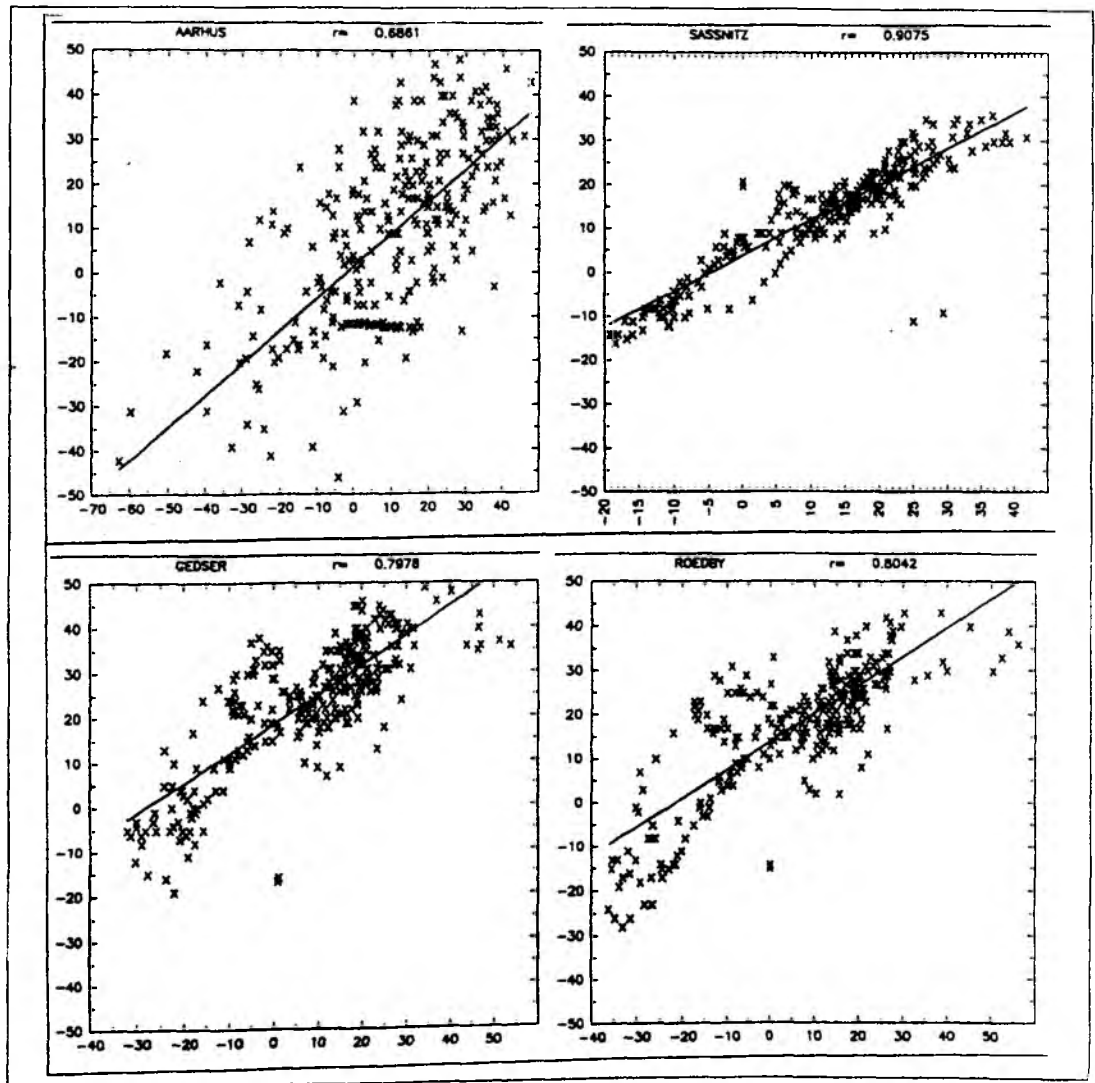

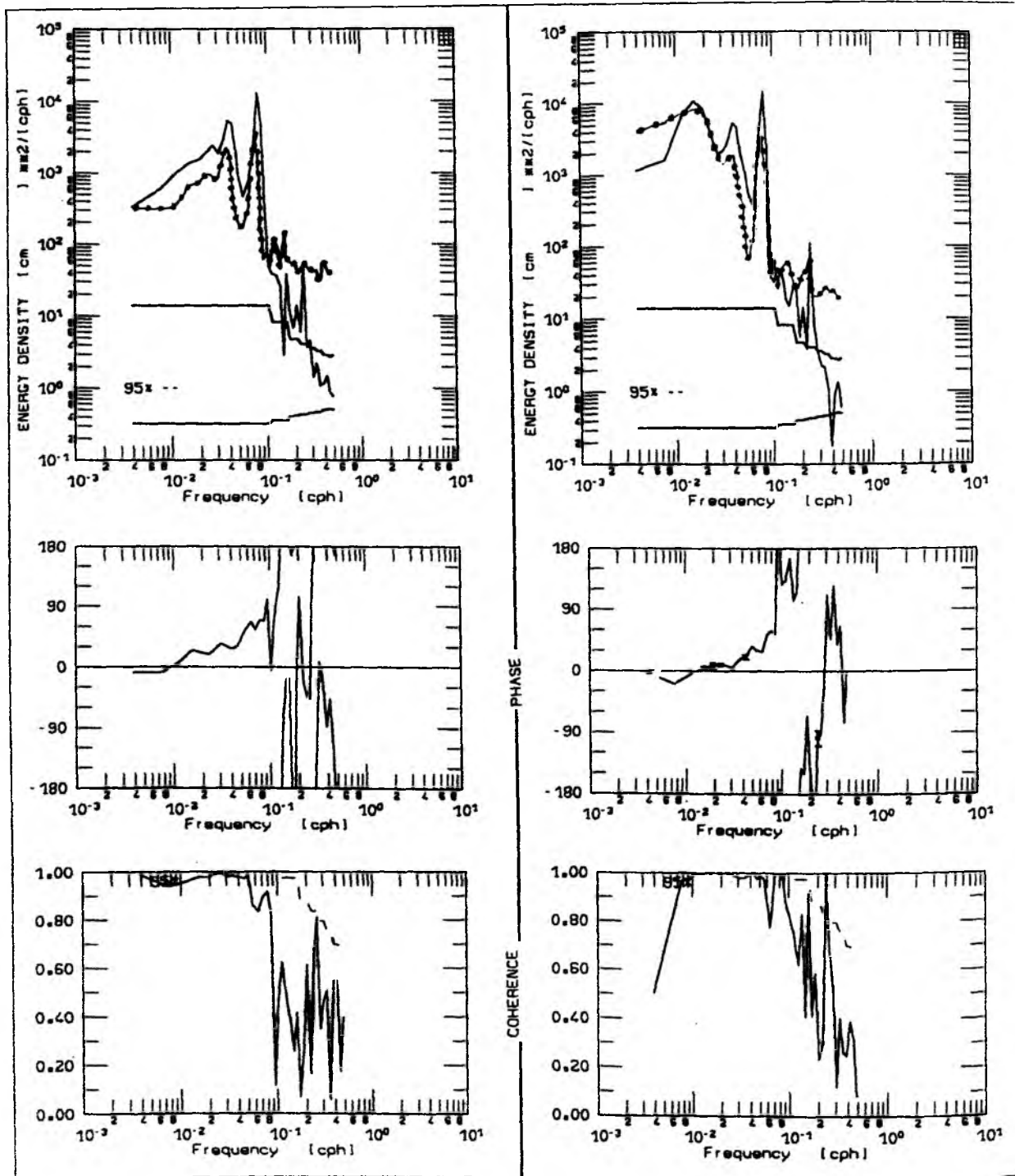Figure 5.10: Linear regression, model surface elevations versus observed ones for 4 stations.

Figure 5.11: Spectral analysis of surface elevations (model results and observations) of the station Aarhus for the months January and November 1989. Upper panel: Energy density. Central panel: Phase. Lower panel: Coherence.
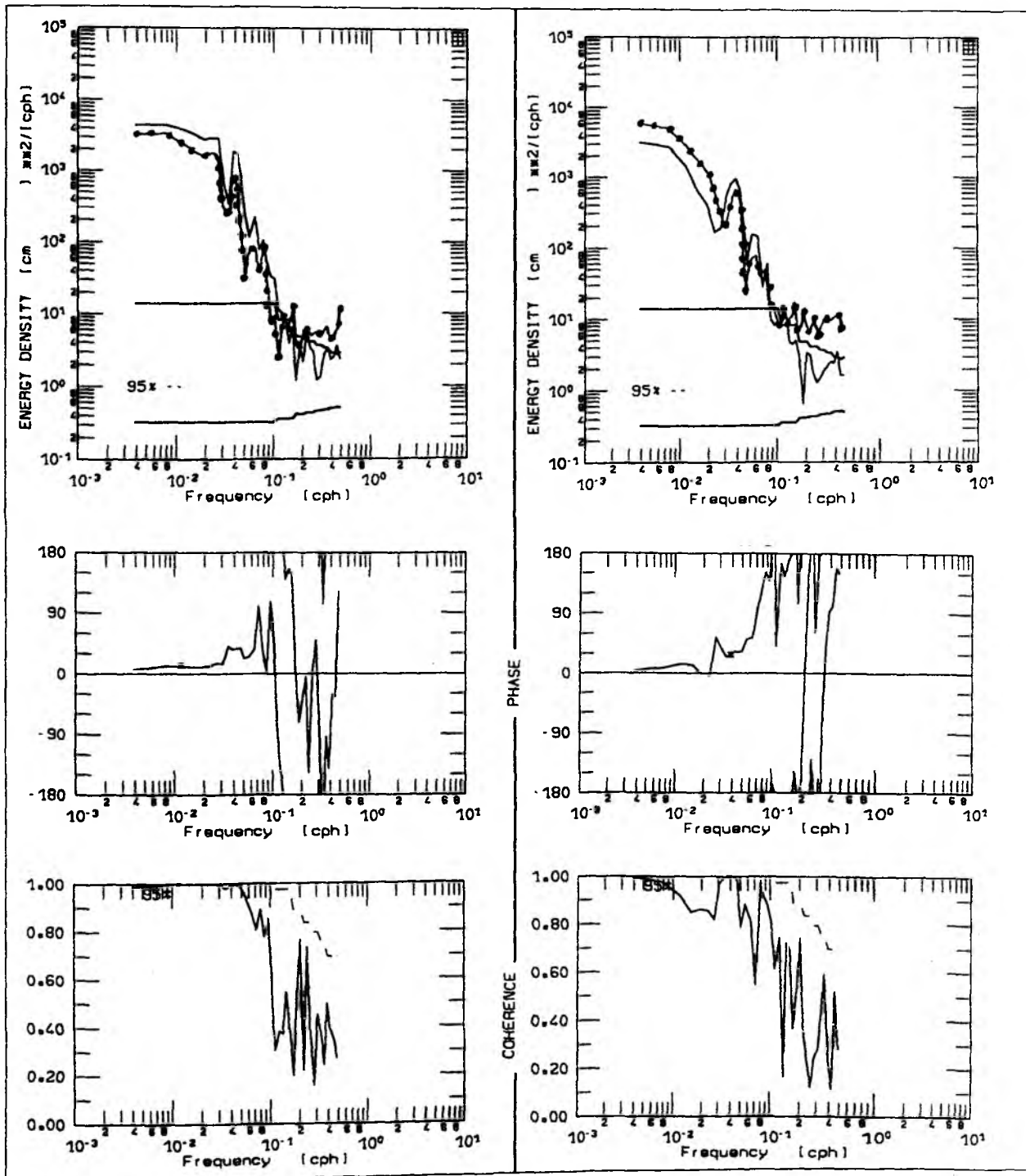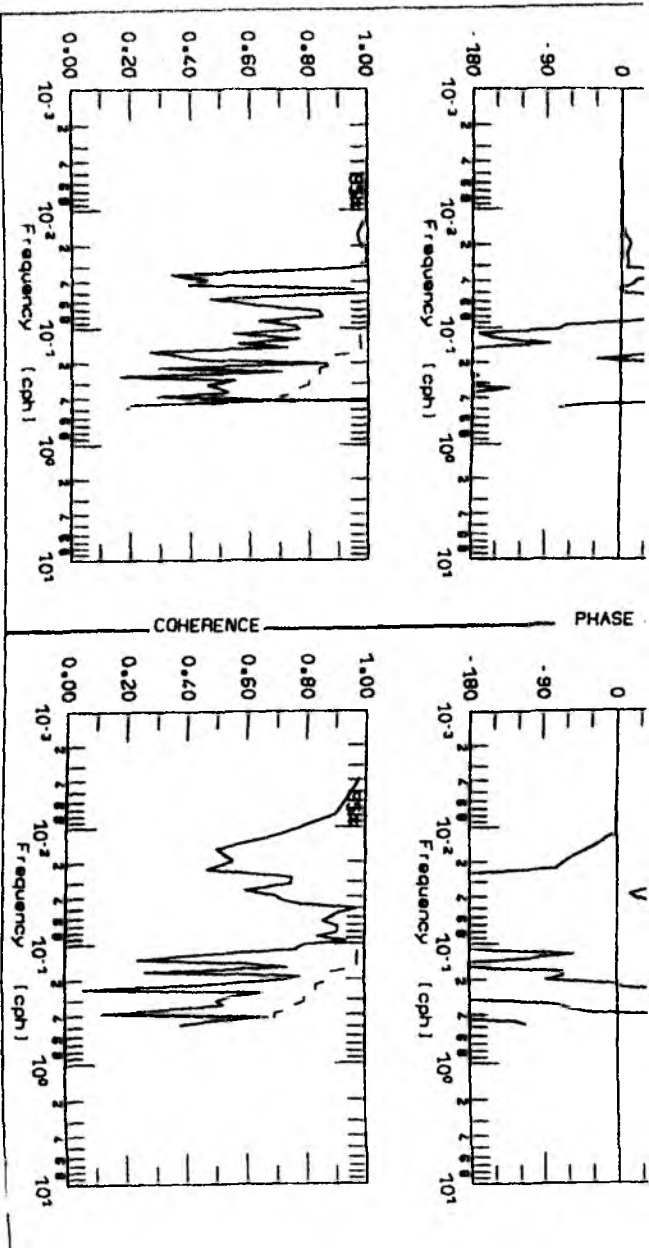
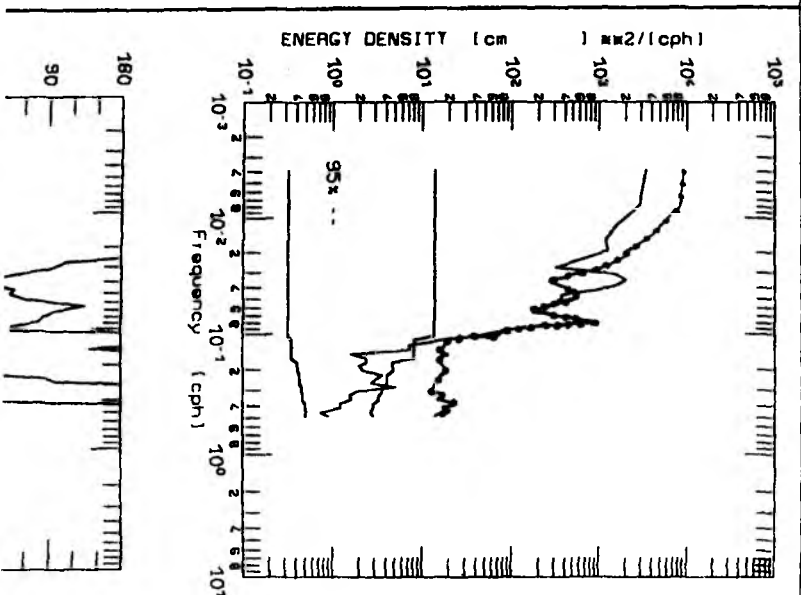Figure 5.12: Same as figure 5.11 for the station Saßnitz.

Figure 5.13: Same as figure 5.11 for the station Gedser.
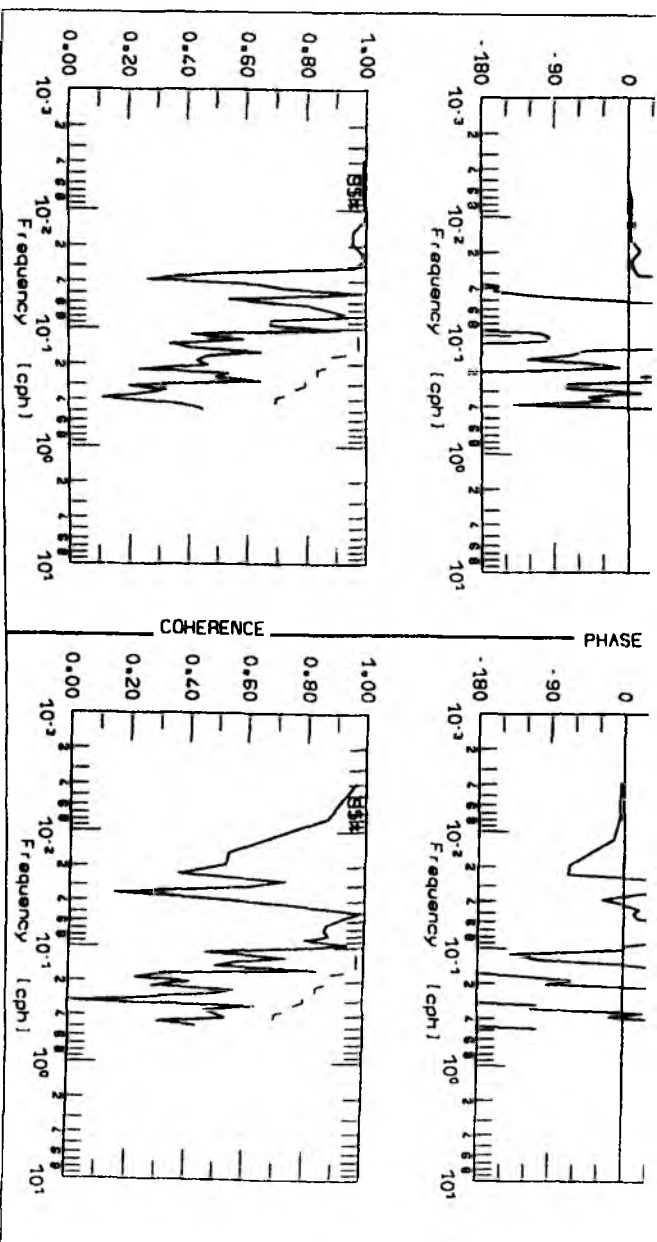
ENERGY DENSITY [cm] ∗∗2/[cph]

ENERGY DENSITY [cm] ∗∗2/[cph]

95% ‥

95% ‥

Frequency (cph)

Frequency (cph)
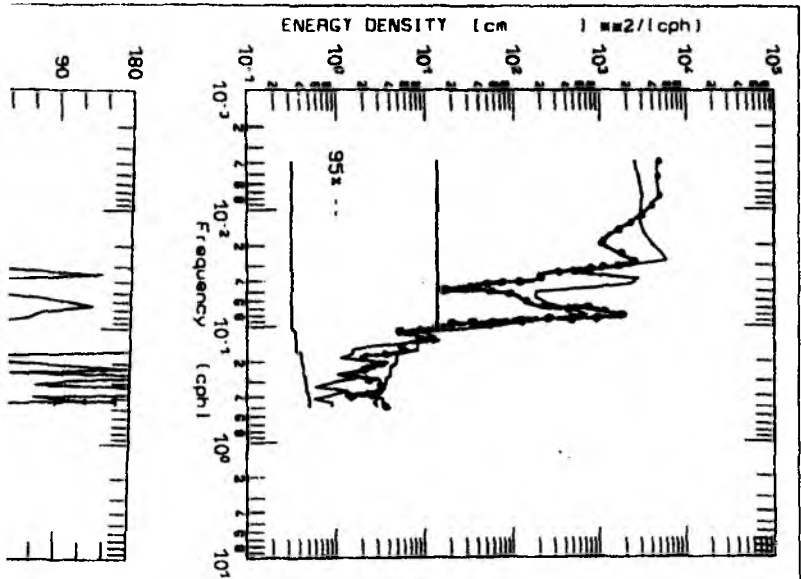
Figure 5.14: Same as figure 5.11 for the station Rödby.

ENERGY DENSITY (cm] ∗∗2/(cph)

95% --

Frequency (cph)

ENERGY DENSITY (cm] ∗∗2/(cph)

95% --

Frequency (cph)
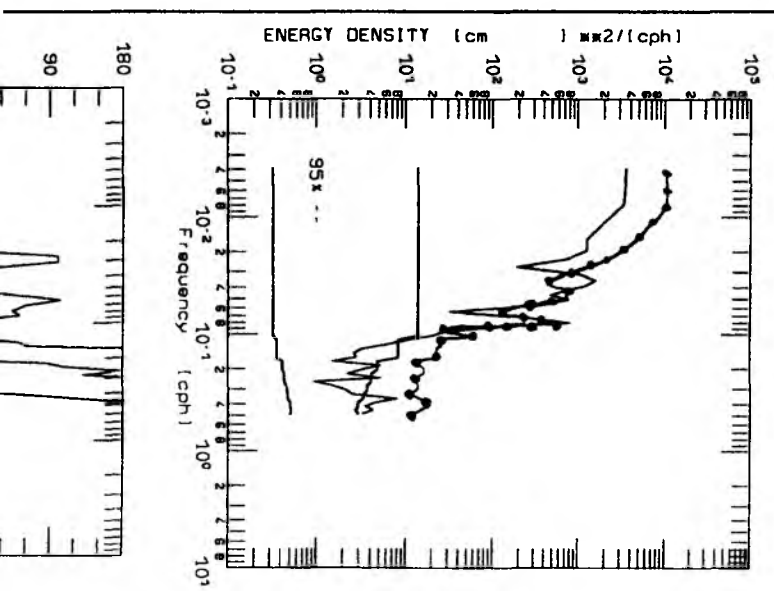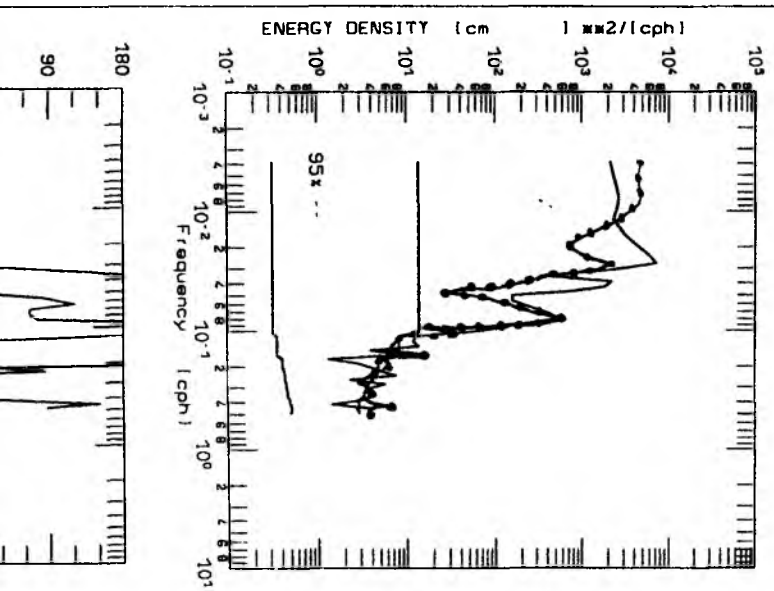
Chapter 6

Conclusions

The results of the two–basin and the Baltic experiments can be summarized as follows:

- Adjustment in a channel has two distinct phases. During the first one geostrophic adjustment takes place in which Kelvin and Poincaré dynamics set up the boundary and interior circulations. The second one is the nonlinear phase, in which topographic effects and stratification play an important role.

- Model transport values were compared with some transport relations. For the outflow case in the Belt the transport may be determined by using the geostrophic relation. The transport values for the inflow case deviate from geostrophy. This can be explained by the generation of internal waves over variable topography. Spectral analysis showed a peak at frequencies slightly higher than the inertial one (inertial waves with a shifted frequency). Internal and inertial waves were often observed in the western Baltic Sea. They have been analysed in the concept of wind-driven circulation by KRAUSS (1978). From results of the present study it can be concluded that internal waves are generated by scattering of Kelvin waves over topography. If the topography intersects the upper layer (topographic breakthrough), then a finite amount of energy is always scattered by topography (KILLWORTH, 1989b).

- The inflowing water forms a dome–like feature in the basin after passing the sill. This convective process is responsible for removing energy from the system. The dense water can only penetrate further by external forcing or after the rim of the dome reaches the next sill.

- The well known relation that 75 % of the total transport in the Danish Straits occurs through the Belt, is established for inflow in the strong stratified case and for inflow and outflow in the weak stratified case with a slightly less percentage. For outflow situations in the strong stratified case this relation is changed.

- In the energy exchange the bottom friction term acts as a sink. This can be interpreted as a drag which is exerted by topography and which leads to the generation of internal waves (GILL, 1982). WAJSOWICZ (1993) stated that frictional drag damps the waves propagating against the mean flow more rapidly than those propagating with it.
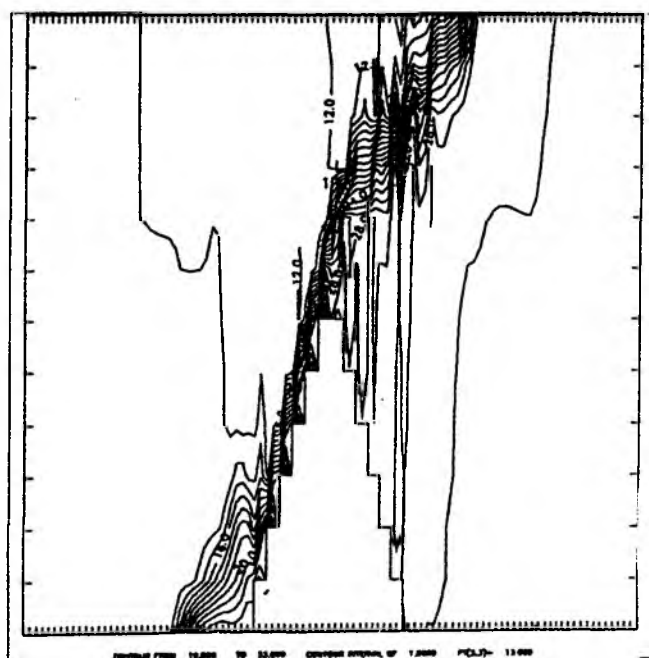

Figure 6.1: Density field along x=19

119

- Triangular features are formed over step–like topography. Figure 6.1 is similar to the figures 3.9b and 3.23b, but the triangular features over the steps of the topography can be better recognizable in figure 6.1. We speculate that the step–like structure produces the following dynamics: the dense water over the steps flows first to the left due to buoyancy force and then to the right due to double Kelvin wave–dynamics. This means that buoyancy causes a decrease of the rotational effect over step–like topography. JOHNSON (1990) examined the scattering of Kelvin waves by stepped and also over smooth topography and found that the short waves are destroyed even with small viscosity. Long waves remain unaltered over smooth topography.

- At the northern coast of the basin solitary waves were detected in the two–basin experiments for the density–driven case. These waves can probably explain the bottom process of the coastal current along the Swedish coast in the Kattegat. In the forced case instead of solitary waves standing waves were found in the northern basin.

Bibliography

[1] AITSAM, A. and J. ELKEN, 1982: Synoptic scale variability of hydrophysical fields in the Baltic proper on the basis of CTD measurements. Hydrodynamics of semi–enclosed seas. J.C.C. Nihoul, Editor, Elsevier, Amsterdam, pp. 433–468.

[2] BAINES, P.G. 1984: A unified describtion of two–layer flow over topography. J. Fluid Mech., 146, 127–167.

[3] BAINES, P.G. and H. GRANEK, 1990: Hydraulic models of deep stratified flows over topography. In: The Physical Oceanography of Sea Straits, edited by L.J. Pratt, 245–269, Kluwer, Boston.

[4] BAINES, P.G., G. HUBBERT and S. POWER, 1991: Fluid transport through Bass Strait. Continental Shelf Res., 11, 269–293.

[5] BELL, T.H., 1978: Radiation damping of inertial oscillations in the upper ocean. J. Fluid Mech., 88, 289–308.

[6] BOCK, K.H., 1971: Monatskarten des Salzgehaltes der Ostsee. Ergänzungsheft zur Deutschen Hydrographischen Zeitschrift, Reihe B, Nr. 12.

[7] BORMANS, M. and C. GARRETT, 1989: The effect of rotation on the surface inflow through the Strait of Gibraltar. J. Phys. Oceanogr., 19, 1535–1542.

[8] BÖNING, C.W., 1989: Influences of a rough bottom topography on flow kinematics in an eddy-resolving circulation model. J. Phys. Oceanogr., 19, 77–97.

[9] BRYAN, K., 1969: A numerical method for the study of the circulation of the world ocean. Jour. Comp. Phys., 4, 347–376.

[10] BRYAN, K., 1989: The design of numerical models of the ocean circulation. In: Ocean Circulation Models: Combining Data and Dynamics. D.L.T. Anderson and J. Willebrand (eds), 465–500.

[11] BRYDEN, H.L. and T.H. KINDER, 1991a: Recent progress in strait dynamics. Reviews of Geophysics, Suppl., 617– 631.

[12] BRYDEN, H.L. and T.H. KINDER, 1991b: Steady two–layer exchange through the Strait of Gibraltar. Deep–Sea Res. , 38, 445–463.

[13] CHAO, S.Y. and W.C. BOICOURT, 1986: Onset of Estuarine Plumes. J. Phys. Oceanogr., 16, 2137–2149.

[14] CHAO, S.Y., 1988: River–forced estuarine plumes. J. Phys. Oceanogr., 18, 72–88.

[15] CHAO, S.Y. and T. PALUSZKIEWICZ, 1991: The hydraulics of density currents over estuarine sills. J. Geophys. Res., 96, 7065–7076.

[16] COX, M.D., 1984: A primitive equation, 3–dimensional model of the ocean. GFDL Ocean Group Tech. Rep. No. 1.

[17] CSANADY, G.T., 1977: The coastal jet conceptual model in the dynamics of shallow seas. In: The Sea (E.D. Goldberg, I.N. McCave, J.J. O'Brien and J.H. Steele, eds.) Vol.6, pp. 117-144. Wiley, New York.

[18] DALZIEL, S.B., 1990: Rotating two–layer sill flows. In: The Physical Oceanography of Sea Straits, edited by L.J. Pratt, 343–371, Kluwer, Boston.

[19] DEFANT, A., 1961: Phsical Oceanography, Vol. II, Pergamon Press, New York, 598 pp.

[20] DIETRICH, G., 1951: Oberflächenströmung im Kattegat, im Sund und in der Beltsee. Dt. Hydrogr. Z., 4, 129–150.

[21] FARMER, D.M. and J.S. MØLLER, 1990: Measurements and modeling in the Great Belt: A unique opportunity for model varification. In: The Physical Oceanography of Sea Straits, edited by L.J. Pratt, 125–152, Kluwer, Boston.

[22] FENNEL, W. and H.U. LASS, 1989: Analytical Theory of Forced Oceanic Waves, Akademic–Verlag, Berlin.

[23] FENNEL, W., T. SEIFERT and B. KAISER, 1991: Rossby radii and phase speeds in the Baltic Sea. Continental Shelf Res., 11, 23–36.

[24] GARRETT, C., M. BORMANS and K. THOMPSON, 1990: Is the exchange through the Strait of Gibraltar maximal or submaximal? In: The Physical Oceanography of Sea Straits, edited by L.J. Pratt, 271–294, Kluwer, Boston.

[25] GARRETT, C., 1991: Marginal mixing theories. Atmosphere–Ocean, 29 (2), 313–339.

[26] GILL, A.E., 1976: Adjustment under gravity in a rotating channel. J. Fluid Mech., 77, 603–621.

[27] GILL, A.E., 1977: The hydraulics of rotating-channel flow. J. Fluid Mech., 80, 641–671.

[28] GILL, A.E., 1982: Atmosphere–Ocean Dynamics. Academic Press, London, 662 pp.

[29] GILL, A.E., 1986: Rossby adjustment over a step. J. Mar. Res., 44, 713–738.

[30] GRIFFITHS, R.W. and E.J. HOPFINGER, 1983: Gravity currents moving along a lateral boundary in a rotating fluid. J. Fluid Mech., 134, 357–399.

[31] HANNAH, C.G., 1992: Geostrophic control with wind forcing: Application to Bass Strait. J. Phys. Oceanogr., 22, 1596– 1599.

[32] HELFRICH, K.R. and W.K. MELVILLE, 1990: Review of dispersive and resonant effects in internal wave propagation. In: The Physical Oceanography of Sea Straits, edited by L.J. Pratt, 391–420, Kluwer, Boston.

[33] HERMANN, A.J., P.B. RHINES and E.R. JOHNSON, 1989: Nonlinear Rossby adjustment in a channel: beyond Kelvin waves. J. Fluid Mech., 205, 469–502.

[34] HOGG, N.G., 1983: Hydraulic control and flow separation in a multi–layered fluid with applications to the Vema Channel. J. Phys. Oceanogr., 13, 695–708.

[35] HOGG, N.G., 1985: Multilayer hydraulic control with application to the Alboran Sea Circulation. J. Phys. Oceanogr., 15, 454–466.

[36] HSIEH, W.W. and A.E. GILL, 1984: The Rosby adjustment problem in a rotating, stratified channel, with and without topography. J. Phys. Oceanogr., 14, 424–437.

[37] HUTHNANCE, J.M., 1980: On natural oscillations of connected ocean basins. Geophys. J. Roy. Astron. Soc., 61, 337–354.

[38] JOHNSON, E.R., 1990: The low–frequency scattering of Kelvin waves by stepped topography. J. Fluid Mech., 215, 23–44.

[39] JOHNSON, E.R. and M.K. DAVEY, 1990: Free–surface adjustment and topographic waves in coastal currents. J. Fluid Mech., 219, 273–289.

[40] KÄNDLER, Von R., 1951: Der Einfluß der Wetterlage auf die Salzgehaltsschichtung im Übergangsgebiet zwischen Nord– und Ostsee. Dt. Hydrogr. Z., 4, 150–160.

[41] KIELMANN, J., W. KRAUSS and K.H. KEUNECKE, 1973: Currents and stratification in the Belt Sea and the Arkona Basin during 1962–1968. Kieler Meeresf. XXIX, 90–111.

[42] KIELMANN, J., 1981: Grundlagen and Anwendung eines numerischen Modells der geschichteten Ostsee. Ber. Inst. f. Meeresk., Kiel Nr. 87a/87b, 158 pp./116 pp.

[43] KILLWORTH, P.D., 1989a: How much of baroclinic coastal Kelvin wave gets over a ridge? J. Phys. Oceanogr., 19, 321–341.

[44] KILLWORTH, P.D., 1989b: Transmission of a two–layer coastal Kelvin wave over a ridge. J. Phys. Oceanogr., 19, 1131–1148.

[45] KILLWORTH, P.D., D. STAINFORTH, D.J. WEBB and S.M. PATERSON, 1989: A free surface Bryan–Cox–Semtner model. Institute of Oceanographic Sciences, Deacon Laboratory Internal Rep. 270.

[46] KILLWORTH, P.D., 1991: The development of a free–surface Bryan–Cox–Semtner ocean model. J. Phys. Oceanogr., 21, 1333–1348.

[47] KILLWORTH, P.D., 1992a: The time–dependent collapse of a rotating fluid cylinder. J. Phys. Oceanogr., 22, 390–397.

[48] KILLWORTH, P.D., 1992b: On hydraulic control in a stratified fluid. J. Fluid Mech., 237, 605–626.

[49] KILLWORTH, P.D., 1992c: Flow properties in rotating, stratified hydraulics. J. Phys. Oceonogr., 22, 997–1017.

[50] KOWALIK, Z., 1972: Wind driven circulation in a shallow stratified sea. Dt. Hydrogr. Z., 25, 265–278.

[51] KRAUSS, W. and L. MAGAARD, 1961: Zum Spektrum der internen Wellen der Ostsee. Kieler Meeresf. XVII, 137–147.

[52] KRAUSS, W., 1973: Methods and Results of Theoretical Oceanography. Vol.1, Dynamics of the Homogeneous and Quasihomogeneous Ocean. Gebrüder Bornträger, Berlin, 302 pp.

[53] KRAUSS, W., 1978: On the energy of the wind stress required to produce internal and inertial waves. Dt. Hydrogr. Z., 31, 31–49.

[54] KRAUSS, W., 1979a: A semi–spectral model for the computation of mesoscale processes in a stratified channel of variable depth. Dt. Hydrogr. Z., 32, 173–189.

[55] KRAUSS, W., 1979b: Inertial waves in an infinite channel of rectangular cross section. Dt. Hydrogr. Z., 32, 247–266.

[56] KRAUSS, W., 1981: The erosion of a thermocline. J. Phys. Oceanogr., 11, 415–433.

[57] KRAUSS, W., 1991: Wind–produced water exchange between the deep basins of the Baltic Sea. J. Phys. Oceanogr., 21, 373-384.

[58] LASS, H.U. and R. SCHWABE, 1990: An analysis of the salt water inflow into the Baltic in 1975 to 1976. Dt. Hydrogr. Z. 43.

[59] LAURENCE, A., 1977: The dynamics of the bottom boundary layer of the deep ocean. In: Bottom Turbulence, edited by J.C.J. Nihoul, 153–164, Elsevier, Amsterdam – Oxford – NewYork.

[60] LAWRENCE, G.A., 1990: Can mixing in exchange flows be predicted using internal hydraulics? In: The Physical Oceanography of Sea Straits, edited by L.J. Pratt, 519–536, Kluwer, Boston.

[61] LeBLOND, P.H. and L.A. MYSAK, 1978: Waves in the Ocean. Elsevier, Amsterdam, 602 pp.

[62] LEHMANN, A., 1992: Ein dreidimensionales baroklines wirbelauflösendes Modell der Ostsee. Ber. Inst. f. Meeresk., Kiel, Nr. 231, 104 pp.

[63] LENZ, W., 1971: Monatskarten der Temperatur der Ostsee. Ergänzungsheft zur Deutschen Hydrographischen Zeitschrift, Reihe B, Nr. 11.

[64] LILLY, D.K. and J.B. KLEMP, 1979: The effects of terrain shape on mountain waves. J. Fluid Mech., 95, 241–262.

[65] LUNDBERG, L. and G. WALIN, 1990: The distribution of the geostrophic flow in a stratified surface layer. Tellus, 42A, 583–593.

[66] MacCREADY, P. and P.B. RHINES, 1993: Slippery bottom boundary layers on a slope. J. Phys. Oceanogr., 23, 5–22.

[67] MAGAARD, L. and W. KRAUSS, 1966: Spektren der Wasserstandsschwankungen der Ostsee im Jahre 1958. Kieler Meeresf. XXII, 155–162.

[68] MAGAARD, L. and G. RHEINHEIMER, 1974: Meereskunde der Ostsee. Springer Verlag, Berlin, 269 pp.

[69] MÄLKKI, P. and R. TAMSALU, 1985: Physical features of the Baltic Sea. Finn. Mar. Res., No. 252, 110 pp.

[70] MAROTZKE, J., 1991: Influence of convective adjustment on the stability of the thermohaline circulation. J. Phys. Oceanogr., 21, 903–907.

[71] MATTHÄUS, W. and H. FRANCK, 1989: Is the positive salinity anomaly in the Kattegat deep water a necessary precondition for major Baltic inflows? Gerlands Beitr. Geophys., 98, 332–343.

[72] McDONALD, N.R., 1993: Topographic dispersal of bottom water. J. Phys. Oceanogr., 23, 954–969.

[73] MIDDLETON, J.F., 1991: Coastal-trapped wave scattering into and out of straits and bays. J. Phys. Oceanogr., 21, 681–694.

[74] MIDDLETON, J.F. and F. VIERA, 1991: The forcing of low frequency motions within Bass Strait. J. Phys. Oceanogr., 21, 695–708.

[75] MÜLLER, P. and N. XU, 1992: Scattering of oceanic internal gravity waves off random bottom topography. J. Phys. Oceanogr., 22, 474–488.

[76] NOF, D., 1984: Shock waves in currents and outflows. J. Phys. Oceanogr., 14, 1683–1702.

[77] NOF, D., 1986: Geostrophic shock waves. J. Phys. Oceanogr., 16, 886–901.

[78] OMSTEDT, A., 1990: Modelling the Baltic Sea as thirteen sub-basins with vertical resolution. Tellus, 42A, 286–301.

[79] ORVIK, K.A. and M. MORK, 1993: Topographic effects in stratified flows resolved by a spectral method. Tellus, 45A, 114–126.

[80] PEDLOSKY, J., 1979: Geophysical Fluid Dynamics. Springer–Verlag, Berlin and New York, 624 pp.

[81] PIERINI, S., 1989: A model for the Alborea Sea internal solitary waves. J. Phys. Oceanogr., 19, 755–772.

[82] PRATT, L.J., 1983: On inertial flow over topography. Part 1. Semigeostrophic adjustment to an obstacle. J. Fluid Mech., 131, 195–218.

[83] PRATT, L.J., 1984a: A time–dependent aspect of hydraulic control in straits. J. Phys. Oceanogr., 14, 1414–1418.

[84] PRATT, L.J., 1984b: On inertial flow over topography. Part 2. Rotating–channel flow near the critical speed. J. Fluid Mech., 145, 95–110.

[85] PRATT, L.J., 1986: Hydraulic control of sill flow with bottom friction. J. Phys. Oceanogr., 16, 1970–1980.

[86] PRATT, L.J., 1987a: Rotating shocks in a separated laboratory channel flow. J. Phys. Oceanogr., 17, 483–491.

[87] PRATT, L.J. and L. ARMI, 1987b: Hydraulic control of flows with nonuniform potential vorticity. J. Phys. Oceanogr., 17, 2016–2029.

[88] PRATT, L.J., 1991: Geostrophic versus critical control in straits., J. Phys. Oceanogr., 21, 728–732.

[89] RAHM, L., 1985: On the diffusive salt flux of the Baltic proper. Tellus, 37A, 87–96.

[90] SEMTNER, A.J., 1974: An oceanic general circulation model with bottom topography. UCLA Dept. Meteorology Tech. Rep. No. 9.

[91] SHEN, S.S.P., 1992: Forced solitary waves and hydraulic falls in two–layer flows. J. Fluid Mech., 234, 583–612.

[92] SIMONS, T.J., 1976: Topographic and baroclinic circulations in the southwest Baltic. Ber. Inst. f. Meeresk., Kiel, Nr. 25.

[93] STERN, M.E., 1980: Geostrophic fronts, bores, breaking and blocking waves. J. Fluid Mech., 99, 687–703.

[94] STIGEBRANDT, A., 1976: Vertical diffusion driven by internal waves in a sill fjord. J. Phys. Oceanogr., 6, 486–495.

[95] STIGEBRANDT, A., 1980: Barotropic and baroclinic response of a semi-enclosed basin to barotropic forcing from the sea. In: Fjord Oceanography, edited by H.J. Freeland, D.M. Farmer and C.D. Levings, 141–163, Plenum, 715 pp.

[96] STIGEBRANDT, A., 1983: A model for the exchange of water and salt between the Baltic and the Skagerrak. J. Phys. Oceanogr., 13, 411–427.

[97] STIGEBRANDT, A., 1987a: Computations of the flow of dense water into the Baltic Sea from hydrographical measurements in the Arkona Basin. Tellus, 39A, 170–177

[98] STIGEBRANDT, A., 1987b: A model for the vertical circulation of the Baltic deep water. J. Phys. Oceanogr., 17, 1772–1785.

[99] SVANSSON, A., 1980: Exchange of water and salt in the Baltic and adjacent seas. Oceanologica Acta, 3, 431–440.

[100] TATRO, P.R., and E.L. MOLLO-CHRISTENSEN, 1967: Experiments on Ekman layer instability. J. Fluid Mech., 28, 531–543.

[101] TOULANY, B. and C. GARRETT, 1984: Geostrophic control of fluctuating barotropic flow through straits. J. Phys. Oceanogr., 14, 649–655.

[102] ÜNLÜATA, Ü., T. OĞUZ, M.A. LATIF and E. ÖZSOY, 1990: On the physical oceanography of the Turkish straits. In: The Physical Oceanography of Sea Straits, edited by L.J. Pratt, 25–60, Kluwer, Boston.

[103] WALIN, G., 1977: A theoretical framework for the describtion of estuaries. Tellus, 29, 128–136.

[104] WELANDER, P., 1974: Two–layer exchange in an estuary basin, with special reference to the Baltic Sea. J. Phys. Oceanogr., 4, 542–556.

[105] WHITEHEAD, J.A., A. LEETMAA and R.A. KNOX, 1974: Rotating hydraulics of strait and sill flows. Geophys. Fluid Dyn., 6, 101–125.

[106] WHITEHEAD, J.A. and A.R. MILLER, 1979: Laboratory simulation of the gyre in the Alboran Sea. J. Geophys. Res., 84, 3733–3742.

[107] WHITEHEAD, J.A., 1986: Flow of a homogeneous rotating fluid through straits. Geophys. Astrophys. Fluid Dyn., 36, 187–205.

[108] WANG, D–P., 1985: Numerical study of gravity currents in a channel. J. Phys. Oceanogr., 15, 299–305.

[109] WRIGHT, D.G., 1987: Comments on "Geostrophic control of fluctuating barotropic flow through straits". J. Phys. Oceanogr., 17, 2375–2377.

[110] WÜBBER, C. and W. KRAUSS, 1979: The two-dimensional seiches of the Baltic Sea. Oceanologica Acta, 2, 435–446.

[111] WYRTKI, K., 1953: Die Dynamik der Wasserbewegungen im Fehmarnbelt I. Kieler Meeresf. IX, 155–170.

[112] WYRTKI, K., 1954a: Der große Salzeinbruch in die Ostsee im November und Dezember 1951. Kieler Meeresf. X, 19–25.

[113] WYRTKI, K., 1954b: Die Dynamik der Wasserbewegungen im Fehmarnbelt II. Kieler Meeresf. X, 162–181.

Danksagung

An dieser Stelle möchte ich mich bei allen bedanken, die mich während meiner Promotionszeit auf verschiedene Weise unterstützt haben.

Vor allem danke ich meinem Doktorvater Prof. Dr. W. Krauß, daß er es ermöglicht hat, daß ich in Deutschland promovieren konnte.

Es war eine große Bereicherung für mich, die Anlagen und Metarialien des Instituts nutzen zu können.

Ganz besonderer Dank gilt meiner Frau Hannelore und meinem Bruder Ercüment Fatih, daß sie mich so lieb unterstützt und mir über meinen Streß hinweggeholfen haben. Auch für die vielen aufmunternden, lieben Worte von Ellen und Jürgen Holtorff bedanke ich mich ganz herzlich.